

**SYNTHESIS AND CHARACTERIZATION OF CARBON
NANOTUBE-BASED COMPOSITES AND THEIR
APPLICATIONS FOR WATER TREATMENT**

BY

TAWFIK ABDO SALEH AWADH

A Dissertation Presented to the
DEANSHIP OF GRADUATE STUDIES

KING FAHD UNIVERSITY OF PETROLEUM & MINERALS

DHAHRAN, SAUDI ARABIA

In Partial Fulfillment of the
Requirements for the Degree of

DOCTOR OF PHILOSOPHY

In

CHEMISTRY

JUNE, 2011


KING FAHD UNIVERSITY OF PETROLEUM & MINERALS
DHAHRAN 31261, SAUDI ARABIA

DEANSHIP OF GRADUATE STUDIES

This dissertation, written by **Tawfik Abdo Saleh Awadh** under the direction of his thesis advisor and approved by his thesis committee, has been presented to and accepted by the Dean of Graduate Studies, in partial fulfillment of the requirements for the degree of **DOCTOR OF PHILOSOPHY IN CHEMISTRY**.

Dissertation Committee



Prof. Vinod Kumar Gupta (Advisor)


Prof. Abdalla M. Abulkibash (Coadvisor)


Prof. Mohammad A. Gondal (Member)


Dr. Basheer Chanbasha (Member)


Dr. Than Htun Maung (Member)


Dr. Abdullah J. Al-Hamdan
Department Chairman

Dr. Salam S. Zummo
Dean of Graduate Studies

23/8/11

[Date]



بسم الله الرحمن الرحيم

DEDICATED

TO

MY PARENTS AND FAMILY

ACKNOWLEDGMENT

First and foremost thanks to Allah who gave me strength, patience and ability to accomplish this research.

Acknowledgment is due to the King Fahd University of Petroleum & Minerals for supporting this research. I wish to express my appreciation to Chair Professor V. K. Gupta, who served as my major advisor, for his guidance and advice through the thesis. Appreciation is also to Professor A. Abukibash, who served as my co-advisor, for his guidance and continuous support. Appreciation is also to Professor M. A. Gondal for his guidance and technical support. I would like also to thank Dr. B. Chanbasha and Dr. T. H. Maung for their suggestions and valuable comments. Thanks are also due to the chairman of chemistry department for providing all the available facilities and continuous support. I would like also to thank Professor El-Ali, who served as graduate advisor, for his continuous guidance. I am also grateful to all faculty members for their direct or indirect help. Special thanks are due to Dr. Al-Daous for his comments. I also acknowledge the assistance of Mr. Hamodi. I gratefully acknowledge the support and help of each member at KFUPM. Finally, I would like to appreciate my family members for their prayers that helped me to complete this work, their continuous support and encouragement cannot be forgotten.

TABLE OF CONTENTS

List of Figures	x
Thesis Abstract	xv
CHAPTER 1 INTRODUCTION.....	1
1.1. OVERVIEW.....	1
1.2. TREATMENT TECHNIQUES	3
1.2.1. Primary Water Treatment Technologies	4
1.2.2. Secondary Water Treatment Technologies	6
1.2.3. Tertiary Water Treatment Technologies	8
1.2.4. Disadvantages.....	18
1.2.5. Advanced oxidation processes	19
1.2.6. General Mechanism.....	20
1.3. NANOTECHNOLOGY	21
CHAPTER 2 LITERATURE REVIEW AND OBJECTIVES	26
2.1. LITERATURE REVIEW.....	26
2.2. OBJECTIVES	30
2.3. SIGNIFICANCE OF THE WORK.....	31
2.4. RESEARCH HIGHLIGHTS.....	31
CHAPTER 3 Activation of Carbon Nanotube.....	32
3.1. INTRODUCTION	32

3.2. EXPERIMENTAL SECTION	35
3.2.1. Materials	35
3.2.2. Oxidation Process	35
3.2.3. Acidity determination	36
3.2.4. Characterization.....	37
3.3. RESULTS AND DISCUSSION	38
3.3.1. Effect of treatment duration.....	38
3.3.2. Effect of Treatment Temperature	38
3.3.3. Characterization of o-MWCNT.....	42
CHAPTER 4 Experimental	53
4.1. MATERIALS	54
4.2. SYNTHESIS STRATEGY	55
4.2.1. Synthesis of CNT/Alumina composite.....	55
4.2.2. Synthesis of magnetic-CNT	56
4.2.3. Synthesis of CNT/Manganese Oxide	56
4.2.4. Synthesis of CNT/Zinc Oxide	57
4.2.5. Synthesis of CNT/Tungsten Oxide.....	58
CHAPTER 5 CHARACTERIZATION: RESULTS AND DISCUSSION.....	62
5.1. INTRODUCTION	62
5.2. OVERVIEW.....	63
5.3. RESULTS AND DISCUSSION	65

5.3.1. CNT/Alumina composite.....	65
5.3.2. Magnetic-CNTs	73
5.3.3. CNT/Manganese Oxide.....	78
5.3.4. CNT/Zinc Oxide.....	85
5.3.5. CNT/Tungsten Oxide	91
CHAPTER 6 APPLICATION OF MWCNT/ALUMINA COMPOSITE.....	99
6.1. INTRODUCTION	99
6.2. HIGHLIGHTS.....	100
6.3. EXPERIMENTAL DESIGN	102
6.4. PARAMETERS OPTIMIZATION	103
6.4.1. Batch mode.....	103
6.4.2. Fixed bed column experiments.....	110
CHAPTER 7 APPLICATION OF MAGNETIC-MWCNT	115
7.1. OVERVIEW.....	116
7.2. EXPERIMENTAL DESIGN	117
7.3. PARAMETERS OPTIMIZATION	118
7.3.1. 2 Results of Batch experiments	118
7.3.2. Results of fixed bed experiments	121
CHAPTER 8 APPLICATION OF MWCNT/MANGANESE COMPOSITE	129
8.1. INTRODUCTION	129
8.2. HIGHLIGHTS.....	129

8.3. EXPERIMENTAL DESIGN	131
8.3.1. Materials	132
8.3.2. Oxidation and adsorption experiments	132
8.3.3. Desorption experiments	133
8.4. RESULTS AND PARAMETERS OPTIMIZATION	133
8.4.1. Contact time effect	133
8.4.2. pH effect	134
8.4.3. Desorption	139
8.5. MECHANISM	143
CHAPTER 9 APPLICATION OF MWCNT/Zinc Oxide COMPOSITE	146
9.1. INTRODUCTION	146
9.2. HIGHLIGHTS.....	147
9.3. EXPERIMENTAL SETUP	148
9.4. PHOTO CATALYTIC DEGRADATION OF CYANIDE.....	149
9.4.1. Parameters' Optimization.....	149
9.4.2. Advantages	154
CHAPTER 10 APPLICATION OF MWCNT/TUNGSTEN OXIDE COMPOSITE	
.....	160
10.1. HIGHLIGHTS.....	160
10.2. EXPERIMENTAL DESIGN	163
10.2.1. Photocatalytic Reaction.....	163

10.2.2. Absorbance Measurement	164
10.3. RESULTS OF PHOTOCATALYTIC ACTIVITY	164
10.3.1. Parameters'' optimization	165
10.3.2. Mechanism	174
CHAPTER 11 CONCLUSIONS	177
References	179
APPENDIX A - LIST OF PUBLICATION	191
APPENDIX B - CURRICULUM VITAE	192

List of Figures

Figure 1-1 Illustration of the water treatment classification and recycling technologies	23
Figure 1-2 Filtration spectrum; micro-, ultra-filtration and reverse osmosis	24
Figure 1-3 Basic design of desalination by RO.....	24
Figure 1-4 Modules of connecting membranes in series.....	25
Figure 3-1 Possible structures of oxygen-containing groups on CNT	34
Figure 3-2 Effect of treatment duration on the acidity of MWCNT oxidized by (a) (a) nitric acid; (b) mixtures of sulfuric and nitric acids (3:1)	40
Figure 3-3 Effect of temperature on the acidity of MWCNT oxidized by (a) nitric acid; (b) mixtures of sulfuric and nitric acids (3:1).....	41
Figure 3-4 EDX spectrum of MWCNTs	46
Figure 3-5 IR spectra of MWCNTs.....	48
Figure 3-6 XRD patterns of MWCNT oxidized with nitric acid at 120 °C.....	49
Figure 3-7 XRD of CNT oxidized with sulfuric and nitric acids mixture at 100 °C.....	50
Figure 3-8 SEM images of MWCNT treated at 140 °C with (a) nitric acid (b) H ₂ SO ₄ / HNO ₃ mixture	51
Figure 3-9 TEM of oxidized MWCNT	51
Figure 3-10 Raman spectra of CNT before functionalization	52
Figure 3-11 Raman spectra of CNT after functionalization.....	52
Figure 4-1 Scheme of MWCNTs oxidation and MWCNT/MnO ₂ preparation.....	59

Figure 4-2 Schematic diagram illustrating the synthesis of MWCNT/ZnO composite using a Ball & Stick model.....	60
Figure 4-3 Scheme of MWCNTs modification and preparation of MWCNT/WO ₃	61
Figure 5-1 SEM images of (a) uncoated MWCNTs (b) alumina-coated MWCNTs	66
5-2 EDX spectrum of MWCNT/alumina composite (a): Inset is the components percentages in the composite sample; (b) is the SEM of the area of the sample from which EDX is measured	67
Figure 5-3 X-ray diffraction of (a) uncoated MWCNTs (b) alumina-coated MWCNTs	68
Figure 5-4 FT-IR spectra of (a) uncoated CNTs and (b) alumina-coated CNTs.....	71
Figure 5-5 Structural representative of possible interaction between alumina and CNT	72
Figure 5-6 SEM images of MWCNTs/nano-iron oxide	75
Figure 5-7 X-ray diffraction MWCNTs/nano-iron oxide.....	76
Figure 5-8 FT-IR spectra of MWCNTs/nano-iron oxide	77
Figure 5-9 FTIR spectra of MWCNT/manganese oxide composite	80
Figure 5-10 FTIR spectra of manganese oxide nanoparticles	81
Figure 5-11 SEM of MWCNT/manganese oxide composite	82
Figure 5-12 EDX of MWCNT/manganese oxide composite	83
Figure 5-13 XRD of MWCNT/manganese oxide composite.....	84
Figure 5-14 XRD of MWCNT (a) and MWCNT/zinc oxide composite.....	87
Figure 5-15 FE-SEM image (a); higher magnification SFM (b); HRTEM image (c); Space Filling model (d) of MWCNT/ZnO composite.....	88
Figure 5-16 UV-vis spectrum of MWCNT/ZnO nanocomposite.....	89

Figure 5-17 FTIR of MWCNT (a) and the MWCNT/ZnO composite.....	90
Figure 5-18 XRD of MWCNT/WO ₃	94
Figure 5-19 FESEM images (a) and Space Filling model (b) and EDX (c) of MWCNT/WO ₃	95
Figure 5-20 IR spectrum of WO ₃ nanoparticles.....	96
Figure 5-21 IR spectrum of MWCNT/WO ₃ composite	97
Figure 5-22 UV-vis spectrum of MWCNT/WO ₃	98
Figure 6-1 Effect of contact time on the percent removal of Pb(II) by uncoated MWCNTs and the alumina-coated MWCNTs. pH=5.5, agitation speed= 150 rpm, adsorbent dosage= 10mg	106
Figure 6-2 Effect of pH on the adsorption of Pb(II) ions. Initial Pb(II) conc. Agitation speed= 150 rpm, adsorbent dosage= 10mg, Contact time 120 min.	107
Figure 6-3 Effect of adsorbent dosage on adsorption of Pb(II) ions. Initial Agitation speed= 150 rpm, pH= 5.5, Contact time 120 min.	108
Figure 6-4 Effect of agitation speed on adsorption of Pb(II) ions. pH= 5.5, contact time 120 min, adsorbent dosage= 10mg.....	109
Figure 6-5 Effect of pH on adsorption of Pb(II) ions, in fixed bed system.....	112
Figure 6-6 Effect of layer thickness on adsorption of Pb(II), in fixed bed system	113
Figure 6-7 Effect of flow rate on adsorption of Pb(II) ions, in fixed bed system	114
Figure 7-1 Effect of contact time on the amount of Cr(III) adsorbed on different adsorbents	123

Figure 7-2 Effect of pH on the amount of Cr(III) adsorbed on the MWCNT/nano-iron oxide	124
Figure 7-3 Effect of agitation speed on the amount of Cr(III) adsorbed on the MWCNT/nano-iron oxide	125
Figure 7-4 Effect of dosage on the amount of Cr(III) adsorbed on the MWCNT/nano-iron oxide.....	126
Figure 7-5 effect of flow rate (ml/min) on the amount of Cr(III) adsorbed on the MWCNT/nano-iron oxide	127
Figure 7-6 Effect of layer thickness on the amount of Cr(III) adsorbed on the MWCNT/nano-iron oxide	128
Figure 8-1 Change in As(III) content in solution vs. time (min) reaction for 0-MWCNTs and MWCNT/MnO ₂	136
Figure 8-2 Change in and As(V) content in solution vs. time (min) reaction for 0-MWCNTs and MWCNT/MnO ₂	137
Figure 8-3 Influence of pH of the solution on As(III) and As(V) adsorption; Experimental conditions: Amount of dosage 0.2g/L; Contact time 60 min.....	138
Figure 8-4 SEM image of MWCNT/MnO ₂ composite after adsorption of arsenic (a); with Energy dispersive X-ray (EDX) spectrum (b).....	140
Figure 8-5 SEM image of MWCNT/MnO ₂ composite after regeneration (a); with energy dispersive X-ray (EDX) spectrum (b)	141
Figure 8-6 Schematic representation of the regeneration process.....	142
Figure 8-7 Proposed mechanism of oxidation and adsorption process of arsenic	145

Figure 9-1 Variation of cyanide elimination with irradiation time in present of dosage of different material	155
Figure 9-2 Proposed mechanism of cyanide photodegradation over CNT/ZnO	156
Figure 9-3 Variation of cyanide elimination with the irradiation energy.....	157
Figure 9-4 Variation of cyanide elimination with pH	158
Figure 9-5 Variation of cyanide elimination with the catalytic composite dosage	159
Figure 10-1 UV/vis spectral changes of RhB under solar irradiation for the composite, spectra from top to bottom refer to irradiation for 0 (after equilibrium), 30, 60, 90, 120 and 150 min, respectively.....	166
Figure 10-2 Apparent first-order linear transform $\ln(C^0 / C) = kt$ of Rh B degradation kinetic plots for the composite and the mixture of MWCNTs	167
Figure 10-3 Equilibrium of Rh B in CNT/tungsten oxide nanocomposite	169
Figure 10-4 Photodegradation of RhB vs irradiation time for several systems	170
Figure 10-5 Photo catalytic degradation of Rh B at various pH values	173
Figure 10-6 Schematic representation of the reasonable reaction mechanism of Rh B photodegradation over MWCNT/WO ₃ presented in this work.....	176

THESIS ABSTRACT

Name: Tawfik Abdo Saleh Awadh,

Title: Synthesis and Characterization of Carbon Nanotube-based
Composites and their Applications for Water Treatment

Major Field: Chemistry

Date of Degree: June 2011

This dissertation describes the synthesis of carbon nanotube/ metal oxides composites including alumina, iron oxide, manganese oxide, tungsten oxide and zinc oxide using sol gel methods and thermal process. The conditions of the reactions were proper optimized. The methods have the additional advantage of reducing cost by minimizing time, amount of reagent consumed, man power required, and simple equipments used, and improved the ability to control the process. Different techniques, scanning electron microscope (SEM), transmission electron microscopy (TEM), Fourier transform Infrared (FTIR) and X-ray diffraction (XRD), and thermal gravimetric analysis (TGA) conducted for the characterization of the synthesized materials. The properties and activities of the synthesized materials have been tested for removal or degradation of various pollutants, such as lead, arsenic, chromium, cyanide and dyes. The composite materials showed better efficiency than the individuals did.

ملخص الرسالة

الاسم: توفيق عبده صالح عوض

عنوان الرسالة: تحضير وتوصيف المركبات المولفه مع انابيب الكربون النانوية وتطبيقاتها لمعالجة المياه

التخصص: كيمياء

تاريخ التخرج: رجب 1432 هجرية

تتناول هذه الدراسة توليف انابيب الكربون النانوية بمركبات متعددة مثل اكاسيد المعادن بطرق كيميائية متعددة. حيث تم تحضير مركبات تتضمن انابيب الكربون ممولفه باكسيد التنجستن واكاسيد المنجنيز واكاسيد الزنك واكاسيد الحديد واكاسيد الالمنيوم وغيرها. وتناولت الدراسة ايضا توصيف المركبات المحضرة باجهزة توصيف متعددة منها ما هي متخصصة في توصيف المواد النانوية الحجم. ومن هذه الاجهزة جهاز المجهر الإلكتروني وجهاز مجهر الانتقال الإلكتروني و جهاز مطيافية الأشعة تحت الحمراء وجهاز مطياف الأشعة السينية الحيود وجهاز طاقة الأشعة السينية المشتتة وجهاز التحليل الطيفي رامان وجهاز مطياف الأشعة فوق البنفسجية وجهاز التحليل الحراري الوزني وغيرها. بينت النتائج ان المركبات الناتجة لها حجم النانو حيث بينت التوصيفات وجود بلورات من اكاسيد المعادن مرتبطة بانابيب الكربون هذه البلورات لها حجم النانو وتتراوح احجامها من 6 الى 50 نانومتر. وتتمتع هذه المركبات بانتظام توزيع البلورات على سطح الانابيب الكربونية. ولاختبار فعالية المواد المحضره فقد تم استخدامها كمواد ادمصاص في تطبيقات متنوعه مثل ازالة ملوثات الرصاص والكروم والزرنيخ وكمواد حفازة في تفكيك السيانيد وبعض الاصباغ. وقد بينت النتائج فعالية عالية لهذه المركبات مقارنة بغيرها.

درجة الدكتوراه

جامعة الملك فهد للبترول والمعادن

2011م

CHAPTER 1

INTRODUCTION

This chapter introduces the techniques and the materials utilized in water treatment; with focus on adsorption processes, advanced oxidation processes, and membrane used in reverse osmoses processes. It discusses the materials used in such techniques. Then, it highlights the disadvantages of the existing techniques and materials. This followed by the rationalization of the role that nanotechnology might play to improve the properties of materials used in such processes.

1.1. OVERVIEW

Freshwater looks like it will become the oil of the future - scarce and expensive. Water scarcity and water pollution are two increasingly pressing problems that easily and quickly could surpass the oil issue. Renewable energy sources can substitute for fossil fuels while freshwater cannot be replaced. This makes the ability to remove toxics from aquatic environments rapidly and efficiently, an important technological challenge.

Many pollutants are present in wastewater however, the toxicity observed beyond a certain limit called permissible limit. The limit is determined based on the type of pollutant. For drinking water quality, the environmental protection agency (EPA) sets

standards called maximum contaminant levels (MCLs) of each pollutant that may be present with no adverse health effects. This level is enforceable public health goal. Another level called the maximum contaminant level goal (MCLG) is non-enforceable public health goal. MCL is higher than the MCLG because of difficulties in measuring small quantities of a contaminant and a lack of available treatment technologies and analytical methods. Point and non-point sources are the sources of water contamination.

Industries, agricultural and municipal wastewater releasing activities play major sources in determining the type of pollutants. There are different types of water pollutants categorized as inorganics, organics, and biologicals in nature. Most common water pollutant inorganics are heavy metals and carcinogenic. Besides, nitrate, sulphate, phosphate, fluoride, chloride and oxalate have also some serious hazardous effects. The toxic organic pollutants include dyes such as rhodamine B, safranin, tartrazine, methyl red, methyl orange, bromothymol blue, alizarin yellow, brom cresol green sodium salt, congo red, ethyl orange, metanil yellow, acid blue, and cyanosine. Pesticides as insecticides, herbicides, fungicides; polynuclear hydrocarbons (PAHs) phenols, polychlorinated biphenyls, halogenated aromatic hydrocarbons, formaldehyde, polybrominated biphenyls, biphenyls, detergents, oils, greases are also found in water. Normal hydrocarbons, alcohols, aldehydes, ketones, proteins, lignin and pharmaceuticals, might be observed in wastewater. Different types of microbes present in wastewater, such as bacteria, fungi, algae, planktons, amoeba, virus and other worms may be responsible for different type of diseases [Droste, 1997].

1.2. TREATMENT TECHNIQUES

Chemical, physical and biological processes are used to decontaminate polluted water. Wastewater treatment methods are classified into three major classes; primary, secondary and tertiary treatment. The primary treatment aims towards preliminary purification of physical and chemical nature. The secondary treatment includes biological treatment of wastewater. The aim of tertiary treatment process is to convert wastewater into good quality water. This water could be used for industrial, agriculture, and different purposes. In a complete water treatment plant, all these three processes are combined together for producing good and safe quality of water

Primary water treatment technologies, used when water is highly polluted, include screening, filtration, coagulation, flotation, and centrifugal separation sedimentation and gravity separation. Secondary water treatment technologies include aeration; aerobic and anaerobic processes. Tertiary water treatment technologies involve distillation, crystallization, evaporation, ozonation, chlorination, high-temperature incineration, solvent extraction, oxidation, ion exchange, micro- and ultra filtration, reverse osmosis adsorption electrolysis and electrodialysis. The treatment processes may be used separately or combined with other processes to enhance the overall treatment efficiency [Nemerow and Dasgupta, 1991]. Moreover, several technical factors should be considered to choose the correct process.

1.2.1. Primary Water Treatment Technologies

At the primary level, water is treated using screening, filtration, centrifuge, sedimentation, coagulation, gravity and flotation methods. These methods are used when water is highly polluted. These methods are described in the following sections.

Screening: The main idea of screening is to remove the solid wastes present in the wastewater. Screening is used as the first step in a wastewater treatment plant. It is used for the removal of large solid pieces such as cloths, papers, wood, cork, hair, fiber, kitchen refuse and fecal solids. The screens of various sizes are used for this purpose and the size of the screen is selected as per size of the solids present in wastewater.

Filtration: Water is passed through a medium having fine pores. Normally, a set-up having pore size of about 0.1 to 0.5 μm is used for this purpose. It is used for the removal of suspended solids, greases, oils, bacteria etc. Different filters, such as membranes and cartridges can be used. The filtration process can be used to remove solids of size below 100 mg/l and to remove oil of 25 mg/l which can be reduced to 99%. The filtration process can be utilized for water treatment. Water produced by filtration is used for adsorption, ion exchange or membrane separation etc. processes. Besides, potable water is produced by filtration systems.

Centrifugal Separation: The suspended non-colloidal solids (size up to 1 μm) is removed by centrifugal separation. The wastewater is applied to the centrifugal devices and rotated at different speeds and the solids (sludge) are separated and discharged. The

extent of separation of suspended solids is directly proportional to their densities. In addition to this, the speed of the centrifugal machine is also responsible for the removal of suspended solids. The applications include the source reduction and separation of oils and greases. The different types of centrifugal machines available and in use are solid-bowl, basket type, counter flow and counter current flow [Franklin, 1991].

Sedimentation and Gravity Separation: The suspended solids, grits and silts are removed by allowing water undisturbed/semi-disturbed for different times of intervals in various types of tanks. The suspended solids get settled down under the influence of gravity. The settling time depends upon the size and density of the solids or velocity if the water is in movement. Sometimes, alums are added to augment the sedimentation process. Gravity separation can reduce the suspended solids up to 60% only. The sedimentation is performed prior to the conventional treatment process. It is very useful method for the treatment of effluents obtained from paper and refinery industries. Water treated in this process is used for industrial water supply, water for ion exchange and membrane process. The technique is also used for the source reduction.

Coagulation: When the suspended solids do not settle down under sedimentation and gravity method, non-settable solids are allowed to settle down by the addition of certain chemicals. Examples of the chemical are alum, starch, iron materials, activated silica and aluminum salts. In addition, synthetic cationics, anionics and non-ionic polymers are very effective coagulants but are usually more costly than natural ones. The most important controlling factors for coagulation process are pH, temperature and contact

time. In biological treatment plant, microbes and other organics floated on the surface are removed by the addition of certain coagulants. It is the main component of a wastewater treatment plant and the applications include wastewater treatment, recycling, removal of heavy metal ions and fluoride.

Flotation: The suspended solids, oils, greases and biological solids are removed by adhering them with either air or gas. The solids get adhered with gas or air and form agglomerates, which in turn accumulate at water surface which can be skimmed off easily. Some chemicals such as alum, activated silica etc. help in the flotation process. The compressed air is allowed to pass through water, which helps in the flotation process. Electro-flotation (electro-flocculation) has been used as an effective process for water treatment and recycling purposes. Suspended solids are removed up to 75% while oil and grease up to 99% by this process. It is very effective technique for the treatment of wastewater of paper and refinery industries.

1.2.2. Secondary Water Treatment Technologies

Secondary water treatment includes biological methods for the removal of soluble and insoluble pollutants by microbes. In this method, water circulated in a reactor that maintains a high concentration of microbes. The microbes convert the organic matters into water, carbon dioxide and ammonia gases. It is possible that the organic matters are converted into other products such as alcohol, glucose, nitrate etc. The microbes detoxify the toxic inorganic matters. The wastewater should be free from toxics. The

maximum concentrations of total dissolved solids (TDS), heavy metals, cyanides, phenols and oil should not exceed by 16000, 2.0, 60.0, 140, and 50 mg/l respectively. The biological treatment includes aerobic and anaerobic digestion of wastewater.

Aerobic Process: When air or oxygen is available freely in dissolved form to wastewater then the biodegradable organic matters undergo aerobic decomposition, caused by aerobic and facultative bacteria. The extent of the process depends on availability of oxygen, retention time, temperature and biological activities of bacteria. Besides, the rate of the biological oxidation of organic pollutants may be increased by the addition of some chemicals required for bacterial growth. The technique is effective for the removal of biological oxygen demand (BOD), chemical oxygen demand (COD), dissolved and suspended organics, volatile organics, nitrate, phosphate etc. The concentration of biodegradable organics can be reduced up to 90%. The disadvantage of the method is the production of a large quantity of biosolids, which require further costly management. The aerobic Process is carried out by trickling filters or activated sludge processes or oxidation ponds. A representation of aerobic decomposition is represented as:

$$\text{Organic matter} + \text{O}_2 + \text{Bacteria} \rightarrow \text{CO}_2 + \text{H}_2\text{O} + \text{New Bacteria} + \text{Byproducts}$$

Anaerobic Process: If free dissolved oxygen is not available to the wastewater then anaerobic decomposition, called putrefaction, occurs. Anaerobic and facultative bacteria convert the complex organic matter into simpler organic compounds of nitrogen, carbon and sulphur. The important gases evolved in this process are nitrogen, ammonia, hydrogen sulphide and methane. This method is used to reduce biological load of

wastewater. The anaerobic process is represented by the following equation.



1.2.3. Tertiary Water Treatment Technologies

Tertiary water treatment technologies are important in wastewater treatment strategy since they are utilized to get the safe water for human consumption. The techniques used for this purpose are distillation, crystallization, evaporation, solvent extraction, oxidation, coagulation, precipitation, electrolysis, electro dialysis, ion exchange, reverse osmosis and adsorption. These methods are described below.

Distillation: Water is purified by heating it up to 100 °C at which liquid water vaporized leaving behind the pollutants. The so generated vapors are cooled into liquid water. The wastewater should be free from volatile impurities and water produced in this technique is about 99% free from impurities. Various types of boilers with multistage and double distillation are used in this process. The size of the boilers depends on the requirement of water quantity. Its applications in water treatment and reclamation include water supplies in laboratories and medicinal preparations. It is an effective tool for the preparation of potable water from sea and brackish water.

Crystallization: Pollutants are removed by raising their concentrations up to a point where they start to crystallize out. This situation is created either by evaporation or by lowering the temperature of water or by mixing other solvents. It is useful for the treatment of wastewater with high TDS including soluble organics and inorganics.

During the process, the other constituents like bicarbonate, ammonia, sulfite etc. may break down into various gases and, therefore, crystallization, sometimes, may be used for pH control. Generally, the crystallization is used for the wastewater released by cooling tower, coal and gas fired boilers, paper and dyeing industries. It is also used for the source reduction. The commonly used devices for crystallization include forced circulation, draft tube baffle, surface cooled crystallizers and fluidized suspension.

Evaporation: Water surface molecules escaped from the surface under the natural conditions and the escaped molecules are collected in form of pure liquid water. Evaporation is used to reduce the waste liquid volume. Mechanical evaporators have been used for water recycling process. Sometimes vacuum evaporation has been used for the wastewater recycling. Evaporation is effective for the removal of inorganic and organic (except volatile organics) contaminants and it works even at very high concentrations (about 10%) of the pollutants. Foaming, scaling and fouling along with the presence of suspended solids and carbonates are the major problems associated with this technique as they create maintenance problem. Evaporation applications include the treatment of wastewater of fertilizer, petroleum, pharmaceutical and food processing industries. In addition, it is used for water supply to ion exchangers and membrane processes. Water from evaporation is used for cooling in towers and boilers. It can be used as the technique of water source reduction.

Solvent Extraction: Organic solvents, immiscible with water and having capacities to dissolve pollutants, are added in wastewater for the removal of pollutants and the

technique is called solvent extraction. The presence of suspended solids may cause a problem in solvent extraction and hence required pre-treatment. A maximum concentration of TDS of 2000 mg/l can be reduced up to 90% by this technique. Most commonly used solvents are benzene, hexane, acetone and other hydrocarbons. Sometimes, small quantity of the solvent remains mixed with water, which is recovered by using distillation technique. The technique is effective to remove only organics, oils and greases. However, certain metal ions and actinide chemicals may be removed by this method. It is used for water treatment and recycling purposes in chemical process plants, phenol, gasoline and acid industries. It is used for water source reduction purpose.

Oxidation: Organic compounds are converted into water and carbon dioxide or some other products such as alcohol, aldehyde, ketone and carboxylic acid which are easily biodegradable. Chemical oxidation is carried out by potassium permanganate, chlorine, ozone, peroxides, air and chlorine dioxides. The rate of chemical oxidation depends on the nature of oxidants and pollutants. Besides, pH, temperature etc. play a crucial role in the rate of chemical oxidation. Ammonia, cyanide, sulphides, phenols, hydrocarbons and some pathogens may be removed by chemical oxidation. Chemical oxidation is used for the wastewater treatment and recycling for industries and irrigation. Besides, it is also useful and effective method for the source reduction purpose.

Precipitation: The dissolved contaminants are converted into solid precipitates by reducing their solubilities and the precipitates are skimmed off easily from water surface. It is effective for the removal of metal ions and organics but the presence of oil

and grease may cause a problem in precipitation. The solubility of the dissolved pollutants is decreased either by adding some chemicals or by lowering the temperature of water. Adding some organic solvents in water may also reduce solubility of the contaminant but this technique is costly at commercial level. These chemicals react with the soluble pollutants to form precipitates. Most commonly used chemicals for this purpose are different types of alum, sodium bicarbonates, ferric chloride, ferric sulphate, ferrous sulphate and lime. pH and temperature are the main controlling factors for precipitation process. About 60% removal of pollutants can be achieved. The applications of this method include wastewater treatment from nickel and chromium plating industries and water recycling. The specific applications include water softening and removal of heavy metals and phosphate from water. The major problem associated with precipitation is the management of the large volume of sludge produced.

Ion Exchange: Toxic ions present in wastewater are exchanged with the non-toxic ions from some solid material called ion exchangers. The ion exchangers are of two types i.e. cation and anion exchangers having the capacities to exchange cations and anions respectively. The ion exchangers are resins of natural or synthetic origins having the active sites on their surfaces. Most commonly used ion exchangers are sodium silicates, zeolites, polystyrene sulfonic acid, acrylic and metha acrylic resins. It is a reversible process and requires low energy contents. Ion exchange is used for the removal of low concentrations of inorganics and organics (up to 250 mg/l). The concentration of organics and inorganics can be reduced up to 95%. The applications include the

production of potable water, water for industries, pharmacy, research, softening, for boiler feed, fossil fuels, nuclear power station, paper and electronic industries. It has also been used for the source reduction purpose. Sometimes, a pre-treatment of water is required; if oil, grease and high concentration of organics and inorganics are present.

Micro- and Ultra Filtration: The removal of particles and other microbes of 0.04 to 1 μ size is required micro and ultra filtration. The filters are used in this process and made of cotton, wool, rayon, cellulose, fiberglass, polypropylene, acrylics, nylon, asbestos and fluorated hydrocarbons polymers. These are arranged in different fashions such as tubular, disc, plates, spiral, and hollow fibers. The life of cartridges varies from 5 to 8 years depending upon the concentration of the dissolved solids. The pre-removal of suspended solids is an important factor for the long life of filters. The operational pressure in this process ranged from 1 to 3 bar. The applications include removal of suspended solids and microbes. Water purified by this technique is used for food and drink industries, soft drinks, pharmaceuticals, photofilm processing, swimming pools and drinking purpose. It has been used as wastewater source reduction technique. Ultrafiltration is a low pressure membrane separation process; capable of removing high molecular weight materials like colloids, pyrogens, microorganisms and suspended solids from wastewater. The membranes are manufactured from a wide variety of polymers such as polysulphonates, polyacrylonitriles, polyamides, PVDF and zirconium oxides. These polymers are having pore size 10-200 Å (0.001-0.02 μ). To achieve the required

filtration, membranes are arranged in tubular, disc, plates, and hollow fiber forms. The life of the membranes varies from 5 to 8 years and may be increased as discussed above.

Reverse Osmosis: known as hyper-filtration, is a classical method of water purification and came into existence for the advancement of semi-permeable membranes. It has achieved a great attention nowadays as the best water recycling technique. The separation and concentration of the dissolved species are achieved due to the hydraulic gradient across the semi-permeable membrane. A pressure greater than the osmotic pressure is applied for the process. Most commonly used membranes are made of cellulose, nylon, polyether, polyethyl urea, polyphenyl oxides, phenylenes and polyamide. Membranes are arranged in tubular, disc, plates, spiral, and hollow fiber forms. The partition coefficients of solutes between water and membrane play the important roles for the removal of water pollutants. Free energy of interaction between water and membrane sites is also responsible for RO process. pH, pressure, size and the molecular weight of the solute and time of operation are considerable factors in RO.

RO has been used as a separation and concentration technique at macro and micro levels for the removal of large, non-polar, ionic and toxic soluble pollutants. The effectiveness and the application of RO on large scale is based on the fact that the total dissolved solids (TDS), organic dissolved matter (ODM) and bacteria can be removed up to 99%. It has been used for the treatment of wastewater of sanitary wastes, municipal leachates, petrochemicals, electroplating, textiles, coal, gasification, pulp and paper, steel and electronic industries. Besides, the rejection of bacteria, virus and other microbes are

hundred percent and, therefore, it is used in the preparation of ultra pure water for pharmacy, medicines and electronics. In addition, it has been used for the purpose of source reduction. RO is today's most economic process for potable water production from saline water.

The working efficiency of RO membrane used is expressed in terms of percentage rejection (PR%) or the removal ratio of solutes and expressed as:

$$PR = \frac{(C_F - C_P)}{C_F} \times 100 \quad \text{or} \quad E = 1 - \frac{C_P}{C_F}$$

where, C_F is the molar concentration of solute in feed water; C_P is the molar concentration of solute in permeate (filtrate) and E is the membrane working efficiency.

The performance of the membrane process is also measured by permeate flux. In desalination and wastewater treatment processes, the solvent or permeate flux is referred to the water and defined as the volume of permeate flux produced per unit membrane area for a time interval and is given by the following equation.

$$MF = \frac{V_P}{S_A t}$$

where MF is the Membrane flux; V_P is the volume of permeate over time t , and S_A is the surface area of the membrane.

Separation of pollutants in RO depends on the basis of partition coefficients of solutes between water and membrane involving free energy of interaction between water and

membrane sites. The percentage of rejection is directly proportional to the number of carbon atoms or the molecular weights of organic/inorganic species but this was not found to be complete description because of the geometry of the molecule, i.e., steric configuration and branching overshadow the former properties. The design of reverse osmosis system plays a role to achieve efficient seawater desalination. Membranes can be connected in series. The flow rate of water through the membrane is given as:

$$F_{rate} = K_f(P_{pump} - P_s)$$

Frate is the flow rate; Kf is the flow rate factor which is determined by the properties of the membrane and its area; P_{pump} is the pressure generated by the pump and controlled by the pressure controller; P_s is the osmotic pressure of the concentrated salt water. The energy in such systems can be recovered with a turbine and an auxiliary pump.

The life of RO membranes has been considered two to five years depending upon the nature of the wastewater to be treated. The flux and the quality of the permeate may decrease over a long period of time due to membrane fouling. After a long period of time, humic acids, bacterial slimes or hardness scales may accumulate on the RO membranes. Phenols have also been found to clog the membranes. To increase the efficiency and life of RO systems, the pre-treatment is necessary to minimize the concentration of colloidal and dispersed solids. Physico-chemical coagulation with lime has been used to minimize colloids, turbidity, dispersed oil phases, metal ions and suspended matters. Sodium hydroxide solution (pH 9-11) has been used to clean RO

membranes in case of silica and sulphate fouling. Besides, silica can also be removed from membranes by ion retarding resins that has a high affinity for strong acids, together with conversion of the weak acid $[\text{Si}(\text{OH})_4]$ into much stronger acid (H_2SiF_6). The bacterial inhibitor solutions are circulated (to check the bacterial growth) in to RO tubules or discs before stopping the process for a long period. Phenolics may be removed from RO membranes by circulating hydrogen peroxide solution.

Adsorption: A surface phenomenon and defined as the increase in the concentration of a particular component at the surface or interface between two phases. The adsorption efficiency depends on a number of parameters such as pH, temperature, concentration of pollutants, contact time, particle size of the adsorbent and nature of adsorbents and the pollutants. The presence of suspended particles, oils and greases reduce the efficiency of the process and, therefore, pre-filtration is required. It is supposed as the universal water treatment and reclamation process as it can be applied for the removal of soluble and insoluble organics, inorganics and biological pollutants. Different types of adsorbents are used in adsorption process. Most commonly used adsorbents are activated carbon, fly ashes, metal oxides, zeolites, moss, biomass, and geothites. At industrial level, pollutants are removed from wastewater by using the columns and contractors filled with the required adsorbents. First all the adsorption is carried out in a batch process and the conditions are optimized. The developed and optimized conditions (batch process) are transferred to the column and contractor experiments. The feasibility of the adsorption is verified by models of Langmuir, Freundlich, Hutchins and Reichenberg.

The extent of the pollutant removal varies from 90 to 99%. Adsorption is used for source reduction, wastewater treatment and reclamation for potable and industrial. The basic problems associated with adsorption are the regeneration of columns and column life. The management of the exhausted adsorbent is also a challenging issue for scientists.

Electrolysis: Soluble inorganics and organics are either deposited or decomposed on the surface of the electrodes by electrochemical redox reaction is called electrolysis. Most metal ions are deposited on the electrode surface while organics are decomposed into carbon dioxide and water or in some other products, which are low or non-toxic. It is used for the removal of turbidity and color from wastewater. This method is effective for the removal of TDS below 200 mg/l and, therefore, requires pre-treatment of the wastewater. The technique comprises a water tank or tanks in series with two or a series of electrodes of the required metal. The electrodes are specific in nature with respect to the dissolved metal ions in wastewater. Most important controlling factors are pH, temperature, amount of current applied and contact time. Electrolysis is not developed completely so far and is still under its development stage. It has been rarely used at commercial level for wastewater treatment. Its applications include the treatment of some industrial effluents specially enriched with metal ions and some organics. It may be used as water source reduction technique. Its advantages comprise the further utilization of the deposited metal ions without any waste management problem.

Electrodialysis: Water-soluble ions are allowed to pass through ion selective semi-permeable membranes under the influence of electric current. The ion selective

membranes are made of ion exchange material and are selective in nature. They may be cation or anion exchangers, which permits the out flow of cations and anions. The process is operated either in a continuous or batch mode having two electrodes on which a voltage is applied. To obtain the desired degree of demineralization, the membranes are arranged either in a parallel or series fashion. The dissolved solids removal depends on pH, temperature, amount of current applied, nature of pollutants, selectivity of the membranes, wastewater flow rate, fouling and scaling of wastewater and number and configuration of stages. The applications include the production of potable water from brackish water. Besides, this technique has been used for water source reduction. A maximum concentration of 200 mg/l of TDS can be reduced up to 90% by electrodialysis. The membrane fouling occurred as in case of reverse osmosis and the cleanup and other precautions should be considered.

1.2.4. Disadvantages

Different methods can be effective for different contaminants with some limitations. Aeration is optimal for removing volatile compounds from water or other kinds of solution. Extraction needs appropriate solvents for separation of solute organics or chemically charged pollutants. Properly designed ion exchange resin may selectively remove some pollutants such as ionic surfactants and detergents by electrostatic force. However, it needs to be regenerated periodically with appropriate solutions. Synthetic non-polar sorbents have high affinities for most volatile organic compounds. Molecular

sieves and zeolite have different pore sizes and affinities towards different kinds of chemical molecules. The concentrated chemicals using the methods discussed above should be taken into further treatment for complete decontamination. Certain kinds of bacteria and chemicals are desirable for digesting some contaminants in biological and chemical treatments and they both need secondary treatments afterwards to further remove or adjust some contents in the solution. Removal of pollutants with high temperature incineration, evaporation and distillation are not energy-efficient.

Alternative methods, such as activated carbon adsorption and dissolved air flotation are not only costly but result in phase transfer of pollutants. Activated carbon has excellent adsorption ability due to its large surface area. Reverse osmosis and filtration including ultrafiltration and nanofiltration require membranes with appropriate size of pores and dynamical equipment to drive the solution through the membranes.

1.2.5. Advanced oxidation processes

To overcome the inconveniences of conventional treatment methods, various chemical oxidation techniques have emerged in the last decades, in particular for the treatment of industrial wastewaters. Among these techniques, the so-called advanced oxidation processes appear to be a promising field of study, which have been reported to be effective for the degradation of soluble organic contaminants in waters and soils. Actually, they can often provide an almost total degradation, under reasonably mild conditions of temperature and pressure. AOPs do not only transform chemically

polluting agents, but present very attractive advantages, such as the complete mineralization of compounds, their oxidation at very low concentrations, the generation of environmentally friendly byproducts, and the low consumption of energy, in comparison with other methods. These processes utilize chemical reactions, electron beams, UV light or ultrasound pulses, for instance, to obtain high oxidation rates through the generation of free radicals (mainly hydroxyl radicals). Highly reactive HO• are thought to be the main active species responsible for the destruction of the pollutants.

There is considerable current interest in developing more cost-effective methods. The combination of UV irradiation with photocatalysts have attracted considerable attention in recent years due to its effectiveness in mineralization of organic compounds. This includes removal of dye pollutants from residual textile treatment waters. Interest in this photocatalytic process stems mainly from its low cost, combined with the non-toxicity, insolubility, stability, high photoactivity of the catalyst. The present study is concerned with the removal of tartrazine by photocatalytic technique.

1.2.6. General Mechanism

In heterogeneous photocatalysis, when aqueous metal oxide semiconductor (SC) suspension is irradiated with light energy greater than its band gap energy ($h\nu > E_g = 3.2$ eV; $\lambda < 390$ nm), conduction band electron (e^-) and valence band holes (h^+) are formed. The photogenerated electrons react with adsorbed molecular O_2 , reducing it to superoxide radical anion $O_2^{\bullet-}$, and the photogenerated holes can oxidize either the

organic molecules directly, or can oxidize OH⁻ ions and water molecules adsorbed on the metal oxide surface to OH. Radicals. These act as strong oxidizing agents that can easily attack any organic molecules adsorbed on or located close to the surface of the catalyst, thus leading to their complete degradation into small inorganic species (eq. 1-5)



Despite of the development of various technologies for water treatment and reclamation, economic, effective and rapid water treatment and reclamation at commercial level is still a challenging problem. The management of the removed pollutants (sludge) should be kept in mind. The systematic approach of water treatment and recycling technologies involves the understanding of the technology which include construction and operational cost, maintenance and management of removed pollutants.

1.3. NANOTECHNOLOGY

Nanotechnology could play an important role in water treatment. An active emerging area of research is the development of novel nanomaterials with increased affinity and capacity for heavy metals and other contaminants.

Carbon nanotubes (CNTs) have been reported to have high adsorption ability which can be explained in two reasons. The first is the presence of high energy adsorption sites,

such as CNT defects functional groups and interstitial and groove regions between CNT bundles [Shih et al., 2008]. These adsorption sites commonly exist on as-grown CNTs, thus heterogeneous adsorption is a general feature. The second reason is condensation, such as surface and capillary condensation of gas or liquid adsorbates. Multilayer adsorption could occur when organic chemicals were adsorbed on CNT surfaces [Gotovac, et al. 2006; Gotovac, et al. 2007]. In this process, the first couple of layers interact with the surface, while molecules beyond the first two layers interact with each other. This process is called surface condensation. The energy of this process varies depending on the distance between the adsorbed molecules and the CNT surface, thus causing a distribution of adsorption energy.

The modification of CNTs can be conducted by forming its composites with metal oxides and polymers. The literature on processing and evaluating carbon nanotube-based composites is still in its infancy but developing rapidly. This situation is not surprising, given that initial attempts to produce such nanocomposites were hindered by the small quantities of nanotubes available; although, more recently, the focus on chemical vapor deposition (CVD) synthesis techniques has enabled the manufacture of large-scale CNTs and drive its cost down, promising for more applications. A number of studies have focused on the effect of nanotubes on the composite stiffness, failing to report other, more relevant, properties such as strength and strain to failure. Nevertheless, some interesting studies have been reported illuminate the potential of nanotube composites.

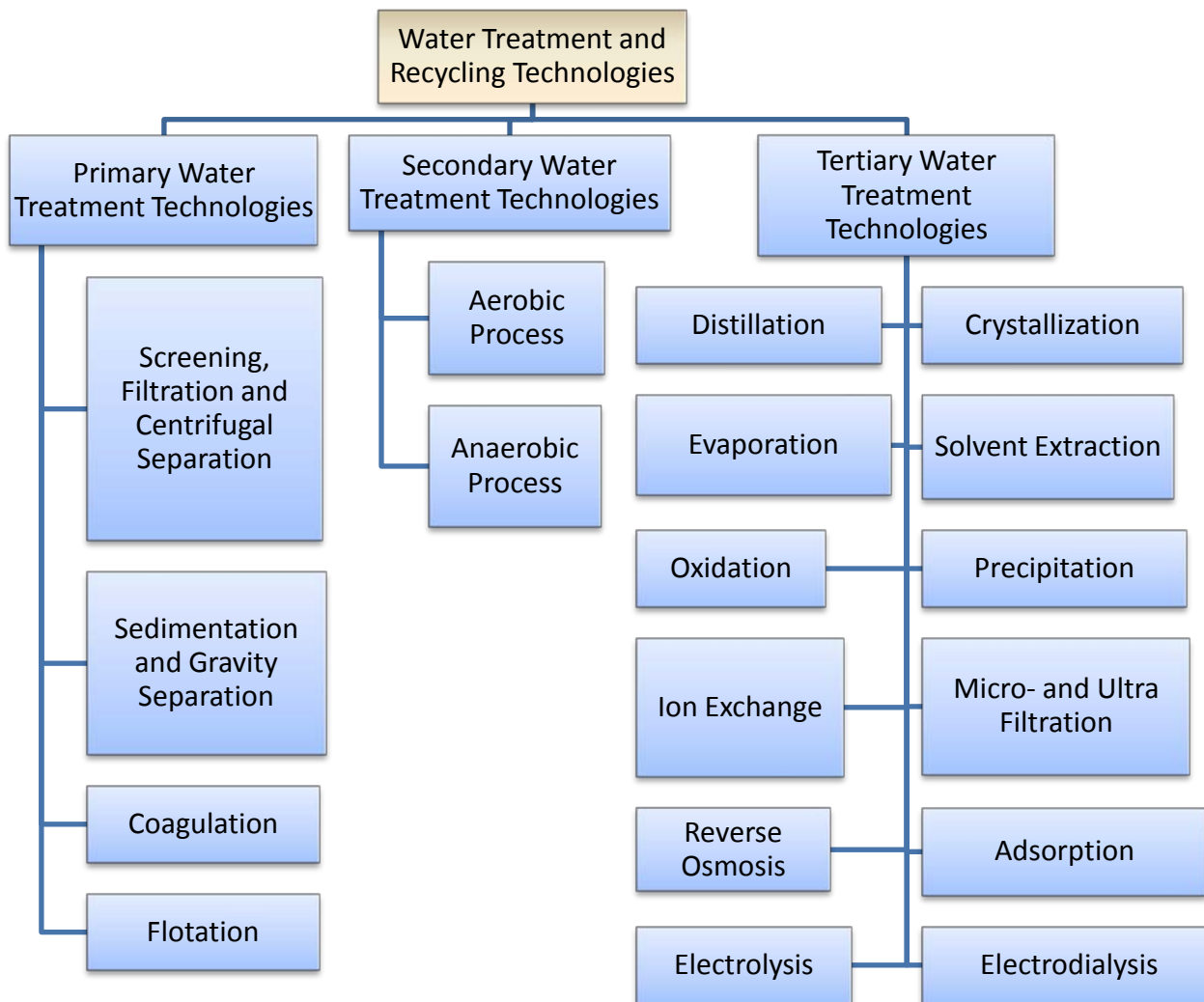


Figure 1-1 Illustration of the water treatment classification and recycling technologies

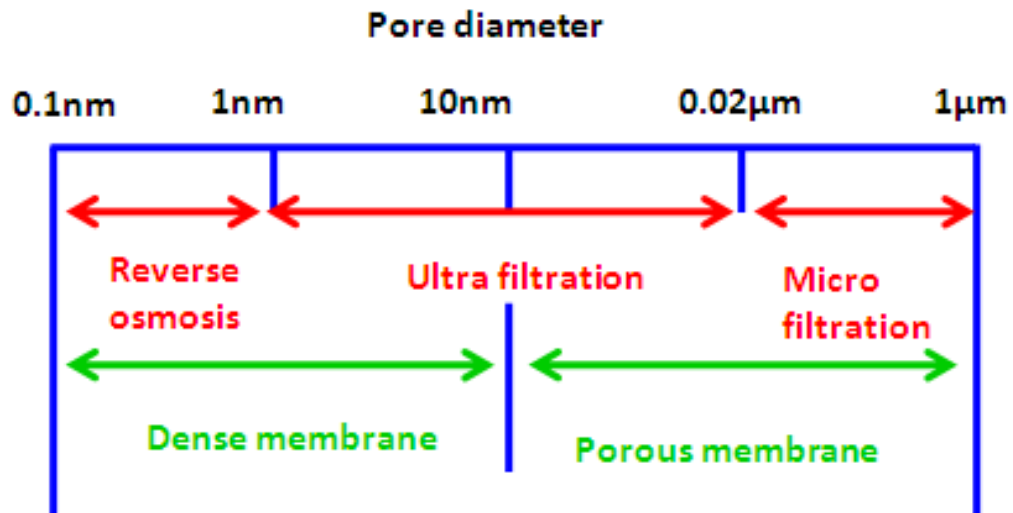


Figure 1-2 Filtration spectrum; micro-, ultra-filtration and reverse osmosis

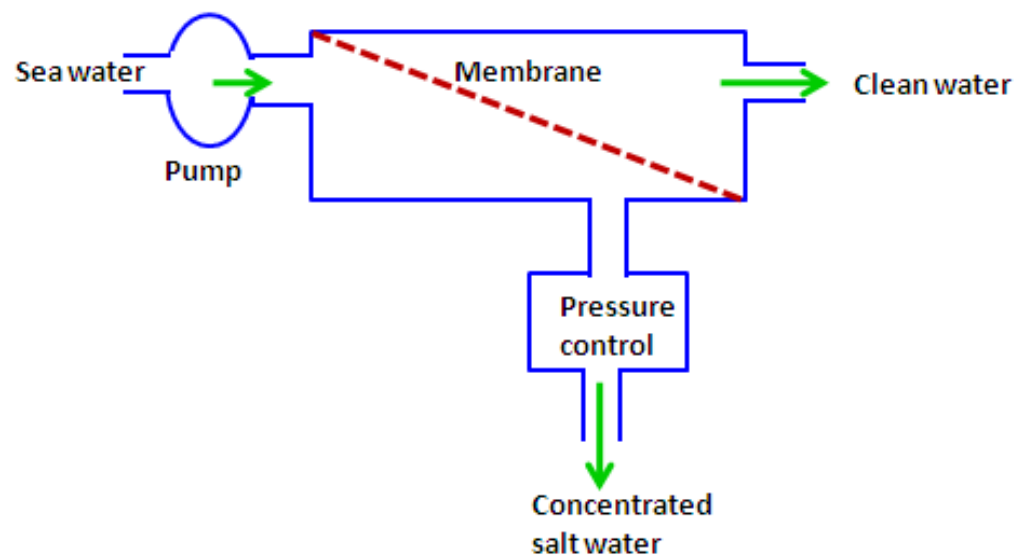


Figure 1-3 Basic design of desalination by RO

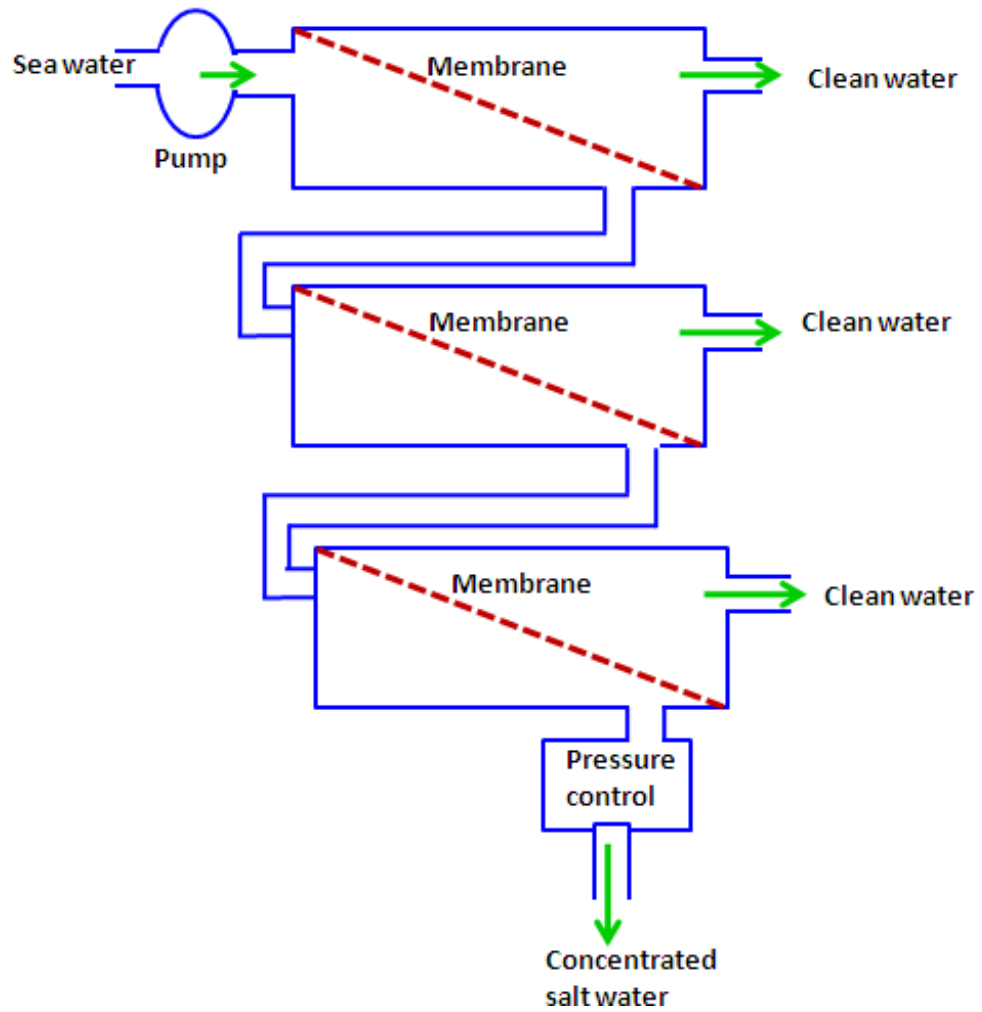


Figure 1-4 Modules of connecting membranes in series

CHAPTER 2

LITERATURE REVIEW AND OBJECTIVES

This chapter highlights the previous work, materials and strategies in water treatment. It contains three sections. The first one is the literature review. The second part presents the objectives. The third part presents the significance of the work. The last part introduces some highlights of the work.

2.1. LITERATURE REVIEW

Several adsorbents were used for removal of heavy metals [Gupta et al. 2009; Gupta et al. 2008]. Aquatic plant was also used for removal of different heavy metal ions from wastewater [Quintelas, C, 2009]. Gupta et al. have used different adsorbents, such as bagasse fly ash, a sugar industry waste material, for removal of lead [Gupta et al. 1998] and for removal of both lead and chromium [Gupta et al. 2004], duolite C-433: a synthetic resin for removal of lead [Gupta et al. 2004], green algae *Spirogyra* species [Gupta et al. 2008], activated carbon [Gupta et al. 1997], and red mud, an aluminum industry waste, for removal of lead and chromium [Gupta et al. 2001].

Adsorbents such as alumina, silica and zirconia are well known by their high surface area, high mechanical properties and good resistivity to thermal degradation, and they are existing in several structures and amphoteric properties. Activated alumina was

applied as an adsorbent for lead and cadmium removal [Tarun et al. 2009]. Activated alumina is one of the common adsorbent used for heavy metal removal, pre-concentration and separation of trace amounts of elements in flow injection- inductively coupled plasma [Jun Yin et al. 2005].

Since their discovery in 1991 [Iijima, 1991], carbon nanotubes (CNTs) have attracted considerable attention due to their unique structural, electrical and mechanical properties. This fascinating new class of materials has shown promising application in many areas. The primary research interests focus on the development of simple and cost effective methods for the synthesis of CNTs. To synthesize single wall carbon nanotubes (SWCNT) and multiwall carbon nanotubes (MWCNT), various techniques have been developed. Examples are laser ablation, arc discharge, and chemical vapor deposition (CVD). However, CVD is considered to be more productive method to produce CNTs with acceptable price. Therefore, the extraordinary properties of CNTs and the continuous decrease in their price make them potentially useful in a wide range of applications like in catalysis, photocatalysis and adsorption.

Due to their large specific surface area; small, hollow, and layered structures; light mass density and strong physical interaction ability, CNTs have already been investigated as promising adsorbents for various organic pollutants and metal ions and can be easily modified by chemical treatment to increase their adsorption capacity. CNTs' adsorption technology has the potential to be used for the removal of pollutants. Unlike many adsorbents, CNTs possess fibrous shape with high aspect ratio, large accessible external

surface area, and well developed mesopores, all contribute to the superior removal capacities. Recently, the applicability of CNTs as adsorbent has been extensively investigated. The applications of CNTs for the removal of pollutants from aqueous solutions have been studied. Numerous experimental studies have already been carried out on the adsorption of heavy metals and hazardous organic materials (Hyung and Kim, 2008; Goering, et al., 2008).

On the other hand, the uses of CNT as support of metallic oxides have still been reported. The advantages of this chemistry is that materials with higher sorption capacity, larger surface area and supported metallic oxides with better orientation degree with regard to net metallic oxides can be obtained.

In recent years, much attention has been paid to the decoration of CNTs by foreign materials, in order to further improve their properties and functions with the aim of extending their applications in various technology fields. Composite of carbon nanotube and alumina was used as a new sorbent for nickel pre-concentration from water samples, using a flow injection system coupled to flame atomic absorption spectrometry [Renata et al 2007, He et al 2009]. A carbon nanotube–alumina composite structure was first prepared by a non-catalytic chemical vapor deposition (CVD) method [Jorg et al., 2008]. Electrophoretic deposition (EPD) has been used to combine multi-walled carbon nanotubes of diameter in the range 20–30 nm and TiO₂ nanoparticles (23 nm particle size) in composite films [Johann Cho, 2008]. Photocatalytic degradation of and

methylene blue [Chen et al. 2009] on MWNT and titania composite catalysts prepared by a modified sol–gel method has been reported.

Researchers suggest that carbon nanotubes could provide a significant advantage over current water treatment technologies, such as reverse osmosis and ultrafiltration. The unique properties of carbon nanotubes would allow water molecules to pass through the interior of the cylinders while chemical and microbial contaminants could not. This is a filtration process called size exclusion. This could be accomplished at a high rate of flow with very little energy (pressure) input to “push” the water through the nanotubes – thus a big advantage over current membrane technologies. Additionally, research has shown carbon nanotubes have a strong ability to adsorb many types of chemical and microbial contaminants [Pan, et al., 2008; Li, et.al. 2008; Upadhyayula, et.al., 2008; Sharma, et.al. 2009].

Wanget al. (2005) report on high-flux filtration membranes with a hydrophilic nanocomposite surface coating. These membranes consist of a dense hydrophilic nanocomposite coating top layer, an electrospun polyvinyl alcohol (PVA) substrate midlayer, and a conventional nonwoven microfibrinous support layer. The incorporation of MWNTs into the hydrophilic top layer improved mechanical strength and durability while simultaneously enhancing water permeability.

In most wastewater flowing systems, as the contact time is not sufficiently long for the attainment of equilibrium, the data obtained under batch conditions are generally not adequate. Hence, it is required to perform equilibrium studies by using columns. Fixed

bed column tests have been widely used to predict the performance of full-scale fixed bed absorbers and to evaluate the mass transport parameters of many contaminants [Westerhoff et al. 2005; Sperlich et al. 2005]. Short bed adsorber column, is a fixed bed column with a bed of sufficiently short length that immediate concentration breakthrough occurs. It simulates the adsorption-related activities occurring in the top layer of a full fixed bed adsorber.

2.2. OBJECTIVES

The objectives of this work can be summarized as follow:

1. Activation of carbon nanotube by wet chemistry methods with optimization of the experimental parameters.
2. Syntheses of MWCNT/metal oxides composites, metal oxides, such as alumina, silica, manganese oxide, iron oxide, and others can be included.
3. Characterization of the produced composites will be performed using different techniques, such as SEM, TEM, FTIR, UV, TGA, and XRD.
4. Designing the fixed bed system with the encapsulation of the materials into fixed bed mode after testing them in batch modes.
5. Applications of the produced materialles for water treatment with efficient separations. Removal of pollutants such as, mercury, lead, arsenic and cyanide.
6. Applications of the produced MWCNT/metal oxides composites for catalytic degradation of some pollutants.

2.3. SIGNIFICANCE OF THE WORK

This work seeks to establish a technology platform for CNT-based composites and a benchmark that relates the performance of CNT-based composites to conventional ones. The benefits using nanomaterials may derive from their enhanced reactivity, surface area and sequestration characteristics.

The coating will greatly enhance material stability and heavy metal removal efficiency of the nanoparticles. Separation based on CNTs will have significant potential for water purification. Polymer composite-based upon aligned CNT forests, is expected to provide near frictionless water flow through the nanotubes, while retaining significant quantities of salt. This offers the possibility of low-energy desalination.

2.4. RESEARCH HIGHLIGHTS

Initially, the research is conducted by synthesis of CNT/metal oxides composites like CNT/alumina, silica, titania, iron oxide composites. This followed by their characterization. In the second stage, the synthesized nano composites have been utilized for the removal of heavy metals, lead, arsenic and chromium and degradation of some organic compounds. In third stage of this work, the synthesized nano composites have been utilized for the and degradation of some organic compounds like dyes under UV irradiation and the natural sun light.

CHAPTER 3

ACTIVATION OF CARBON NANOTUBE

3.1. INTRODUCTION

Purification and activation or functionalization of CNTs is essential process for further enhancement the activity and adsorption ability of CNTs and for further functionalization of CNT with other nanoparticles. Purification is necessary to remove the impurities, like catalyst particles, soot, amorphous carbon and other forms, which are often found, mixed with CNTs. Impurities can reduce the adsorption by their coating on the surfaces of CNTs, and as a result influencing the adsorption on the external surface of the nanotubes. Activation process is performed via oxidation treatment (Cho, et al., 2010). The enhancement in the adsorption ability of CNTs via oxidation treatment is most probable ascribed due to an increase in hydrophilicity of CNTs.

Oxidation treatment of CNTs results in creating new functional groups on the surface of nanotubes. It can be performed using oxidizing agents; such as nitric acid, sulfuric acid, mixtures of sulfuric acid and nitric acid, potassium permanganate, sulfuric acid in presence of potassium permanganate, hydrogen peroxide in presence of nitric acid, hydrogen peroxide, ozone. Other methods are oxygen-based atmosphere by an inductively coupled plasma or microwave energy and water (Wang et al., 2009; Smith et al., 2009; Peng et al., 2011; Hojati-Talemi & Simon, 2009).

Treatment with different oxidizing agent might introduce different functional groups on the CNTs surface including alcoholic, carboxylic, aldehydic, ketonic, and esteric oxygenated functional groups, see Fig.1. Hydroxyl groups (b) on the edge of nanotube could be of phenolic character. Oxygen could be substituted for edge carbon atoms in xanthene- or ether-type (d). Carboxyl groups (a) might give carboxylic anhydrides (e) if they are close together. In addition, carbonyl groups might condense to lactone groups (f) or form lactols (g) if they are in close to hydroxyl groups or carboxyl groups. The existence of carbonyl groups could be isolated (c) or arranged in quinone-like structure (h). The groups (a, b, e, f, and g) have weak acidic character.

Synthesis of CNT/MO requires the nanotubes' surface to have mainly alcoholic and carboxylic functional groups, which can facilitate the binding of the nanoparticles into the nanotubes. Over other methods, treatment of CNTs by nitric acid or mixtures of sulfuric acid and nitric acid have been expected to mainly graft carboxylic and alcoholic functional groups onto the CNTs surface [Wepasnick et al., 2011]. Thus, in the study, CNT is oxidized by nitric acid or mixtures of sulfuric acid and nitric acid (3:1; v:v)

Despite several efforts [Chiang et al., 2011; Wepasnick et al., 2011; Wang et al., 2009], the effect of treatment duration and temperature on the extent of the acidity of MWCNT remain unclear. In the present work, these factors have been investigated. In the following sections, the experimental results of the effect of the treatment duration and temperature on the acidity of MWCNTs will be discussed.

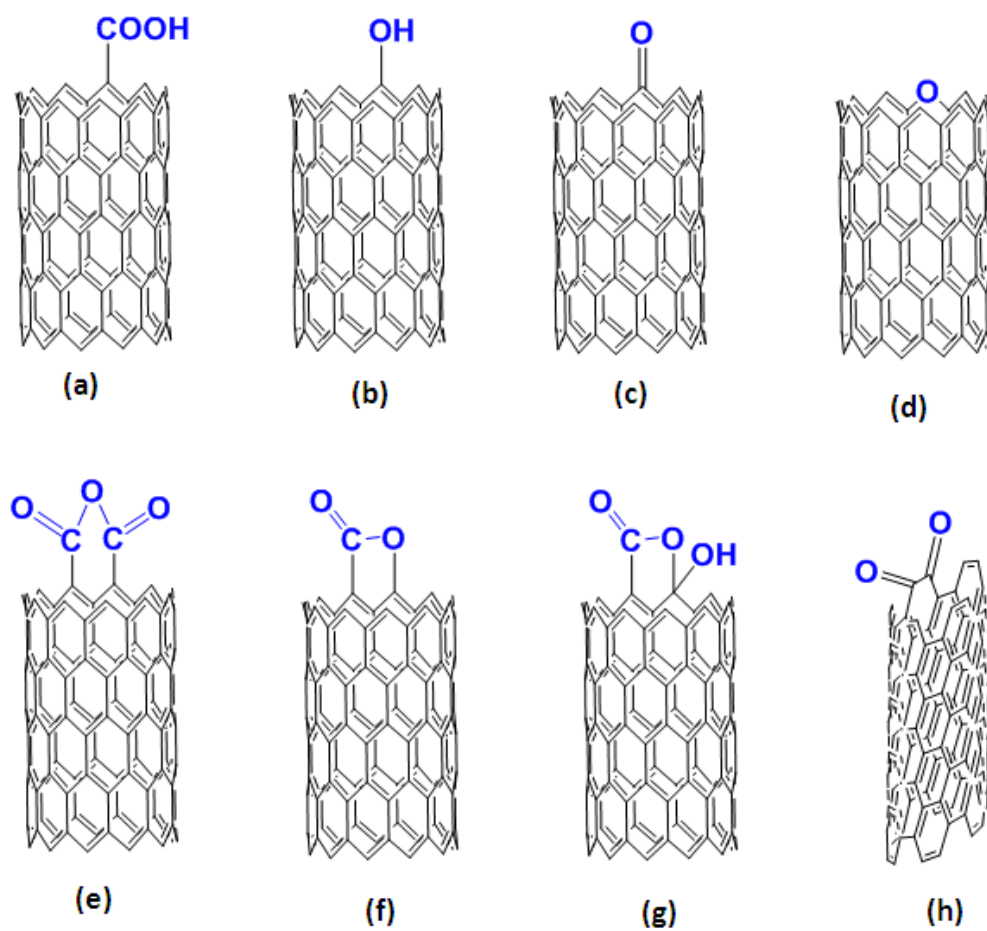


Figure 3-1 Possible structures of oxygen-containing groups on CNT

3.2. EXPERIMENTAL SECTION

3.2.1. Materials

MWCNTs was purchased from Cheap Tubes Com. Their specifications are as follows; purity, >95%; outer diameter, 30-50 nm; inside diameter, 5-10 nm; length, 10-20 μm ; average specific surface area, 60 m^2/g ; Electrical Conductivity: >100 S/cm; Bulk density: 0.28 g/cm^3 ; True density: $\sim 2.1 \text{ g}/\text{cm}^3$. The 70% nitric acid and 95% Sulfuric acid of analytical grade were obtained from Sigma-Aldrich. The solutions of 0.01M base and 0.01M acid for titration process were prepared from sodium hydroxide and hydrochloric acid.

3.2.2. Oxidation Process

MWCNTs were initially dispersed for 1 h by sonication in HNO_3 . Typically, 1g of the nanotubes was dispersed in 100 mL of 70% nitric acid. Then, the MWCNT- HNO_3 mixture was refluxed while stirring vigorously for 6h at a specific temperature. After refluxing process, the mixture was allowed to cool at room temperature. The same process was repeated using mixtures of nitric acid and sulfuric acid. To investigate the duration effect, the refluxing time was varied as 2, 4, 6, 8, 10 and 12 h for each oxidant. To investigate the temperature effect, temperatures of the refluxing solution was varied as 60, 80, 100, 120 and 140 $^\circ\text{C}$ for each oxidant.

The *oxidized MWCNT* (o-MWCNTs) was purified by extraction from the residual acids by repeated cycles of dilution with distilled water, centrifugation and decanting the solutions until the pH was approximately 5. After the purification process, o-MWCNTs were dried overnight in an oven at 100 °C. After that, the dry o-MWCNTs were pulverized in a ball-mill. Characterization and acidity determination was performed.

3.2.3. Acidity determination

The acidity of the o-MWCNTs was determined based on a typical acid–base or Boehm titration [Boehm, 1994]. The o-MWCNT samples, each weighing 5 mg of the material were immersed in 50 mL of the NaOH solution, which was selected to neutralize the acidic sites. Then the mixture was dispersed by sonication bath for 5 min in closed flask.

Reference samples of 50 ml of each solution were prepared and treated in the same way as the CNTs' samples. Closed flasks containing the samples were placed on a rotary shaker at room temperature with continuous stirring for 24 h to reach the equilibration. Then, the samples were filtered carefully. 50 mL of acid solution (HCl) was added into the filtrate and washings. Then, the mixture was boiled for 20 min to degas the carbon dioxide from the solution. After cooling at room temperature, the excess HCl was slowly titrated with NaOH solution up to the neutral point, pH 7.0, and the pH was monitored using a pH meter. The blank sample which contained no MWCNTs was also titrated as described. Titrations were performed in triplicate. The titration process includes the following steps:

Step (1): $\text{MWCNT-COOH} + \text{NaOH (excess)} \rightarrow \text{MWCNT-COO}^- \text{Na}^+$

Step (2): Filtration process to separate the $\text{MWCNT-COO}^- \text{Na}^+$ from the excess NaOH

Step (3): Addition of HCl excess into the filtrate

Step (4): Determination of HCl excess by titration with NaOH of the same concentrations

It has been shown that the treatment of MWCNTs with nitric acid or mixtures of nitric acid and sulfuric acid mainly leads to the formation of carbonyl, lactone and phenol groups on the nanotubes' surface. Surface acidity of oxidized MWCNTs is contributed by many types of surface oxygen-containing functional groups such as carboxylic groups, lactonic groups and phenolic groups. It can be titrated by NaOH neutralizing carboxylic, phenolic and lactonic groups [Wepasnick et al., 2011; Boehm, 1994].

3.2.4. Characterization

Various tools characterized the presence of functional groups. X-ray powder diffraction (Shimadzu XRD 6000) was used for the structure phases of the o- MWCNTs. Field emission scanning electron microscope (FESEM, FEI Nova-Nano SEM-600, Netherlands) was used for characterization. IR spectra in the range of $400\text{-}4000\text{ cm}^{-1}$ were recorded in KBr pellets using a Thermo Nicolet FT-IR spectrophotometer at room temperature on. Sample were prepared by gently mixing 10 mg of each sample with 300 mg of KBr powder and compressed into discs at a force of 17 kN for 5 min using a manual tablet presser. pH measurements were monitored with a Fisher model 25 pH meter calibrated with three buffered (pH 4, 7, and 10) solutions.

3.3. RESULTS AND DISCUSSION

The results of the treatment duration and temperature effect on the extent of acidity of the nanotubes will be discussed. The effect of treatment duration is discussed in the first part while the second part introduces the effect of the treatment temperature.

3.3.1. Effect of treatment duration

Effect of treatment duration on the acidity of MWCNTs was investigated. Boehm acid-base titration method was used to determine the acidity of the MWCNTs treated by either nitric acid or a mixture of mixture of sulfuric and nitric acid for different durations, 2, 4, 6, 8, 10 and 12 h and under constant temperature of 120 and 100 °C respectively. In Fig. 2, mmol of acidic oxygen-containing surface groups per mg of MWCNT material is given as a function of treatment duration. It was found that the total amounts of acidic groups on o-MWCNTs gradually increased with increasing the treatment period using both nitric acid and the mixture of sulfuric and nitric acid.

3.3.2. Effect of Treatment Temperature

The effect of oxidation temperature on the acidity of MWCNT was investigated by changing the reflux temperature and keeping the treatment time constant, 6h each. As can be seen in Fig. 3a, the total amounts of acidic groups on o-MWCNTs gradually increased, under nitric acid treatment, with increasing the temperature between 60 °C and 120 °C. Further increase in the temperature results in no significant increase of the

acidity of MWCNTs under nitric acid treatment for 6h. Thus, optimum treatment temperature that can be selected is 120 °C, at which 0.026 mmol/mg amount of acidity was obtained. Based on mentioned experimental conditions, the most favorable reaction temperature for an efficient oxidation of MWCNTs with nitric acid treatment has been quantitatively determined by titration method to be 120 °C.

Fig. 3b depicts the effect of temperature on the oxidation process by mixtures of sulfuric and nitric acid. It can be observed that the acidity increase from 0.011 mmol/mg under treatment temperature of 60 °C to 0.04 mmol/mg at 100 °C. The acidity increased sharply to 0.08 and 0.15 mmol/mg when the treatment temperature increased to 120 and 140 °C respectively. However, there was a mechanical lost at treatment conditions of 120 or 140 °C for 6h. It is likely that the nanotube lattice became severely destroyed at this stage, creating new defect sites and facilitating formation of functional groups. A treatment temperature of 100 °C, with 6h oxidation duration, was selected to be the optimum when a mixture of sulfuric and nitric acid was used for MWCNTs oxidation.

It is worth mentioning that Boehm titration results for the reference, unfunctionalised MWCNTs, showed 0.0005 mmol/mg acidity, which is very low. The presence of some acidity on the surface of the unfunctionalized nanotube is probably because of the purification process. The purification of the as-produced CNTs is conducted to remove the catalyst particles and amorphous carbons (impurities). It is conducted by treating CNTs with acid under specific conditions. Thus, there is a possibility of forming some acidic groups on the nanotube surface, during removing the impurities.

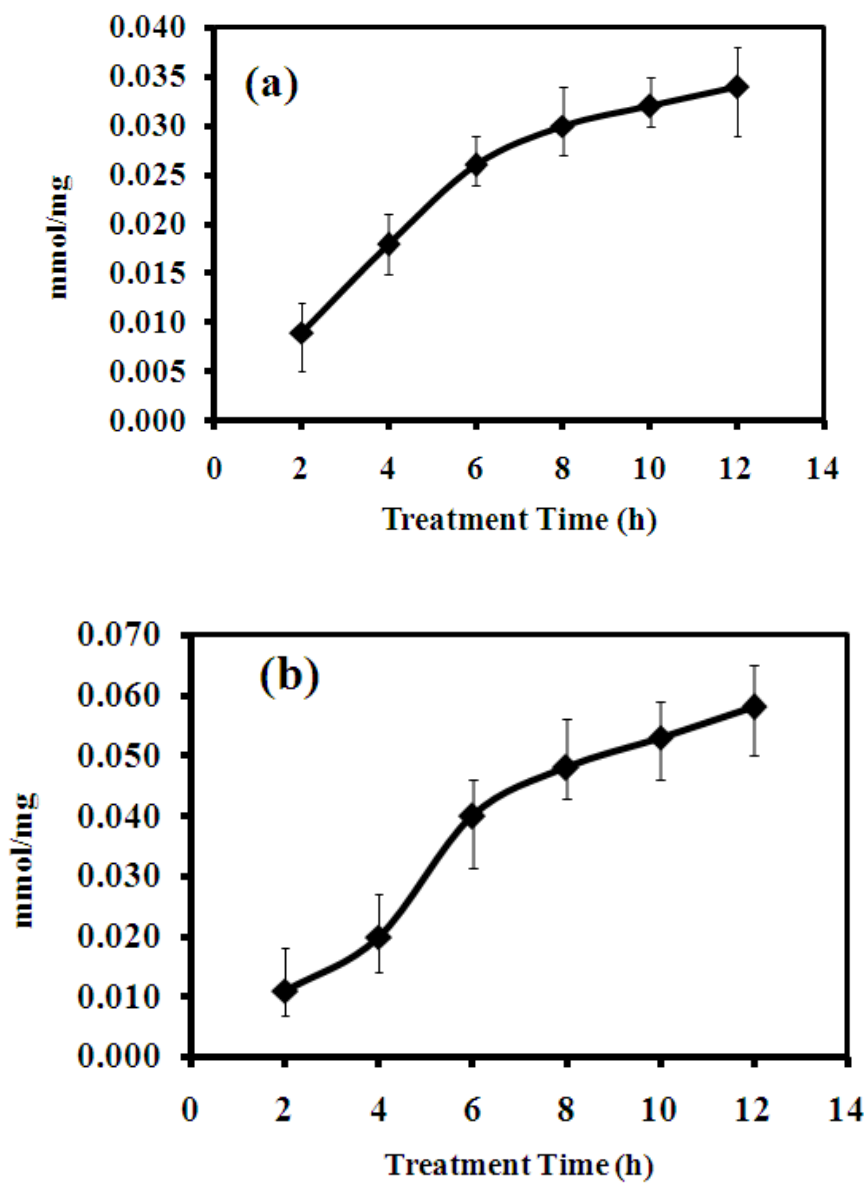


Figure 3-2 Effect of treatment duration on the acidity of MWCNT oxidized by (a)

(a) nitric acid; (b) mixtures of sulfuric and nitric acids (3:1)

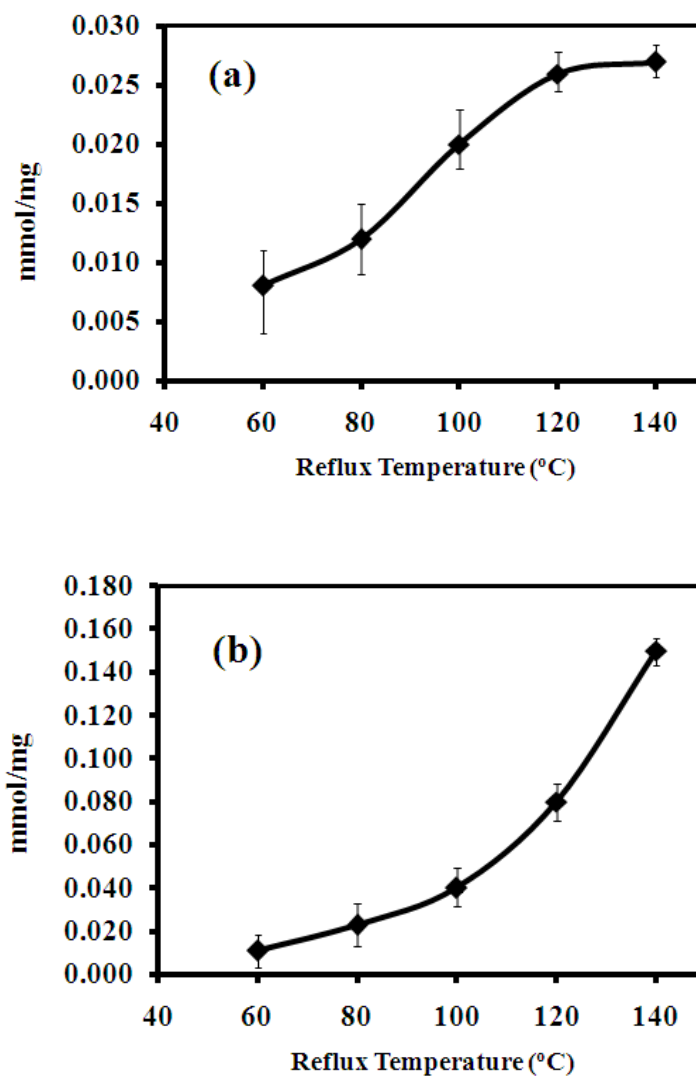


Figure 3-3 Effect of temperature on the acidity of MWCNT oxidized by (a) nitric acid; (b) mixtures of sulfuric and nitric acids (3:1)

3.3.3. Characterization of o-MWCNT

Characterization techniques were used to confirm the presence of functional groups on the surface of oxidized MWCNT (o-MWCNT). The change in acidity was confirmed by energy dispersive X-ray spectrometry (EDX). The measurements showed the quantitative representation of oxygen presented in the samples. Fig. 4 shows the results of EDX measurements. Fig. 4(a) represents the results of untreated MWCNT as a reference that shows 2.61 atomic percentage. The percentage increases up to 4.50 (Fig. 4b) and 9.49 (Fig. 4c) when MWCNT was treated with HNO₃ at 80 and 120 °C, respectively. However, when MWCNT was treated with mixtures of H₂SO₄/ HNO₃ at 80 and 100 °C, oxygen percentage increased to 8.33 and 14.33, respectively (Fig. 4d,e). A further increase in the percentage was also observed under H₂SO₄/ HNO₃ mixture treatment. Unfortunately, though the acidity is high in the treatment with H₂SO₄/ HNO₃ mixture, at temperatures of 120 and 140 °C, a mechanical loss was noticed.

FTIR spectra of untreated and treated MWCNTs are shown in Fig. 5. IR spectrum of untreated MWCNTs, Fig. 5a, shows a characteristic peak at 1582 cm⁻¹ assigns C=C bond in MWCNTs. The band at about 1160cm⁻¹ is assigned to C–C bonds. Fig. 5b depicts the IR spectrum of MWCNTs treated with HNO₃ for 6h at 80 °C. The spectrum shows the carbonyl characteristic peak at 1638 cm⁻¹, which is assigned to the carbonyl group from quinone or ring structure. The carboxylic characteristic peak is not intense enough to be clear in the spectrum. This may indicate that the oxidation conditions are not strong. By increasing the temperature to 120 °C, the carboxylic characteristic peak at

1710 cm^{-1} became clear as presented in Fig. 5c which depicts the IR spectrum of MWCNTs treated with HNO_3 for 6h at 120 $^\circ\text{C}$.

Fig. 5d depicts the IR spectrum of MWCNTs treated with $\text{H}_2\text{SO}_4/\text{HNO}_3$ for 6h at 80 $^\circ\text{C}$. In the spectrum, the peaks at 1705 and 1638 cm^{-1} are present and can be assigned to carbonyl groups in ester and ring structure. The peak at 1582 cm^{-1} is also present and assigns C=C bond in MWCNTs. Increasing the temperature to 100 $^\circ\text{C}$ with $\text{H}_2\text{SO}_4/\text{HNO}_3$ for 6h results to increase the intensity of carboxylic characteristic peak, as seen in Fig. 5e which depicts the IR spectrum of MWCNTs treated with $\text{H}_2\text{SO}_4/\text{HNO}_3$ for 6h at 100 $^\circ\text{C}$.

In the spectra of the treated MWCNTs, the peaks which are identified at 1360 and 3402 cm^{-1} characterize C-O and O-H bonds in acid modified MWCNTs. The spectra of the other samples (not shown), i.e. samples of MWCNTs treated at mentioned temperatures, display similar results.

Therefore, the observation of IR spectra corresponding to the oxidized MWCNTs suggests the presence of carboxylic groups at MWCNT surface. FT-IR, EDX and the titration results support each other very effectively. Thus, the above observations suggest that oxidation was promoted in all treatments, and that the most effective treatments for MWCNT acidity, without mechanical lose, are those treated with nitric acid at 120 $^\circ\text{C}$ or with $\text{H}_2\text{SO}_4/\text{HNO}_3$ mixture at 100 $^\circ\text{C}$.

Typical XRD patterns of MWCNTs treated for 6h with HNO₃ at 120 °C, Fig. 6, and XRD of MWCNT treated with H₂SO₄/ HNO₃ mixture at 100 °C, Fig. 7. The strongest diffraction peak for the samples at the angle (2θ) of 25.54° can be indexed as the C(002) reflection of the hexagonal graphite structure. The other characteristic diffraction peaks of graphite at 2θ of about 43.2°, 53.7° and 77.6° are associated with C(100), C(004) and C(110) diffractions of graphite, respectively.

There is no significant difference between the two patterns since d_{002} is 0.348492 nm and 0.343874 nm; and FWHM is 2.1334° and 1.9927° of MWCNTs oxidized by treatment with H₂SO₄/ HNO₃ and HNO₃ respectively. The sharpness of the peak at the angle (2θ) of 25.54° indicates that the graphite structure of the MWCNTs was acid-oxidized without significant damage since any decrease in the order of crystalline in MWCNTs will make the XRD peaks broader and shift the peak diffraction towards lower angles.

In order to know the effects on the nanotubes after each treatment, SEM was conducted. SEM images confirmed that there is no damage effect or cutting on the nanotubes, even under the strongest oxidation treatment, of using nitric acid and mixtures of nitric acid sulfuric acid. As examples, the SEM and TEM images, Fig. 8 and 9 shows that there is no effect on the nanotubes treated at 140 °C with nitric acid or with H₂SO₄/ HNO₃ mixture at 140 °C.

Figure 10 shows the Raman spectrum of CNTs before oxidation process. Two bands were observed, in the high-frequency region of spectrum. These bands are the graphite band (G band) and the disorder and defects of the structure, D band. Figure 11 shows the Raman spectrum of CNTs after fictionalization by oxidation process. It also shows the two bands.

The ratio between the intensity of the D band and the G band ($I_{D/G}$), is related to the degree of disorder of the nanotube (Osorio et al., 2008). An increase in $I_{D/G}$ value corresponds to a higher proportion of sp^3 carbon, which is ascribed to the presence of more structural defects because of creating oxygen-containing functional groups on the surface of the nanotube.

As can be observed in Raman spectrum of both samples, the characteristic peaks of CNTs, named the D band at 1330 cm^{-1} and the G band at 1580 cm^{-1} , are identified. This indicates that the acid treatment does not damage the structure of CNTs. Comparing the ratio $I_{D/G}$ values of functionalized and nonfunctionalized CNTs, it is observed that the ratio values increase after functionalization by oxidation process. The oxidation of CNTs breaks some of its bonds and inserts chemical groups (oxygen-containing groups) that can be interpreted as defects on the structure.

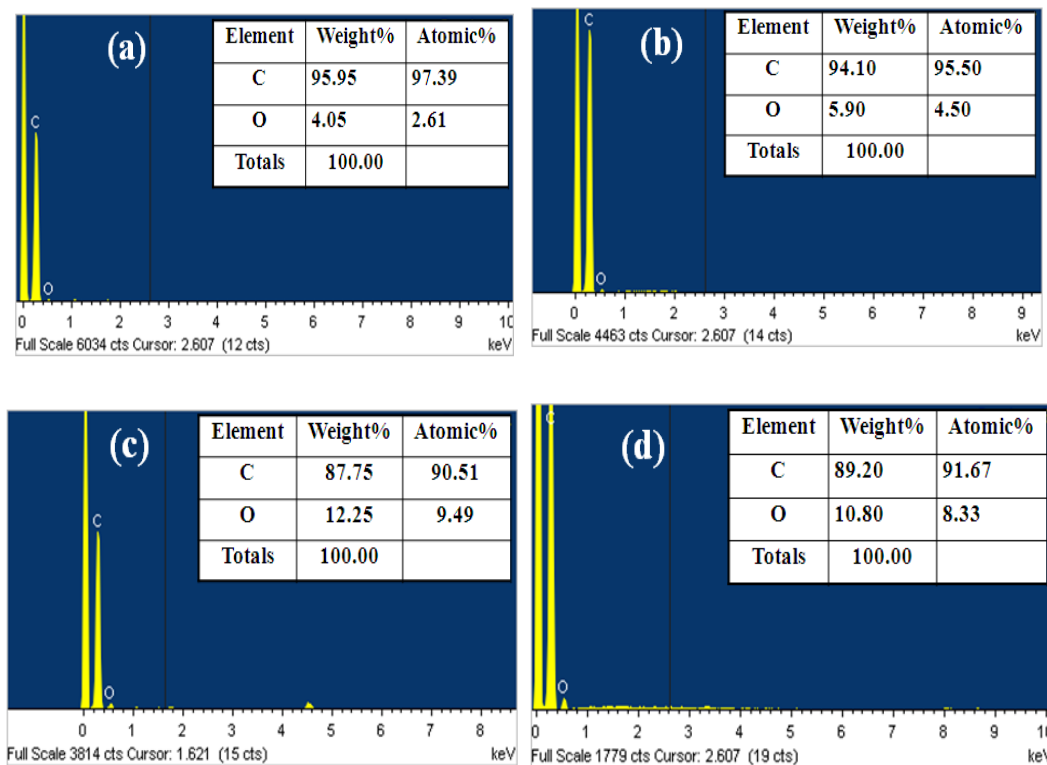
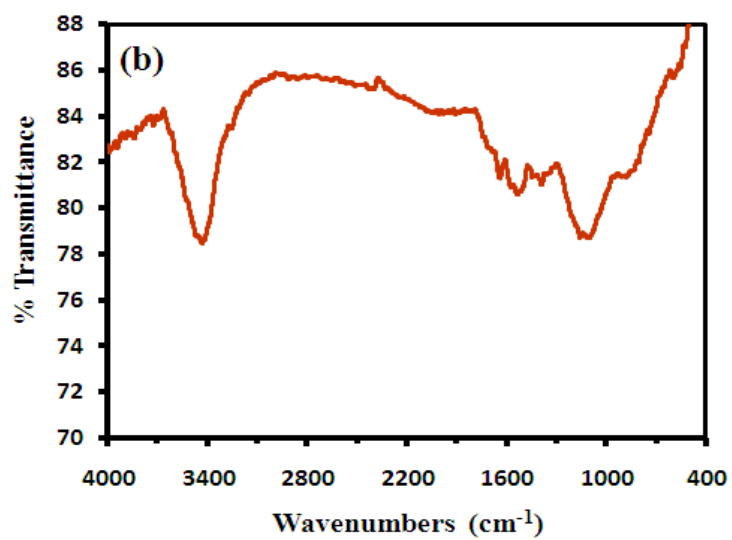
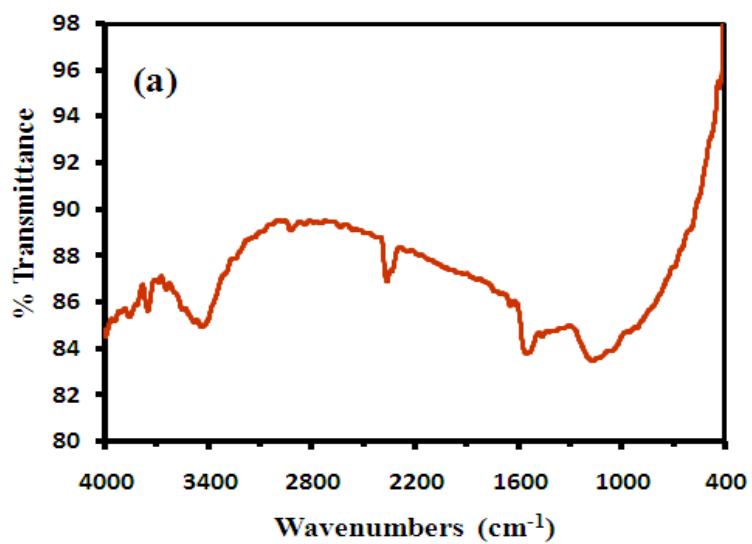


Figure 3-4 EDX spectrum of MWCNTs

Raw MWCNT (a), MWCNT oxidized with HNO₃ at 80 °C (b), at 120 °C (c); and MWCNT oxidized with H₂SO₄/HNO₃ mixture at 80 °C (d); Insets are the components percentages in each sample



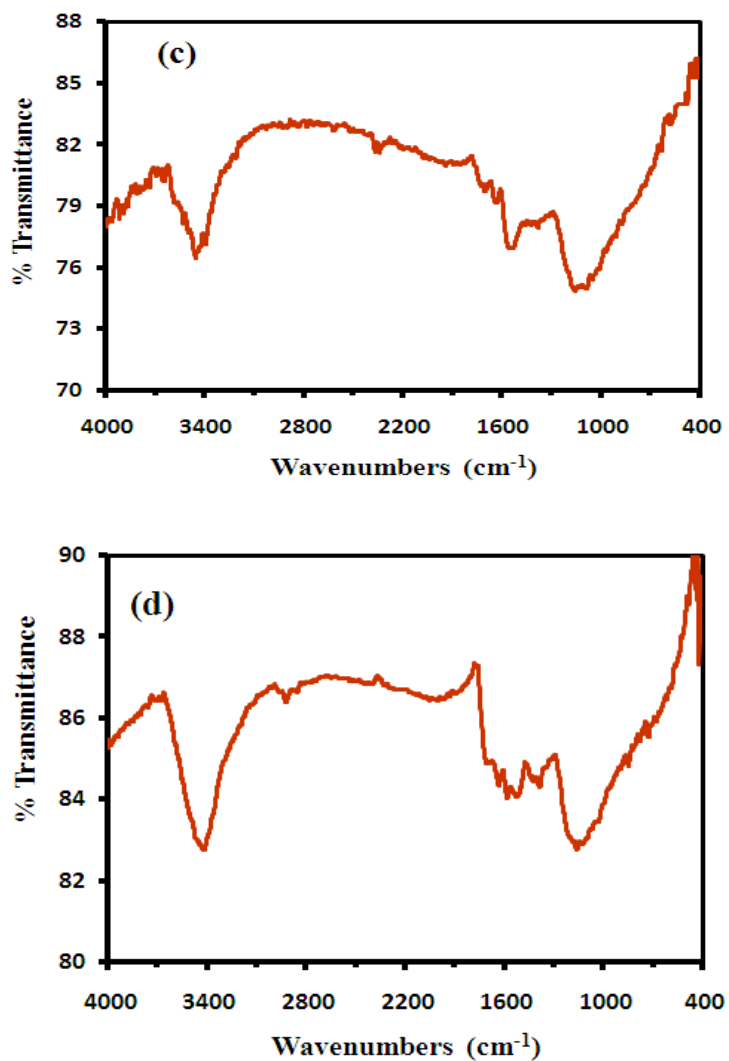


Figure 3-5 IR spectra of MWCNTs

FTIR spectra of raw MWCNT (a), MWCNT oxidized with nitric acid at 80 °C (b), at 120 °C (c); and MWCNT oxidized with mixtures of sulfuric and nitric acids at 80 °C (d),

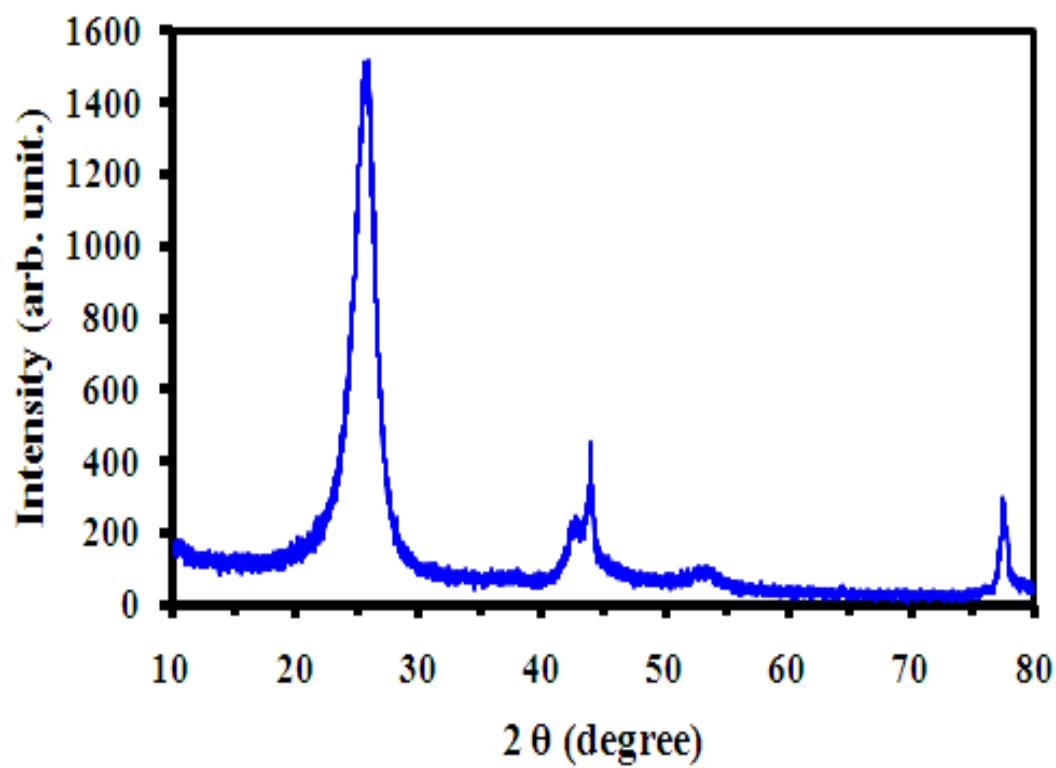


Figure 3-6 XRD patterns of MWCNT oxidized with nitric acid at 120 °C

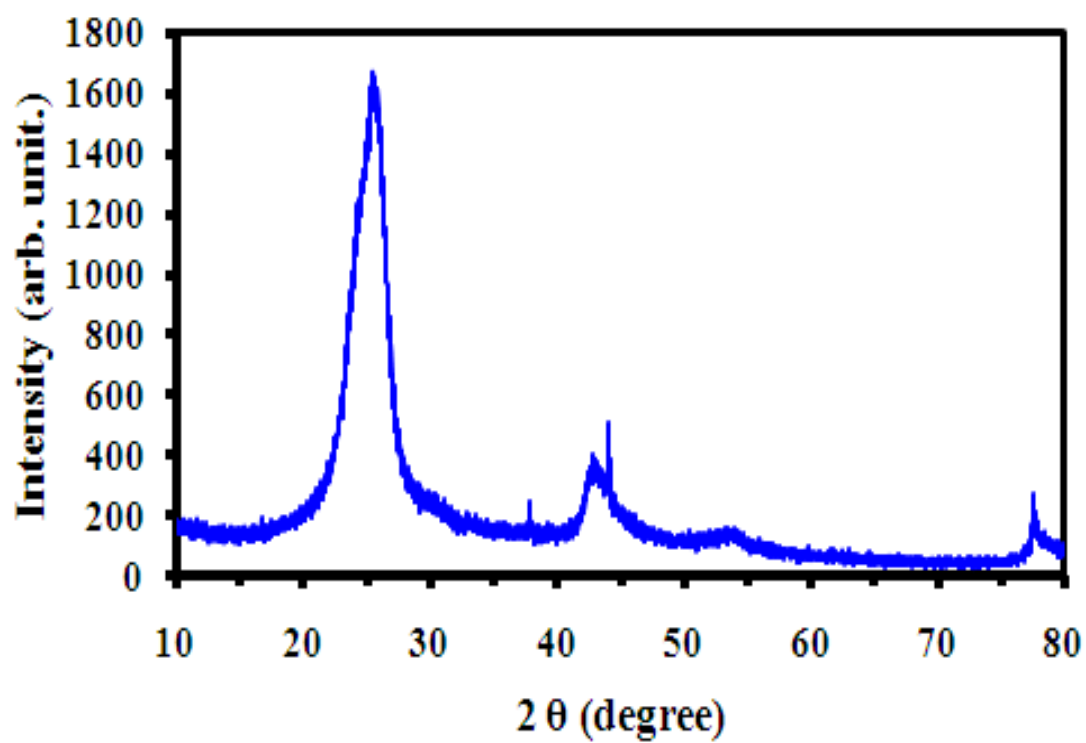


Figure 3-7 XRD of CNT oxidized with sulfuric and nitric acids mixture at 100 °C

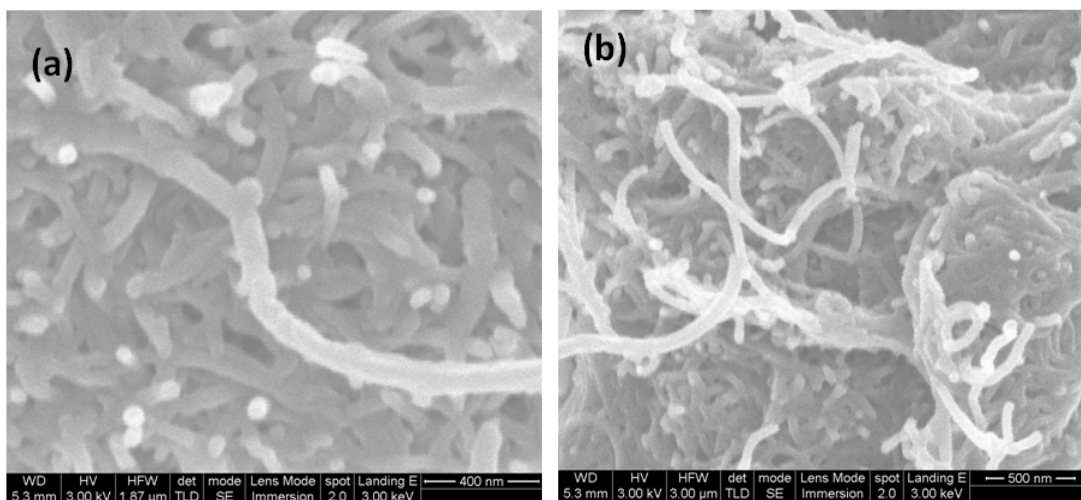


Figure 3-8 SEM images of MWCNT treated at 140 °C with (a) nitric acid (b) $\text{H}_2\text{SO}_4/\text{HNO}_3$ mixture

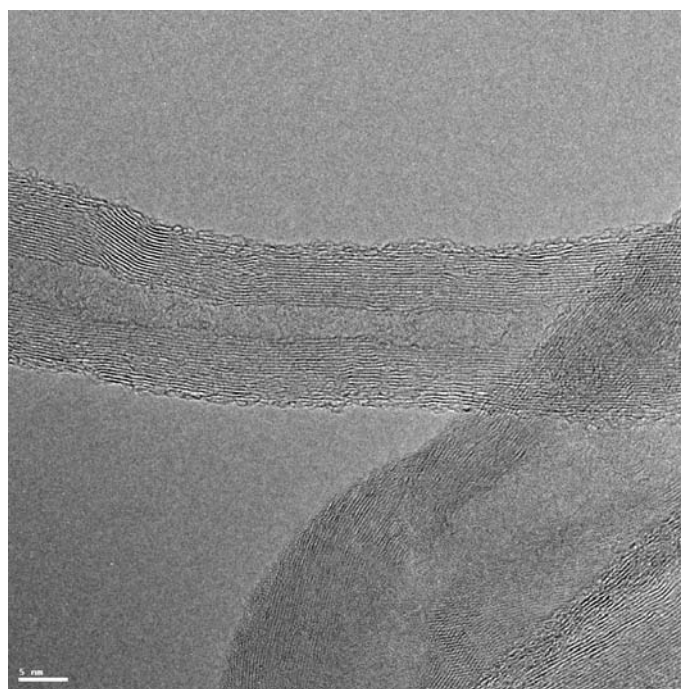


Figure 3-9 TEM of oxidized MWCNT

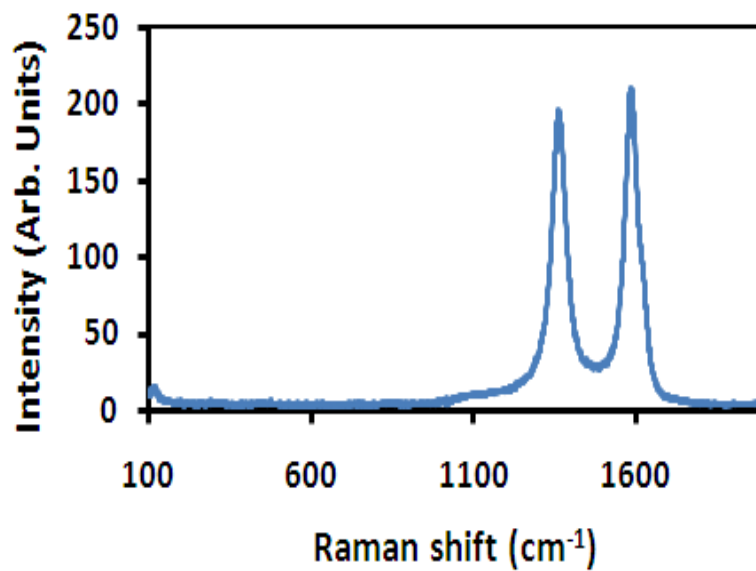


Figure 3-10 Raman spectra of CNT before functionalization

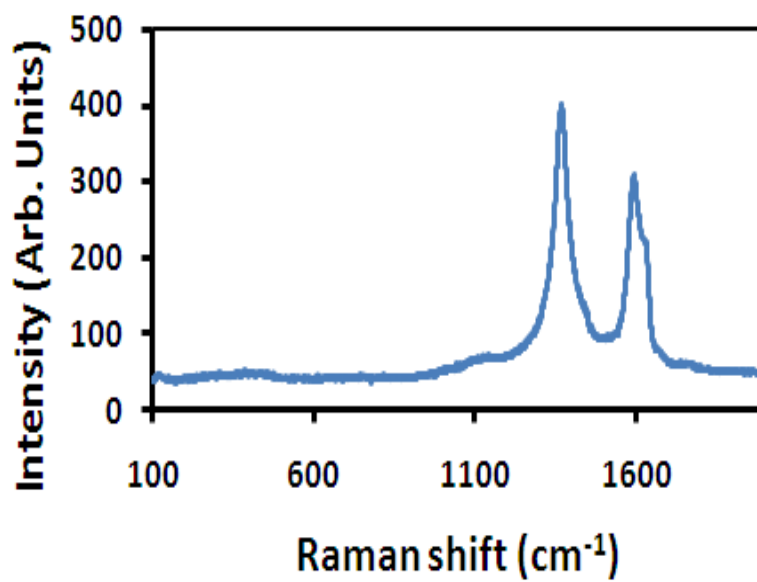


Figure 3-11 Raman spectra of CNT after functionalization

CHAPTER 4

EXPERIMENTAL

Composites combine two or more materials with different properties in a way that takes advantage of each individual property of the components. In contrast, hybrid materials are materials combinations, which take advantage of interfacial charge and heat transfer processes that create new synergistic functions and properties. Recent years show the introduction of next-generation nanocomposites, which additionally take advantage of interfacial processes that greatly improved their properties and even created new properties.

Carbon nanotube (CNT) and graphene–inorganic hybrids are the most promising examples of new exciting class of functional materials (Eder, 2010). In contrast to the classical nano-composites, where CNTs are mechanically dispersed in an inorganic matrix, hybrids, in which a thin inorganic layer coats CNTs, combine their properties in a way that creates new properties distinct from those of either building block.

Recently, there has been a growing interest in the synthesis of nanoscale composites for different applications. Carbon nanotube-metal oxides (CNT/MO) composites are one of the most exciting fields of research nowadays. The formation of CNT/MO is both of fundamental and technological interest since the composite combines the unique properties of CNTs and metal oxide nanoparticles, and in addition exhibit some new

extraordinary properties caused by the interaction between them. Thus, a new class of nanocomposites can be made with extraordinary properties meeting a wide range of applications in different disciplines. For example, alumina is one of the most widely used ceramic materials because of its high hardness, good oxidation resistance and chemical stability. However, its applications are limited because of its low fracture toughness. Mechanical mixing of CNTs with alumina has been used to reinforce and increase the fracture toughness of alumina owing to their unique one-dimensional structure with robust mechanical and thermal properties.

CNT/MO composites can be prepared via various methods as mentioned earlier in this section. Here, the focus is on the wet chemistry methods where the functional groups on CNTs act as nucleation sites for the metal oxides.

This chapter introduces the experimental methods that have been used for the synthesis of different carbon nanotube-based metal oxides composites. Thus, the objective of this chapter is to detail how to synthesize carbon nanotube-metal oxide composites. The characterization will be discussed in the next chapter.

4.1. MATERIALS

Nitric acid, hydrochloric acid, sulfuric acid, aluminum nitrate, ferric and ferrous chlorides, potassium permanganate, zinc nitrate, were obtained from Sigma–Aldrich. Stock solutions were prepared daily by dissolve in distilled water. Solutions of different initial concentrations were prepared by diluting the stock solution in appropriate

proportions. In order to prevent contamination from laboratory glassware, glassware was kept overnight in 10% (v/v) HNO₃ solutions. All other chemicals were of analytical grade.

4.2. SYNTHESIS STRATEGY

In this part of the chapter, the synthesis of the carbon nanotube-based composites with different metal oxides is discussed. The composites, that have been synthesized, are CNT/alumina, CNT/iron oxide, CNT/manganese oxide, CNT/zinc oxide, and CNT/tungsten oxide.

4.2.1. Synthesis of CNT/Alumina composite

The MWCNT/alumina composite was prepared via thermal method. Typically, some amounts of o-MWCNTs were dispersed into deionized water and magnetically agitated 6h until acceptable level of dispersion was observed. A specific amount of aluminum nitrate was properly dissolved in deionized water. Carefully, the aluminum nitrate solution was drop-wise added into dispersed MWCNTs. Between consecutive drops, there should be an appropriate time for the aluminum to reach, appropriately disperse and engage to the nanotubes' surface. After that, the suspension was dried at 110 °C. The obtained material was heated up to 400 °C for 90 min, where the pyrolysis process resulted in alumina formation supported onto the nanotube surface.

4.2.2. Synthesis of magnetic-CNT

A composite of magnetic-MWCNT was prepared as follows. A mixture of 0.1M ferric chloride hexahydrate and 0.05M ferrous chloride tetrahydrate with a molar ratio of one to two was prepared. Subsequently, a specific amount of oxidized-MWCNTs was suspended in the mixed solution for 2h. Then, at constant temperature of 70 °C, 5M- NH_4OH solution was added drop wise to precipitate iron oxides. The mixture was adjusted to pH 10 and then aged for 1h under stirring.

After the completion of the reaction, the suspension was allowed to cool. A magnet was used to separate the product. Then, it was washed by distilled water and ethanol respectively. The obtained composite was dried in an oven at 100 °C for 2h.

4.2.3. Synthesis of CNT/Manganese Oxide

Preparation of composites of MWCNTs with MnO_2 nanoparticles was performed as follows. o-MWCNTs were dispersed in de-ionized water by ultrasonic vibration for 3 h. 0.5 M solution of KMnO_4 was then drop-wise added, with the rate of 1ml/2min, into the o-MWCNTs, dispersed in deionized water, under continuous vigorous stirring at room temperature. The slow addition was necessary for MnO_4^- dispersion onto the surface of the nanotubes and interacts with the active sites. Once start heating the mixture, the

color of the mixture immediately turned to dark brown, which indicates the formation of MnO_2 .

In a typical experiment, 1 g of o-MWCNTs was dispersed in 100 mL of de-ionized water and 100 mL of 0.5 M KMnO_4 . Then the mixture was refluxed at 130 °C with magnetic stirring. The rate of increasing temperature was slow, 1 °C/min. After refluxing for 8h, the composite was allowed to cool at room temperature. After that, it was filtered and washed by de-ionized water. Then, it was dried overnight at 110 °C. The process of the composite preparation is illustrated in Fig. 1.

4.2.4. Synthesis of CNT/Zinc Oxide

For the preparation of MWCNT-ZnO nanocomposites, an appropriate amount of $\text{Zn}(\text{NO}_3)_2 \cdot 6\text{H}_2\text{O}$ was dissolved in doubly deionized water. Then ammonia was added drop-wise under continuous stirring into the solution until a clear solution was formed. After that, an appropriate amount of the oxidized MWCNTS was added into the solution. After soaking for 60 min, the composite were separated and dried at 80 °C. The product was then calcined in vacuum at 300 °C for 24h. The product was then characterized by different analytical techniques mentioned below. Fig. 2 depicts a schematic showing the process of MWCNT/ZnO composite synthesis.

4.2.5. Synthesis of CNT/Tungsten Oxide

To prepare MWCNT/WO₃ composites, MWCNTs was added into a mixture of 50% ethanol in distilled water. Then it was sonicated 8 h for complete dispersion. While ammonia was added drop-wise into a slurry suspension of WO₃ in distilled water under vigorous stirring for almost 8 h until a very clear solution was observed.

Then, the latter was added drop-wise into the dispersed MWCNTs under sonication. This is a very critical step and care should be taken during the addition; be patient. This step was followed by stirring the mixture for 12 h at room temperature followed by heating at 60-70 °C for 12 h under stirring also. Then, dry the composite overnight. The final step is the calcinations for 2 h at 350-400 °C, Figure 3. Then, the composite was characterized.

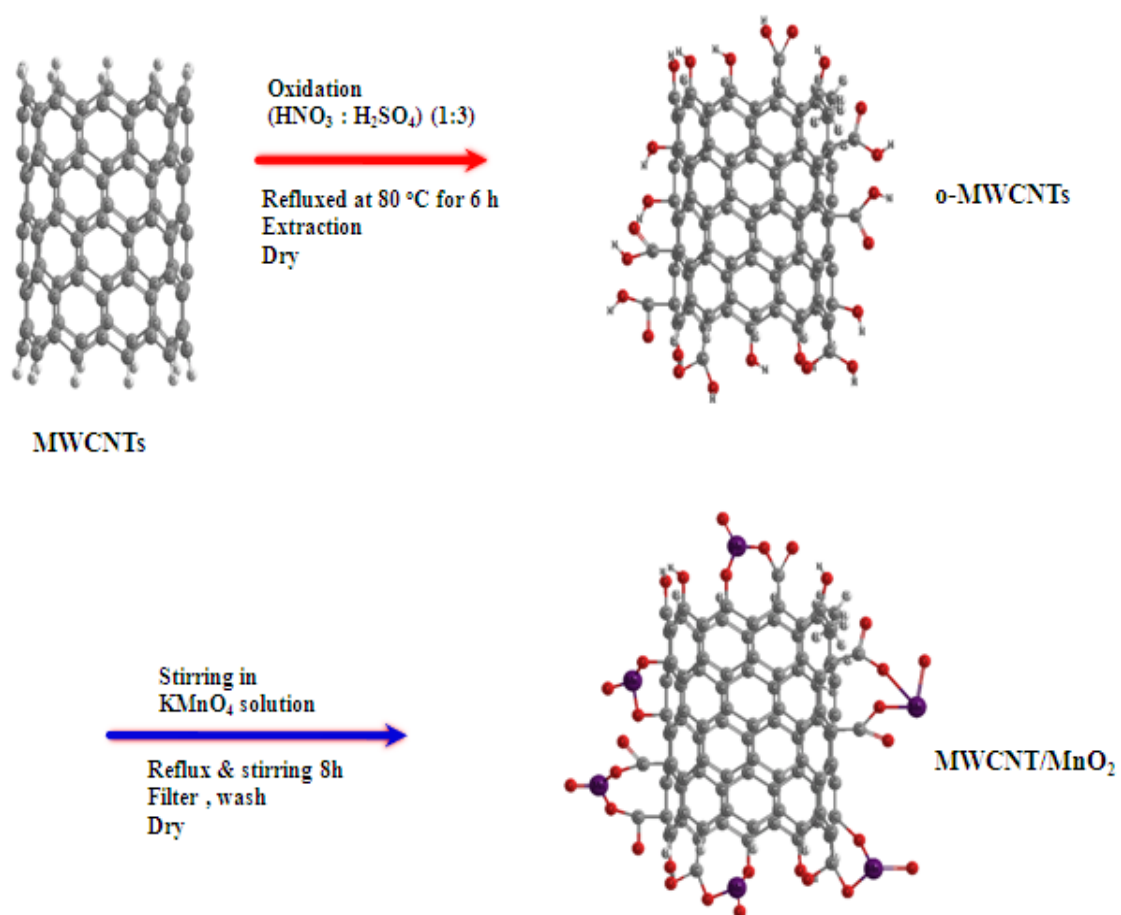


Figure 4-1 Scheme of MWCNTs oxidation and MWCNT/MnO₂ preparation

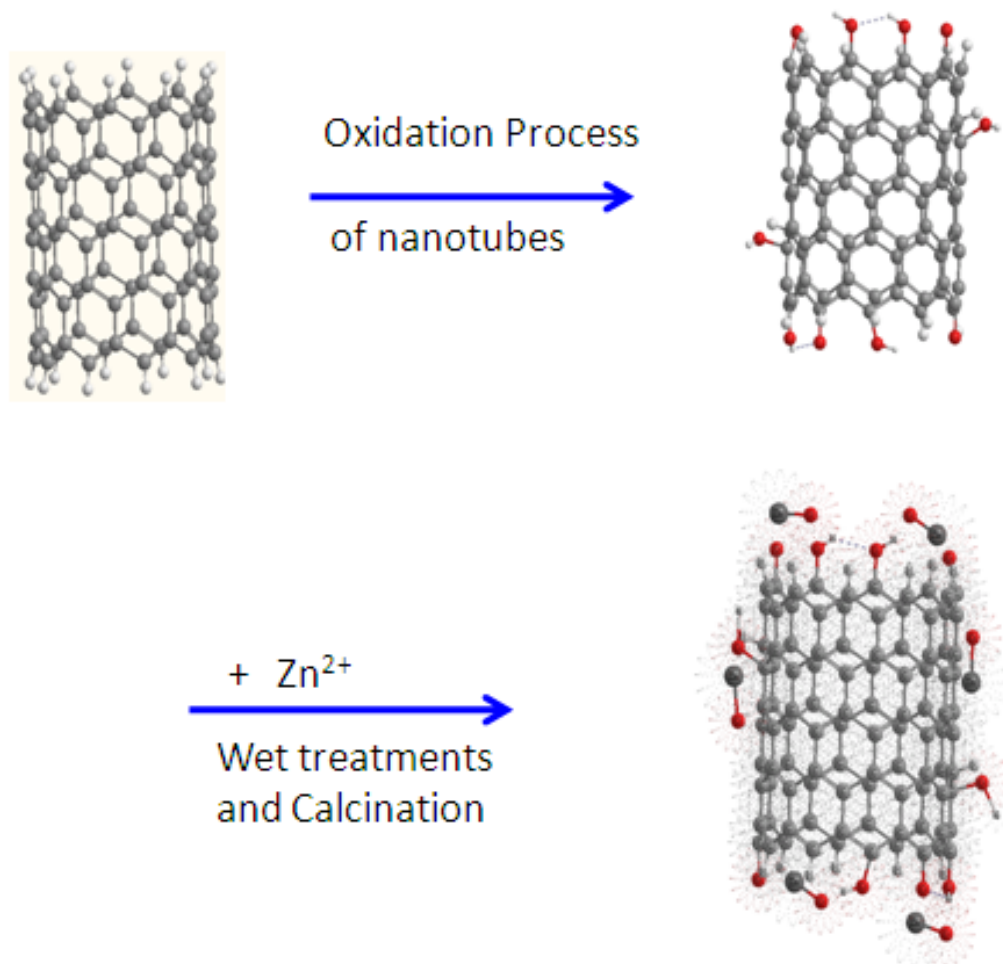


Figure 4-2 Schematic diagram illustrating the synthesis of MWCNT/ZnO composite using a Ball & Stick model

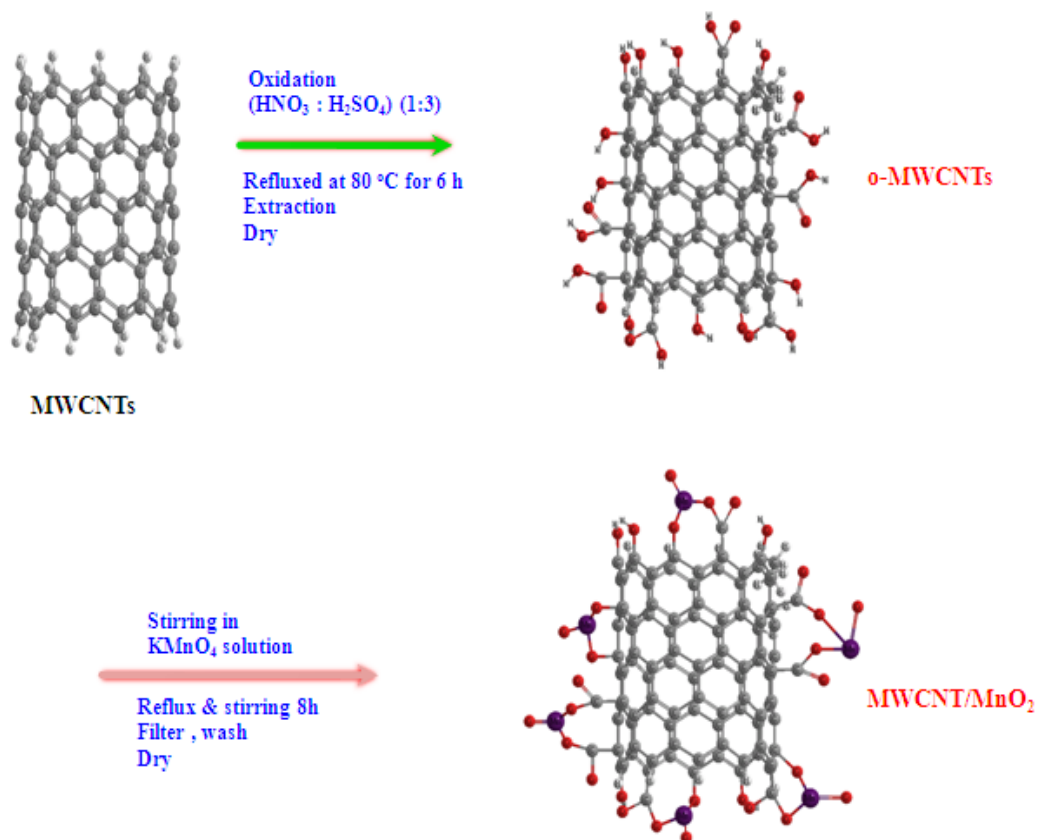


Figure 4-3 Scheme of MWCNTs modification and preparation of MWCNT/ WO_3

CHAPTER 5

CHARACTERIZATION: RESULTS AND DISCUSSION

This chapter presents, in the first part, general discussion of the instruments and techniques used to characterize the synthesized materials. The second part highlights the importance of each technique for the characterization of such composites. The third part presents the characterization results of the nanocomposite materials with interpretation.

5.1. INTRODUCTION

Characterization of the as-prepared carbon nanotube/metal oxides (CNT/MO) nanocomposite is conducted by means of different characterization tools. For example, high resolution transmission electron microscope (HRTEM), field emission scanning electron microscope (FESEM), energy dispersive X-ray (EDX), thermogravimetric analysis (TGA), Raman spectroscope, UV-vis spectrometer and fourier transformed infrared spectroscope (FT-IR), X-ray photoelectron spectroscope (XPS) and photoluminescence (PL) technique; in addition to electrochemical techniques. The techniques are complementary.

Detailed discussion to explain the morphology of the composites, crystalline phases and average size will be presented in the third part. The characterization of each composite is introduced and interpreted separately. The composites prepared in this work are;

CNT/alumina, magnetic-CNTs, CNT/manganese Oxide, CNT/zinc Oxide and CNT/tungsten Oxide composite.

5.2. OVERVIEW

The importance of each technique for the characterization of the composites is highlighted. HRTEM image indicates the shape and distribution of nanoparticles on the surface of the nanotubes. The average size and diameters of the nanoparticles can also be determined from the TEM images. Particularly, TEM is employed to observe the loading state of the nanocomposites. Specifically, TEM images show the surface of the nanotubes coated, decorated or embedded with the nanoparticles. It might be also used to compare the surfaces o-CNTs with that of CNT/MO nanocomposite in term of the roughness and compact.

SEM micrograph is used to investigate the surface morphology and the general morphological features of the prepared composites nanomaterials. It also reveals the uniformity of dispersion of the nanoparticles on the nanotubes. The average particle size can also be measured by SEM.

The EDX or EDS measurements are usually used to confirm the percentage, the atomic ratio, of the components on the nanocomposites surface. It should be noticed that EDX spectrum be better measured for large surface area of the sample for better representation, in other words; low errors.

Thermo gravimetric analysis is used to confirm the presence of metal oxides particles in the nanocomposite. From TGA of CNT/MO nanocomposites, it is expected to have initial weight loss between 250 to 500 °C and can be attributed to condensation reactions of metal-hydroxyl residual groups on the surface of the prepared nanocomposites materials.

XPS analysis is also of important. In the C1s XPS spectra, the main peak is usually observed at 284.6 eV that is attributed to the C–C bonds. Additional peaks are observed at 285.8 eV, 286.8 eV and 289.3 eV; and are assigned to C–O and C=O bonds; and COO groups (Jitianu et al., 2004). The shift of these peaks to higher binding energy could be indicative of binding of metal oxide to the nanotubes. The XRD patterns are used to characterize the crystalline structure of the CNT/MO nanocomposites. FTIR spectra are important and indicative of the presence of functional groups.

Raman spectroscopy is a powerful characteristic technique that is employed to distinguish between the characteristic peaks of TiO₂ and those of CNTs since peaks from each components; nanotube and metal oxide are in most cases separated in frequency, and thus the phases are distinguishable. It is worth mentioning that to run samples on Raman, the energy power should be as low as possible to prevent the effect on the nanotube absorption and get good results. The energy power is preferably to be selected between 10 and 100 mW.

5.3. RESULTS AND DISCUSSION

In this section the characterization results of the prepared composites, CNT/alumina, CNT/ iron oxide, CNT/MnO₂, CNT/ZnO, and CNT/WO₃, is introduced.

5.3.1. CNT/Alumina composite

The morphologies of MWCNTs and synthesized MWCNT/Alumina adsorbent were obtained by SEM, Figure 1 (a) and (b). It should be noticed that after the acidification of MWCNTs, their surface presents polar groups, such as hydroxyl or carboxyl groups, that are able to interact, by hydrogen bonding with Al₂O₃ surface. It was observed that aluminum oxide nanoparticles were successfully coated on the surface of MWCNTs to form multi-wall carbon nanotube aluminum oxide composites. EDX spectrum of MWCNT/alumina composite is depicted in Fig 2a, the inset is the percentage of the components in the composite sample. Fig 2b is the SEM of the sample area from which EDX is measured. Figure 3(a) and (b) show the XRD patterns of MWCNTs and MWCNT/alumina composites. It was observed that the two peaks corresponding to the structure of MWCNTs (Figure 3a) also exist in the XRD pattern of the MWCNT composites (Figure 3b). The broad peak of MWCNT in XRD was narrow in the XRD of the composite because MWCNT in the composite was coated with alumina. The observed XRD of the synthesized Al₂O₃-coated MWCNTs was in convenience with that reported for the synthesis of alumina carbon nanotube composite using thermal pressure method (Schneider et al., 2008).

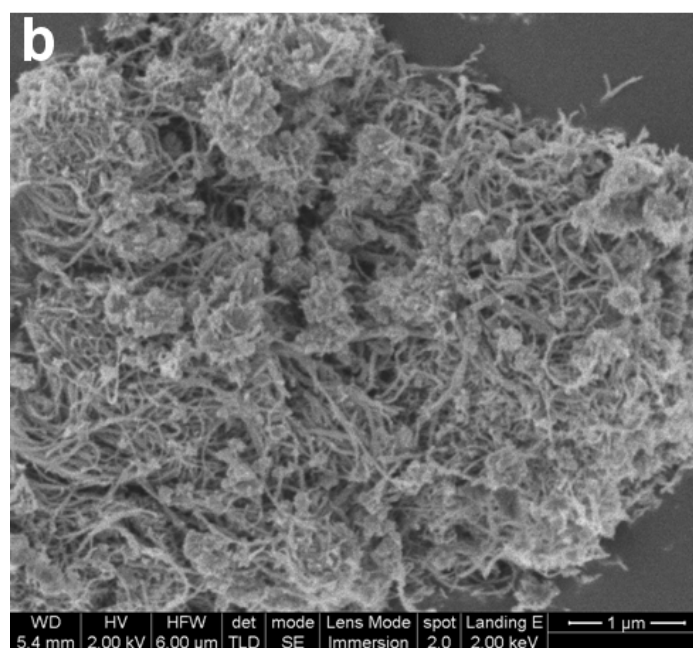
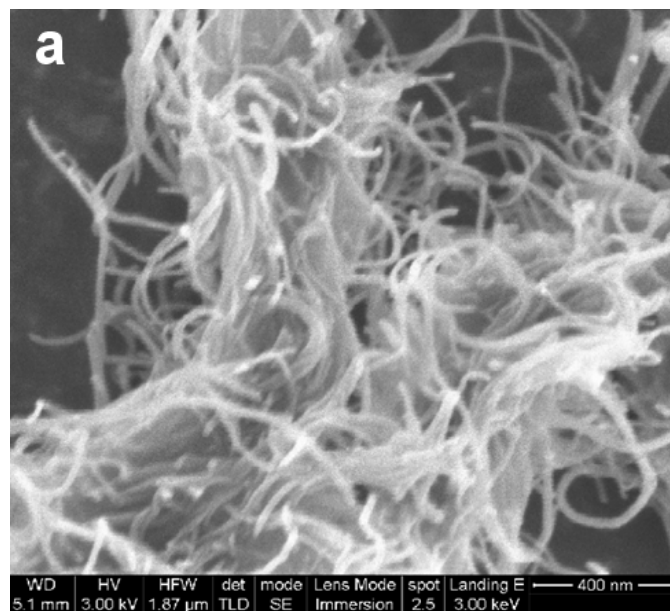
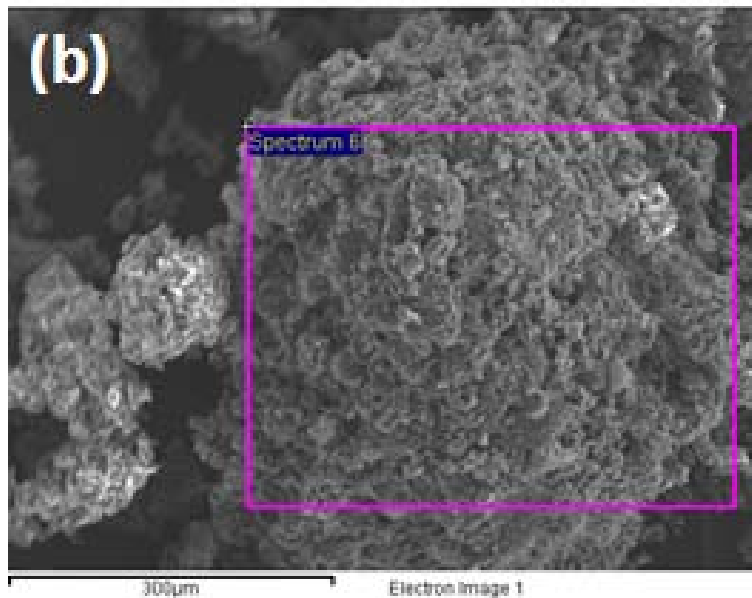
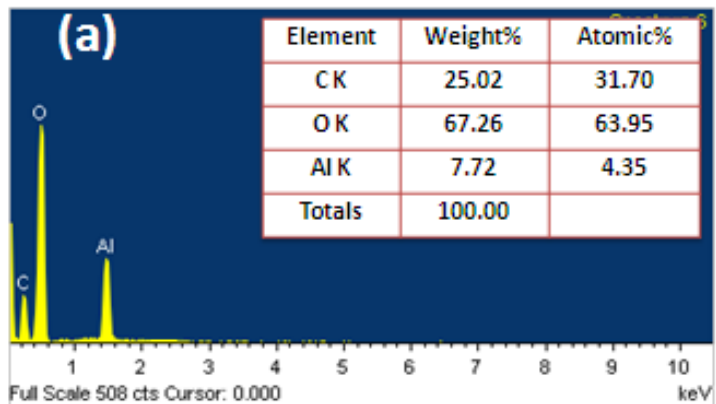


Figure 5-1 SEM images of (a) uncoated MWCNTs (b) alumina-coated MWCNTs



5-2 EDX spectrum of MWCNT/alumina composite (a): Inset is the components percentages in the composite sample; (b) is the SEM of the area of the sample from which EDX is measured

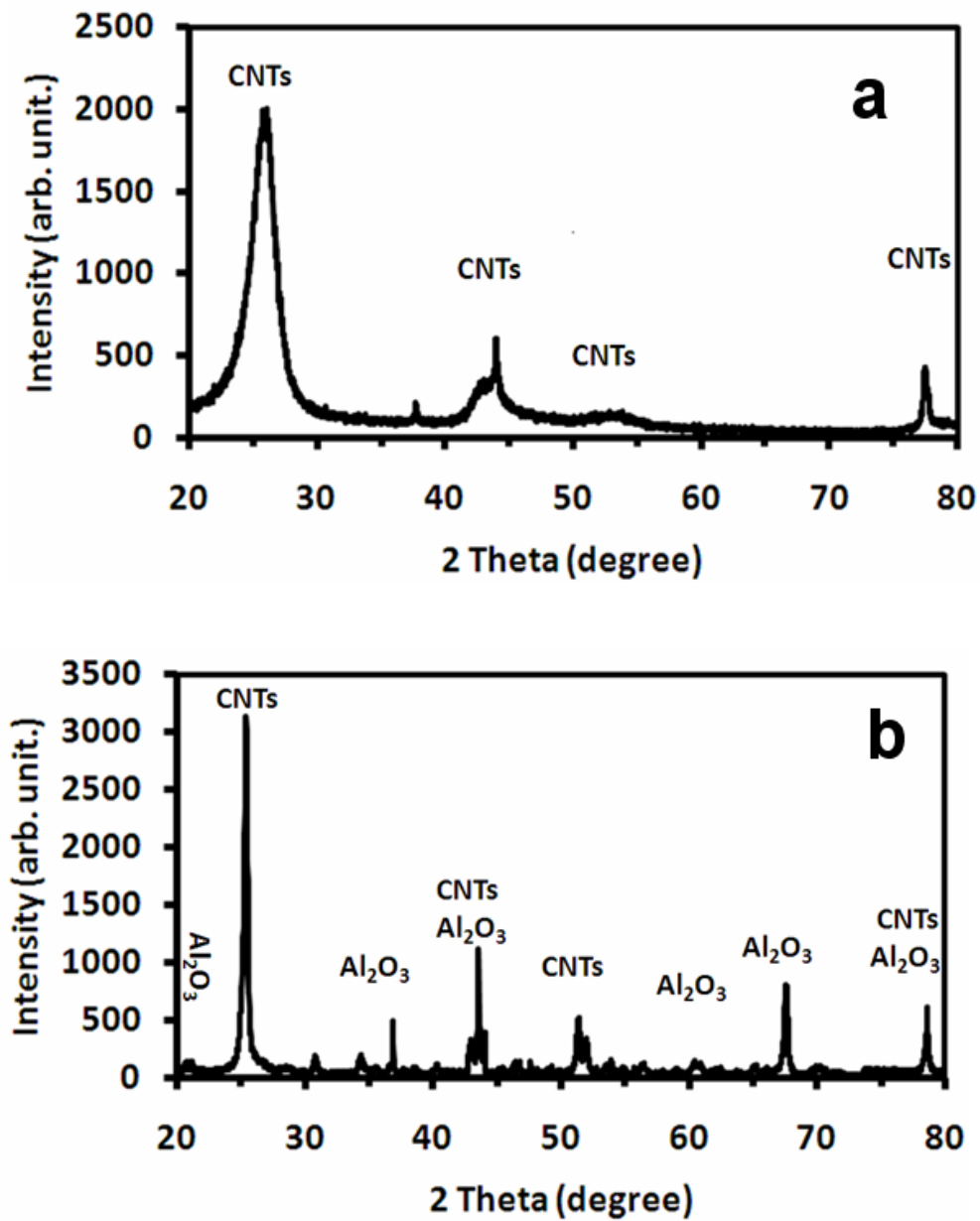


Figure 5-3 X-ray diffraction of (a) uncoated MWCNTs (b) alumina-coated MWCNTs

FTIR spectra are used in order to confirm the formation alumina on the surface of MWCNTs. FTIR spectra, Fig. 4, of uncoated MWCNTs and synthesized Al_2O_3 -coated MWCNTs were performed for a better comprehension of the structure and composition of these materials. An absorption band revealing the vibrational properties of Al-O bond is observed at about 500cm^{-1} . This band is mainly assigned to the stretching vibrations of Al-O ($\nu\text{Al-O}$).

The broad absorption peaks in the range of $3410\text{-}3465\text{ cm}^{-1}$ correspond to -OH group, indicating of existence of the hydroxyl groups on the surface of the composites or it can be attributed to the adsorption of some atmospheric water during FTIR measurements. Those at $1500\text{-}1650\text{ cm}^{-1}$ are the C=O stretching mode of the functional groups on the surface of the MWCNTs or arising from the absorption of atmospheric CO_2 on the surface of the composites. The peak at 3420cm^{-1} is attributed to the stretching vibration of O-H band. The two peaks at 2920 and 2854 cm^{-1} correspond to the C-H stretch vibration, originated from the surface of tubes, Figure 3a, are obviously weak in Figure 3b, suggests that the surface of MWCNTs covered by Al_2O_3 .

Based on the characteristic results, XRD, SEM and FTIR, a schematic diagram of structural nature of alignment of Al_2O_3 on the surface of MWCNTs is depicted in Figure 5. One explanation is based on the assumption that aluminum atom of alumina is aligned closer to the oxygen atom of the carbonyl group (C=O) of MWCNTs which enhanced by the affinity of aluminum atom to interact with the pair of electrons on the oxygen. The

oxygen atom of Al_2O_3 is aligned close to the hydrogen atom of hydroxyl group of MWCNTs due to the hydrogen bond formation. In addition, the attractive Van der Waals forces are expected to play a role.

As shown in IR spectra, the shift of the carbonyl peak of carboxyl group on the nanotube toward lower wavenumber in the composite can be attributed to formation of chemical bond between alumina and the nanotube.

Understanding the interaction may give a possibility to control the nanoparticles on the surface of the nanotube. This may give chance to prepare a control composite of a promising future for the application of MWCNTs in materials systems, such as reinforcing structural ceramic components.

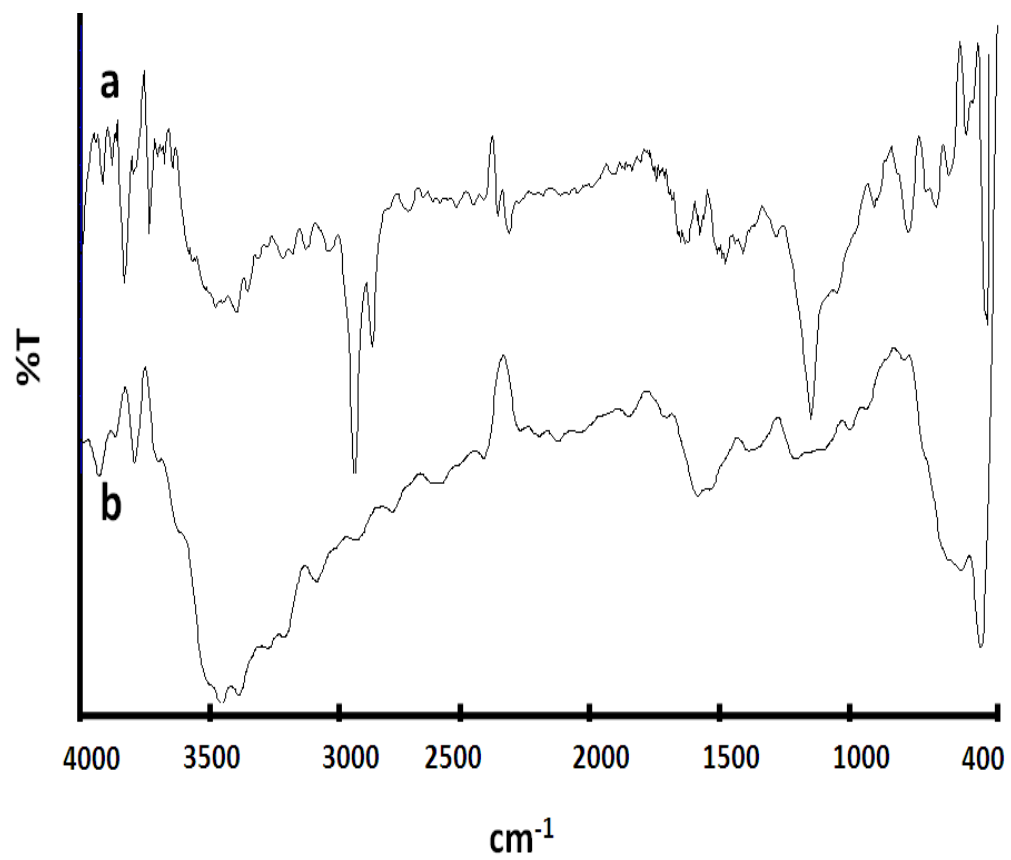


Figure 5-4 FT-IR spectra of (a) uncoated CNTs and (b) alumina-coated CNTs

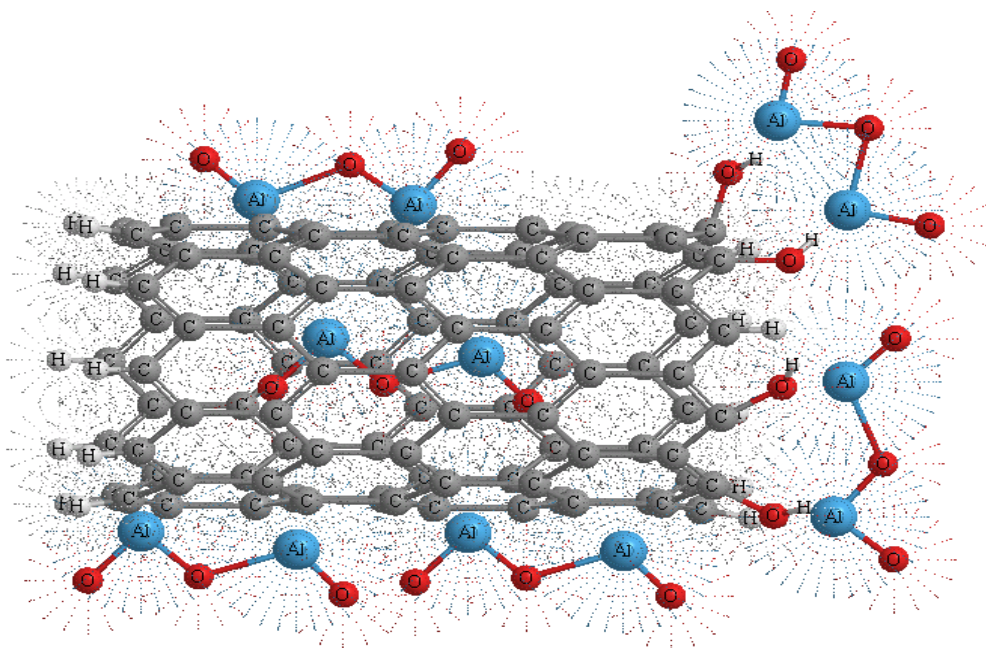


Figure 5-5 Structural representative of possible interaction between alumina and CNT

5.3.2. Magnetic-CNTs

After the synthesis of MWCNT/nano-iron oxide composite, a test with the magnet showed that the whole material is magnetic and completely attracted to the magnet. The morphologies of uncoated MWCNTs and synthesized MWCNT/nano-iron oxide were obtained by SEM. Fig. 5 shows the SEM images of the composites. SEM image (Fig. 5) of the composites depicts an entangled network of oxidized MWCNTs with clusters of iron oxides attached to them. Surface area of the prepared composite was measured using BET method. The specific surface area of MWCNT/nano-iron oxide composite was $92 \text{ m}^2/\text{g}$

Under the reaction conditions employed, four iron oxides are commonly formed. These are Fe_3O_4 (magnetite), $\gamma\text{-Fe}_2\text{O}_3$ (maghemite), $\alpha\text{-Fe}_2\text{O}_3$ (hematite) and $\alpha\text{-FeO(OH)}$ (goethite). Among them two magnetite and maghemite are magnetic (Perez et al., 1998). Fig. 6 shows the X-ray diffraction patterns of MWCNTs and MWCNTs/nano-iron oxide composites. The two peaks corresponding to the structure of MWCNTs also exist in the XRD pattern of the magnetite composites.

The XRD pattern of the magnetic composites reveals a cubic iron oxide phase. Their indexes diffraction peaks as shown in Fig. 6B support the presence of maghemite and magnetite as the magnetic phase in the composite. The average grain size 'd' of the iron oxide was estimated by using the standard equation known as Debye Scherrer formula (Yu, et al., 2009)

$$d = \frac{0.9\lambda}{\beta \cos \theta}$$

where λ = wavelength of the X-ray, β = FWHM (Full Width at Half Maximum) width of the diffraction peak, θ = diffraction angle. The average size of iron oxide on the surface of the nanotube was calculated and found to be 18 nm.

FTIR measurements are used in order to confirm the formation iron oxide. FTIR spectra, Fig. 7 synthesize MWCNTs/nano-iron oxide were performed for a better comprehension of the structure and composition of these materials. An absorption band revealing the vibrational properties of Fe-O bond is observed for in around 477cm^{-1} . This band is mainly assigned to the stretching vibrations of Fe-O ($\nu\text{Fe-O}$). The broad absorption peaks in the range of $3300\text{-}3500\text{ cm}^{-1}$ correspond to -OH group, indicating of existence of the hydroxyl groups on the surface of the composites or it can be attributed to the adsorption of some atmospheric water during FT-IR measurements. Those at $1570\text{-}1655\text{ cm}^{-1}$ are the C=O stretching mode of the functional groups on the surface of the MWCNTs. The two peaks, in IR of nanotube, at 2920 and 2854 cm^{-1} correspond to the C-H stretch vibration, originated from the surface of tubes are obviously weak in IR of the composite Fig. 7.

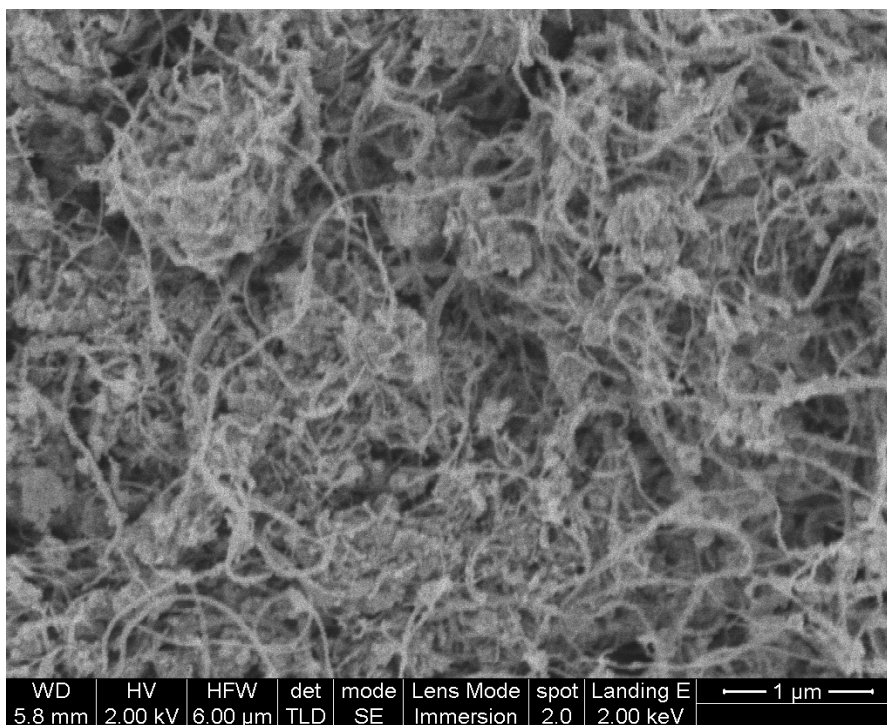


Figure 5-6 SEM images of MWCNTs/nano-iron oxide

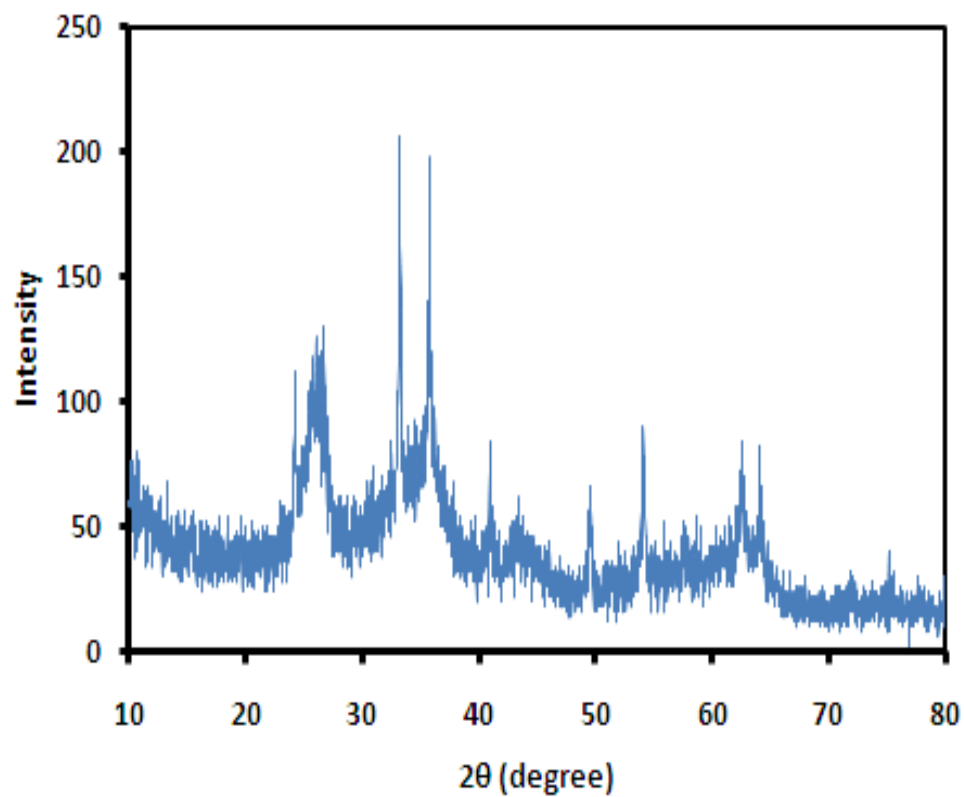


Figure 5-7 X-ray diffraction MWCNTs/nano-iron oxide

where Mn: Magnetite (Fe_3O_4); Mh: Maghemite ($\gamma\text{-Fe}_2\text{O}_3$)

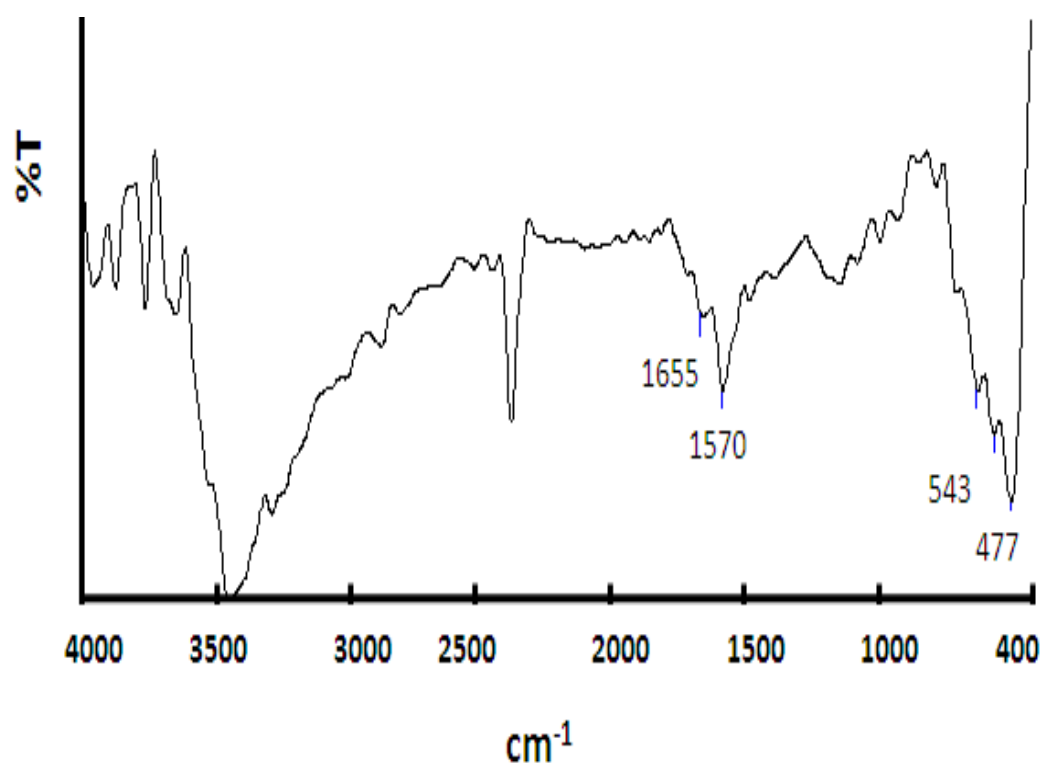


Figure 5-8 FT-IR spectra of MWCNTs/nano-iron oxide

5.3.3. CNT/Manganese Oxide

The functionalization of MWCNTs with oxygen containing groups is an important step for the preparation of MWCNT/MnO₂ nanocomposites. Once the presence of oxygen-containing groups on MWCNTs is confirmed by FTIR, the synthesis of the composite was followed. The binding of manganese to o-MWCNTs was confirmed by FTIR as shown in Fig. 8. The appearance of a peak at 1383 cm⁻¹ is indicative of the symmetric carboxylate stretching mode. It is well known that the positions of symmetric COO-stretching bands considerably change within 1450-1300 cm⁻¹ in metal complexes depending on the coordination structures. The strong peak assigned to C=O stretching band at 1680 cm⁻¹ in the spectrum of o-MWCNTs is shifted to 1610 cm⁻¹ in the spectrum of the composite. This indicates that the double bond between carbon and oxygen become longer and weaker because of formation of electrostatic ionic bond with manganese that withdraw the electrons. As a result, the Mn-O bond in the MWCNT/MnO₂ is stronger than the same bond in MnO₂.

To confirm this, MnO₂ nanoparticles were prepared from the same precursor and its FTIR spectrum was measured as shown in Fig. 9. Comparing FTIR of MnO₂ with that of the composite shows the blue shift from about 505 cm⁻¹ to 547 cm⁻¹.

The FESEM was used to investigate the morphology of the as synthesized MWCNT/MnO₂ and o-MWCNTs. SEM image and EDX spectrum of MWCNT/MnO₂ composite material are presented in Fig. 10. The chemical composition of the composite derived from the EDX is presented in the inset of EDX spectra. Fig. 11 presents the

high-resolution FESEM image of MWCNT/MnO₂ nanocomposite, which indicates that the surface of MWCNTs is embedded with MnO₂.

The phase and structure of the composite was investigated by XRD. The strong graphite peak of plane 002 at $2\theta = 25.8^\circ$ is clear in both XRD patterns of o-MWCNTs and MWCNT/MnO₂ composite. The other diffraction peaks related to MWCNTs at the angle 2θ of 42.7° , 43.9° , 53.5° and 77.5° can be indexed to the (100), (101), (004) and (110) planes of MWCNTs. The four broad peaks corresponding to MnO₂ (001), (002), (110) and (020) reflections are revealed in XRD pattern Fig. 12. From the XRD pattern and using the Debye–Scherrer formula, the average size of MnO₂ nanoparticle in MWCNT/MnO₂ nanocomposite was estimated to be 12 nm.

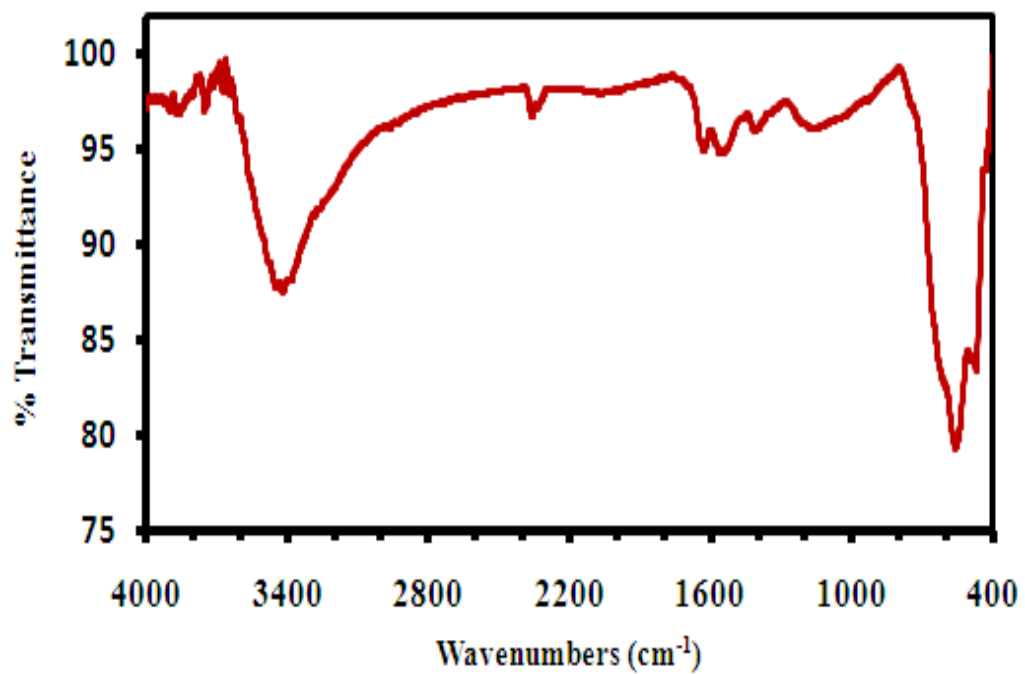


Figure 5-9 FTIR spectra of MWCNT/manganese oxide composite

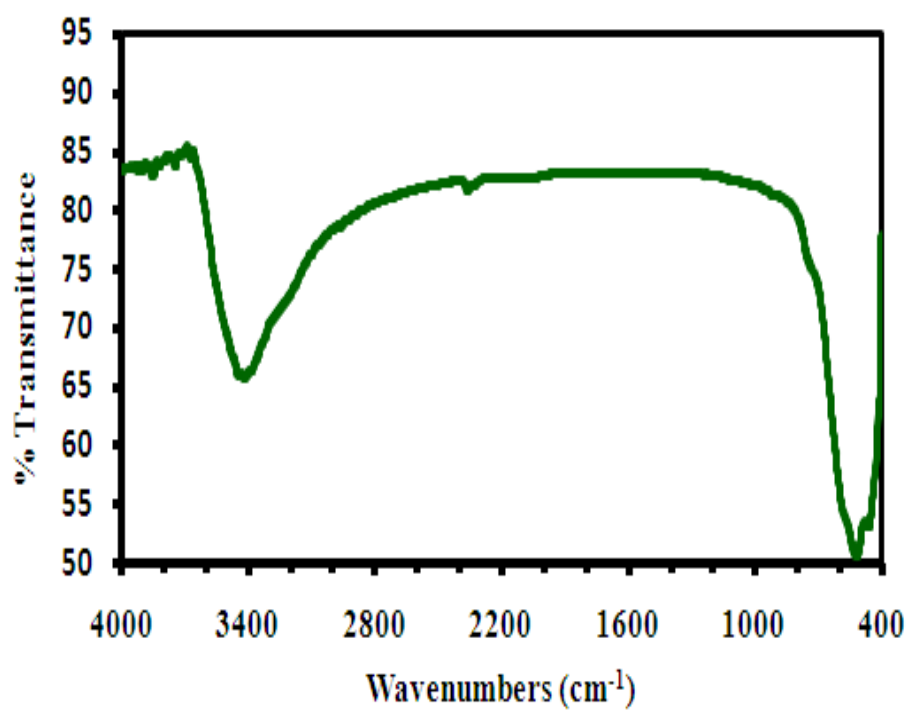


Figure 5-10 FTIR spectra of manganese oxide nanoparticles

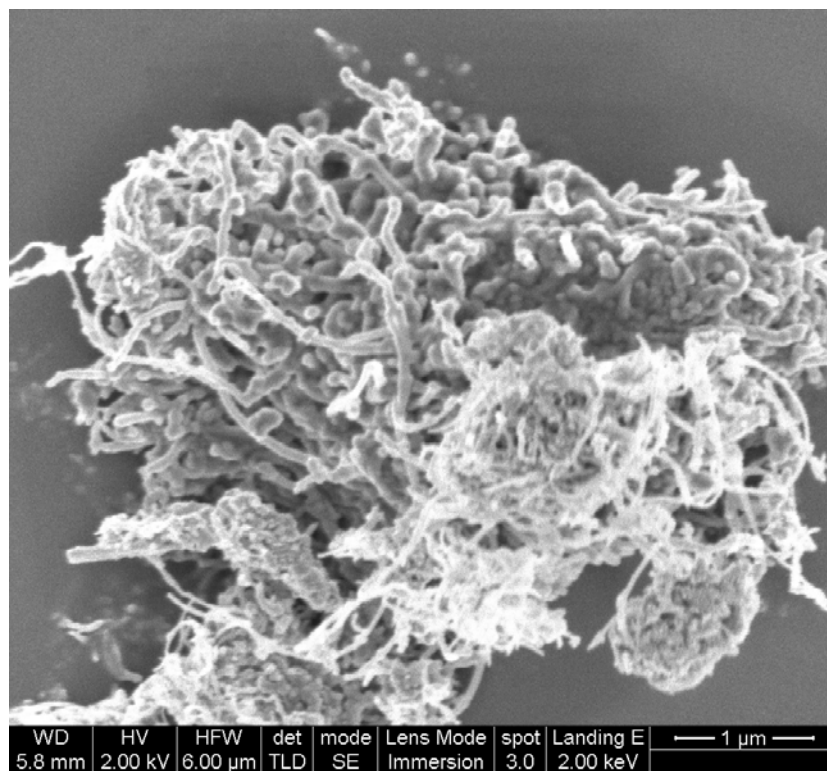


Figure 5-11 SEM of MWCNT/manganese oxide composite

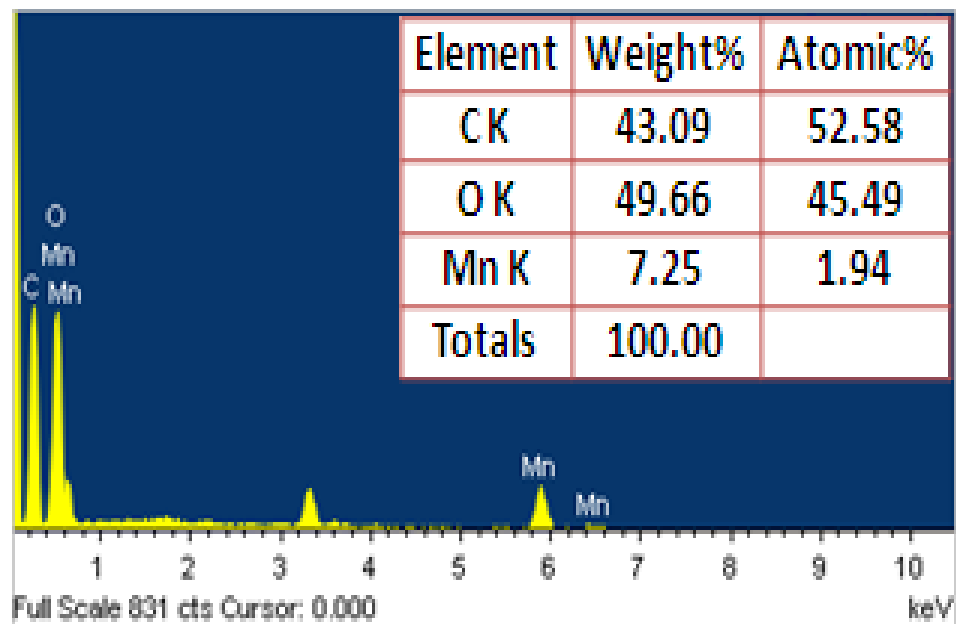


Figure 5-12 EDX of MWCNT/manganese oxide composite

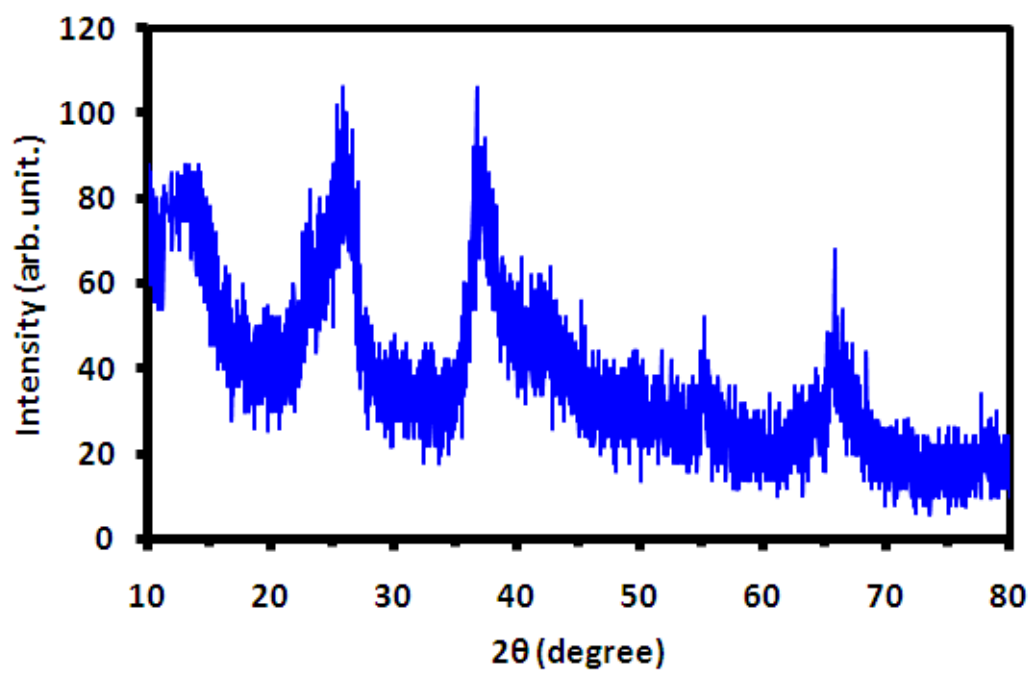


Figure 5-13 XRD of MWCNT/manganese oxide composite

5.3.4. CNT/Zinc Oxide

Fig. 13 depicts the XRD patterns of MWCNT and the MWCNT/ZnO nanocomposite. Diffractions of both MWCNTs and ZnO could be observed. The main dominant peaks for ZnO were identified at $2\theta = 31.77^\circ$, 34.44° , 36.25° , 47.53° , 56.57° , 62.85° , 66.37° , 67.92° , 69.03° and 77.5° ; which can be indexed as (100), (002), (101), (102), (110), (103), (200), (112), (201), (004) and (202). XRD results of ZnO showed prominent 100, 002 and 101 reflections among which 101 is of highest intensity. The average particle size of ZnO in MWCNT-ZnO nanocomposite can be roughly estimated using the Debye-Scherrer formula for spherical particles and the estimated size was around 18nm and the lattice parameters a and c of the ZnO was estimated using hexagonal structure formula which gives values of $a = 0.3257$ nm and $c = 0.5257$ nm.

Fig.14 a-b shows the morphology of MWCNT/ZnO nanocomposite. As clear from FE-SEM image of MWCNT/ZnO composite, a dark ZnO sheath on the surface of the MWCNTS core has been appeared, which reflects that the MWCNTs had been embedded by zinc oxide. The morphology, particle size and shape of MWCNT/ZnO were investigated by high-resolution transmission electron microscope (model: JEM-2100F (HR)), at a voltage of 200 kV. Transmission electron micrograph illustrates directly the size and shape distribution. The powders are dispersed in acetone by stirring in an ultrasonic tank for 15 minutes. A drop of this suspension was then mounted on a carbon-coated copper grid for analysis. Fig. 14c illustrates the TEM images of MWCNT/ZnO composite. Fig. 14c clearly illustrates that the surface of MWCNT was

embedded uniformly with ZnO nanoparticles. Based on morphological studies a space-filling model representing the MWCNT/ZnO composite is depicted in Fig. 14d.

In order to study the optical properties, the prepared MWCNT/ZnO composite were first dispersed in water. The UV-VIS optical absorption characteristics of the MWCNT/ZnO nanocomposites were investigated using UV spectrophotometer. The measured absorption spectrum is presented in Fig. 15. The excitonic absorption peaks are observed due to the ZnO nanoparticles at 270 nm and 370 nm which lie below the band gap wavelength of 388 nm ($E_g = 3.2$ eV) of bulk ZnO.

FTIR spectra are useful to understand further the formation of MWCNT/ZnO composite. Fig. 16 reveals different surface chemistry of MWCNTs and the MWCNT/ZnO composite. In the high frequency region, broadened bands around 3420 cm^{-1} can be observed in Fig. 16A-B, which can be assigned to the bending vibrations of adsorbed molecular water and stretching vibrations of OH groups. The two peaks at 2920 and 2854 cm^{-1} correspond to the C-H stretch vibration, originated from the surface of tubes. Compared with MWCNTs (Fig. 16-A), the two peaks of composite (Fig. 16-B) are obviously weak, which suggests that the surface of MWCNTs has been covered by ZnO. The peaks at 1650 cm^{-1} can be inferred as CO_2 stretching vibration of the two samples, which is lower in the composite than that of MWCNTs. Furthermore, peaks observed at low frequency region (around 500 cm^{-1}) in MWCNT/ZnO composite are assigned to the Zn-O.

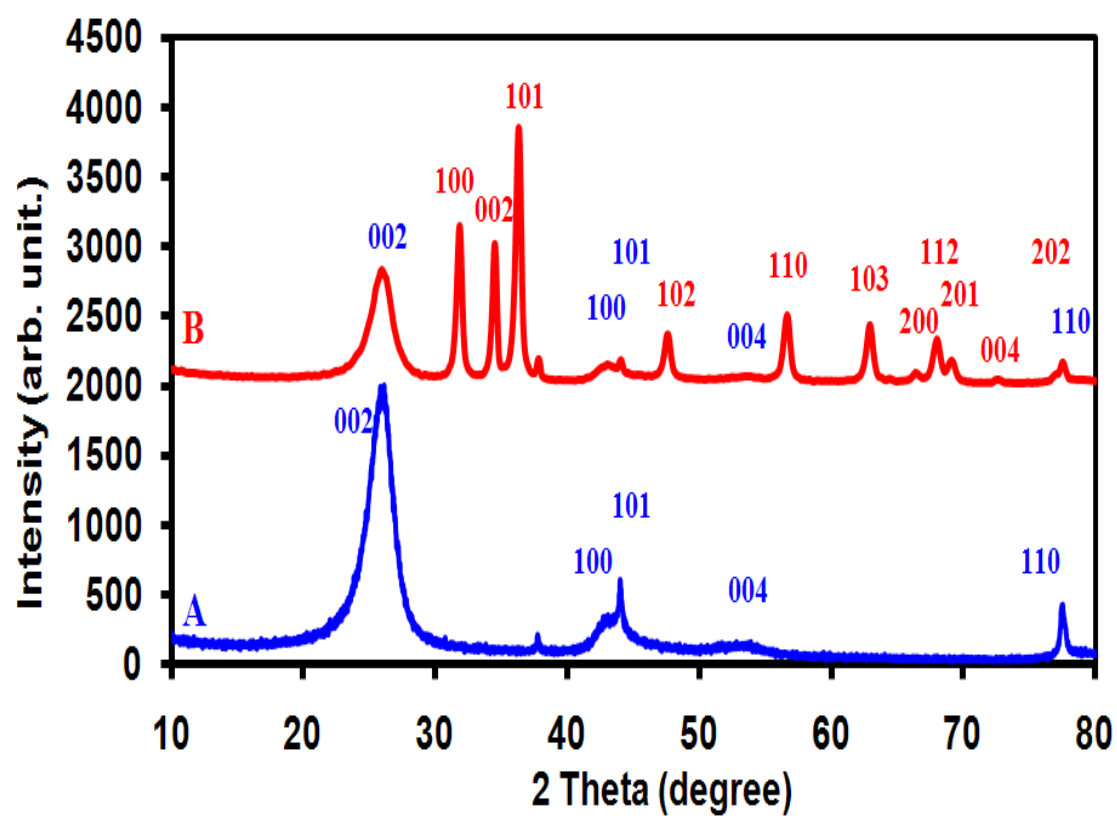


Figure 5-14 XRD of MWCNT (a) and MWCNT/zinc oxide composite

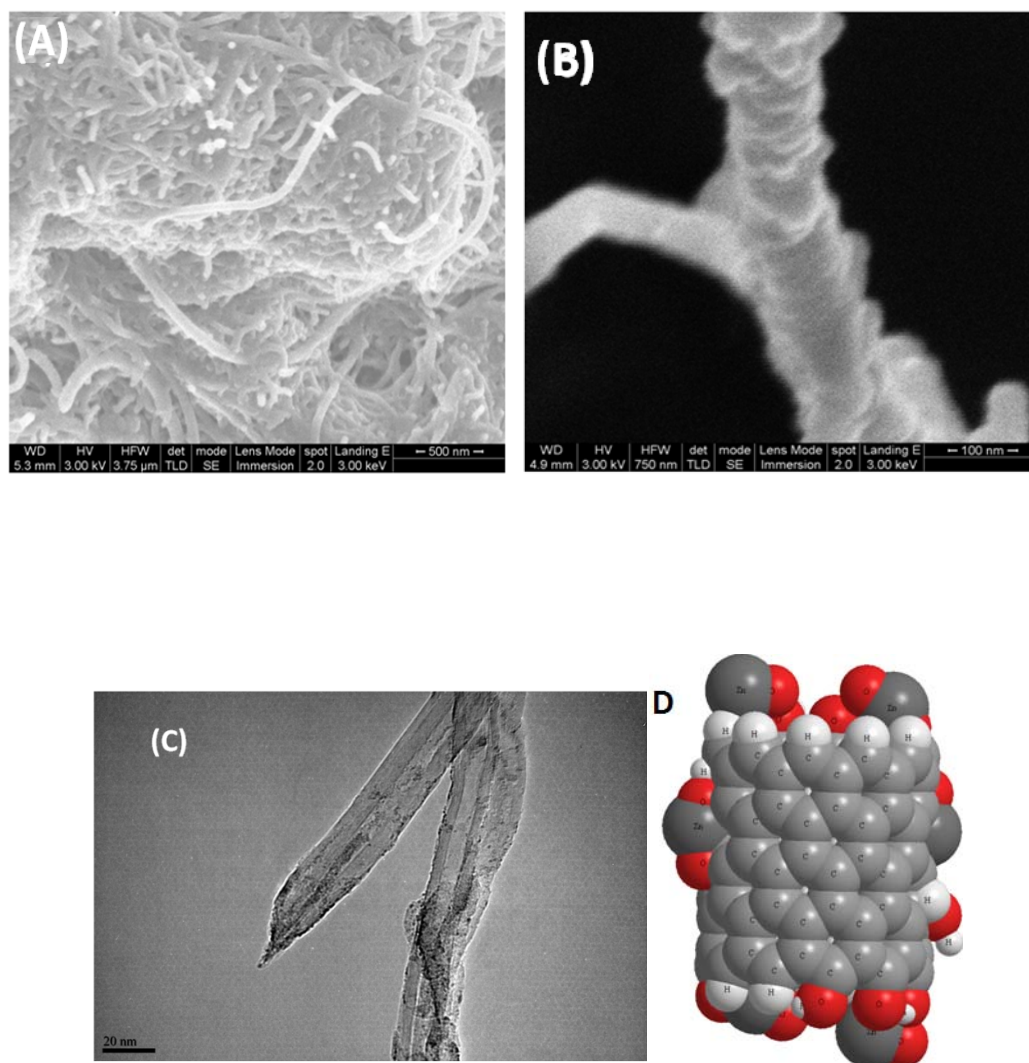


Figure 5-15 FE-SEM image (a); higher magnification SFM (b); HRTEM image (c); Space Filling model (d) of MWCNT/ZnO composite

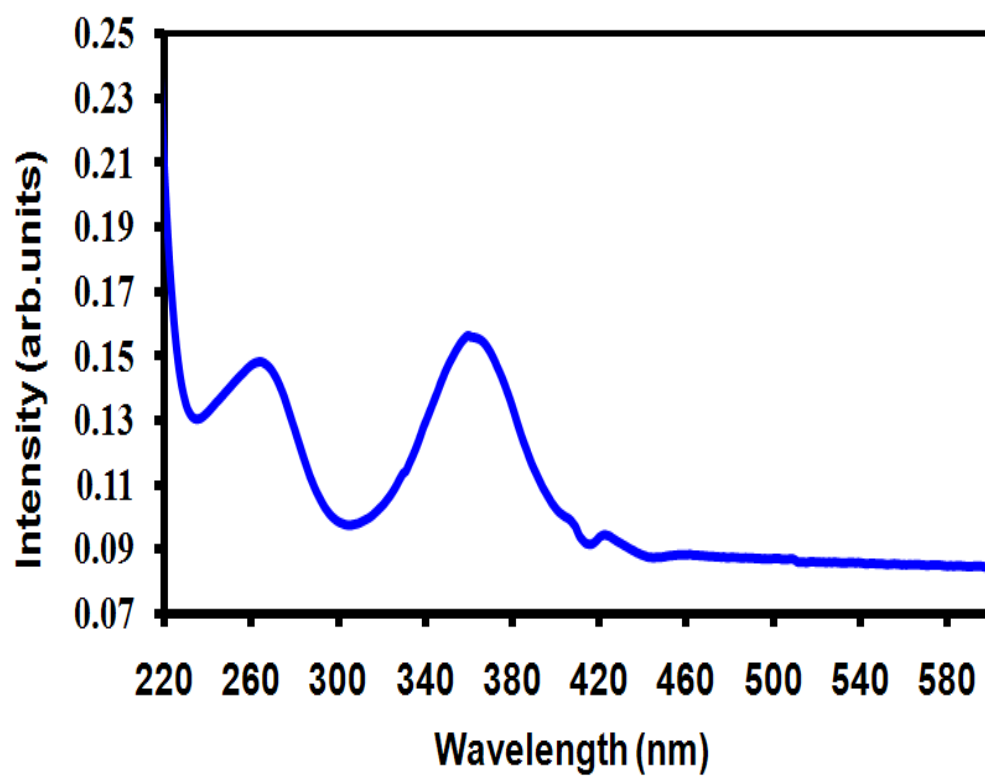


Figure 5-16 UV-vis spectrum of MWCNT/ZnO nanocomposite.

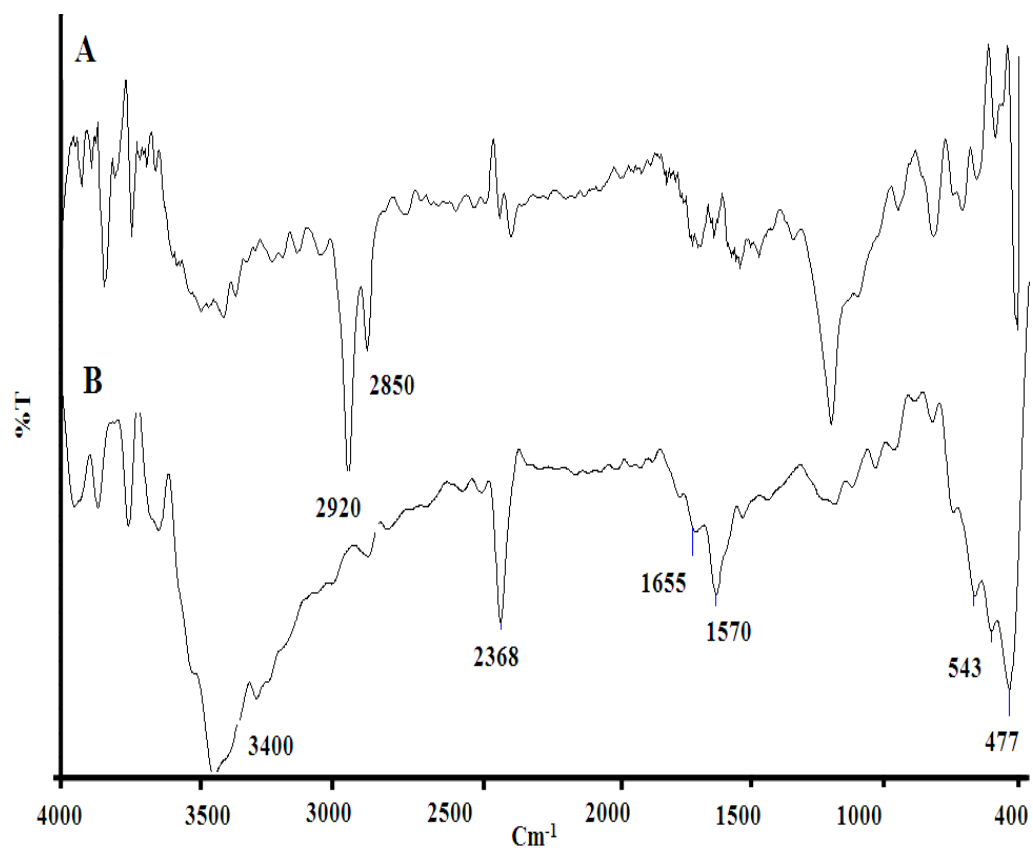


Figure 5-17 FTIR of MWCNT (a) and the MWCNT/ZnO composite

5.3.5. CNT/Tungsten Oxide

To verify the formation of tungsten oxide, the prepared composites after chemical treatment process were analyzed by XRD. Analysis of the diffraction peaks revealed the presence of hexagonal, JCPDS 85-2460, (see green colored rows in Fig. 17b) and orthorhombic, JCPDS 71-0131, (see red colored rows in Fig. 2b tungsten oxide nanoparticles by analyzing their corresponding XRD patterns, respectively [Wang et al., 2009]. The peaks attributed to WO_3 were very likely broadened by the small particle size. Using the Scherrer's formula for peak broadening, a value of 9 nm was calculated for the average size of the WO_3 crystallites nanoparticles. It was found that diffraction peaks assigned to the (002) plane of MWCNTs at $2\theta = 25.8^\circ$ be clearly distinguished in both XRD patterns, indicating that the graphite structure of MWCNTs was not destroyed after heat-treatment process. However, this peak becomes sharper and the reason could be the presence of WO_3 peaks that might lead to the shielding of MWCNT peak at 25.8.

The morphology and microstructure of MWCNT/ WO_3 composite were examined by SEM. Fig. 18 illustrates that MWCNTs were decorated with WO_3 . The quantitative microanalysis of C, O and W as major elements for the composite was performed by EDX. The spectrum shows the presence of C and O with strong W peaks as component elements and there are no impurities in the as-synthesized composite.

After the purification and oxidation of MWCNTs, the functional group formed on the surface was examined using FTIR. The band at 2910 cm^{-1} and 2847 cm^{-1} ascribe to

C-H stretching vibration originated from the tubes' surface. The band at 1670 cm^{-1} , ascribe to C=O stretching vibration. It can be noted that the frequency of the carbonyl stretching absorption is reduced because of the internal hydrogen bonding effect, which is higher than the effect of intermolecular hydrogen bonding. The band at 1562 cm^{-1} can be assigned to unsaturated structural of C=C [Stobinski et al., 2010]. The bands in the range of $1300\text{--}950\text{ cm}^{-1}$ prove the presence of C-O bonds in various chemical surroundings. The band at 3450 cm^{-1} ascribes to stretching vibrations of isolated surface -OH moieties and/or -OH in carboxyl groups and in sorbed water. These observations suggest that oxidation was promoted in all treatments, and these formed functional groups can increase the active sites on the surface of MWCNTs.

In Fig. 19 the broad characteristic peak observed around 701 cm^{-1} broaden to 1000 cm^{-1} in the FTIR spectrum of WO_3 , can be assigned to W-O bonds vibrations. Fig. 20 depicts the FTIR spectrum of the composite. The peak of W-O covalent bond is shifted from 701 cm^{-1} to 770 cm^{-1} , which confirm the existence of a close interaction between WO_3 and MWCNTs and thus the formation of the ionic chemical bond between WO_3 and MWCNTs through the oxygen of carboxylate anion. The band assigned to C=O stretching vibration is shifted from 1670 to 1606 cm^{-1} . Also, the appearance of the band at 1403 cm^{-1} formation could be assigned to the symmetrical stretching of the carboxylate anion proven the formation of ester bonds (-COO-W-). This illustrates that carboxylic acid groups on the surface of MWCNTs and hydroxyl groups on tungsten could interact with each other and form the chemical bond. The existence of the peak, in the IR spectrum of the composite, at around 3450 assigned for the O-H free stretching

vibration could indicate that not completely the sites on the surface of MWCNTs have been occupied or be assigned to sorbed water.

UV-vis absorption spectra were recorded to evaluate the optical property of the as-prepared MWCNT/WO₃ composites, together with MWCNTs. The absorption spectra of dispersed MWCNT/WO₃ composite and MWCNTs in water were measured (Fig. 21). MWCNTs have a broad absorption area while the as-prepared composite shows the typical absorption with an intense transition in the UV-vis region of the spectra. However, the absorption edge of WO₃ nanoparticles is about 450 nm which is due to electron promotion from the valence band to the conduction band of WO₃ [Xiang et al., 2010]. The presence of MWCNTs leads to strong absorption band and leads to the continuous absorption band in the range of 400-800 nm [Xu et al., 2010]. This result suggests that the composites combined the features of MWCNTs and WO₃ together, and generated new properties, which would be favorable to widening the absorption.

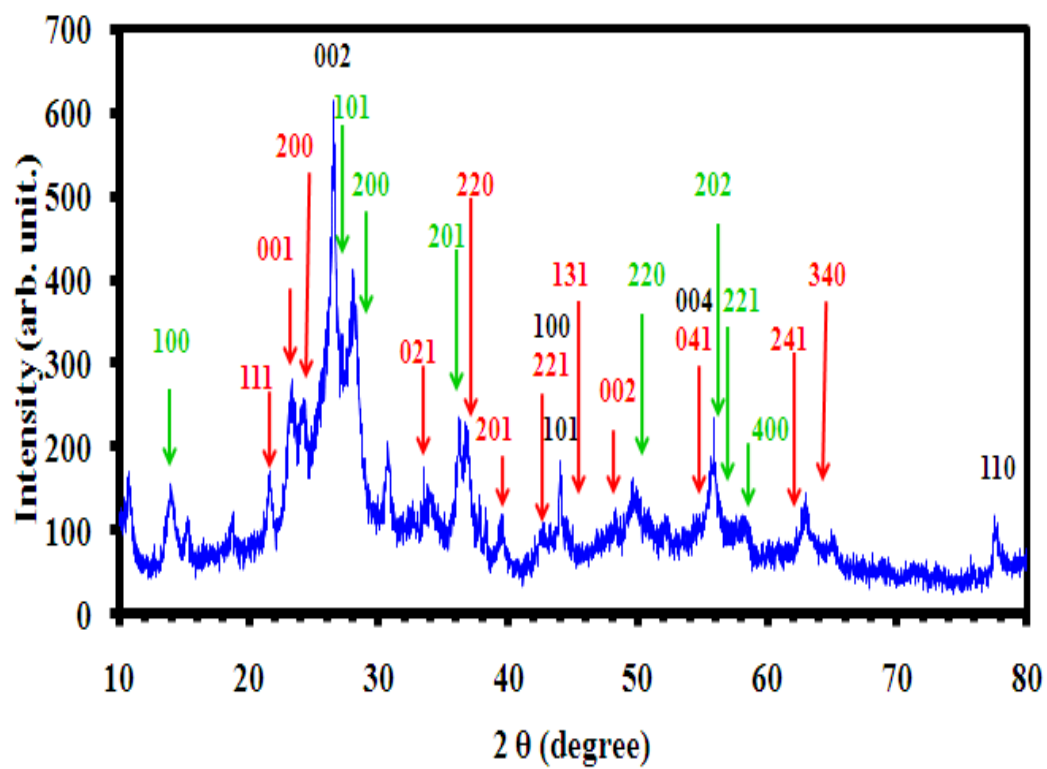


Figure 5-18 XRD of MWCNT/WO₃

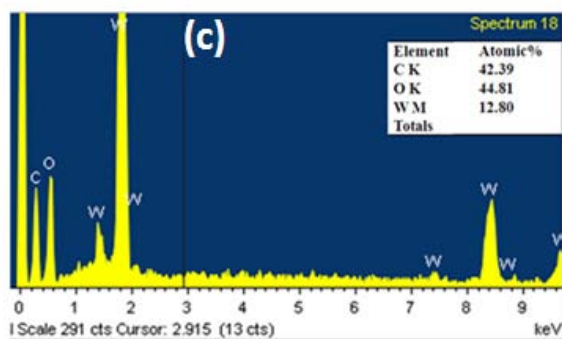
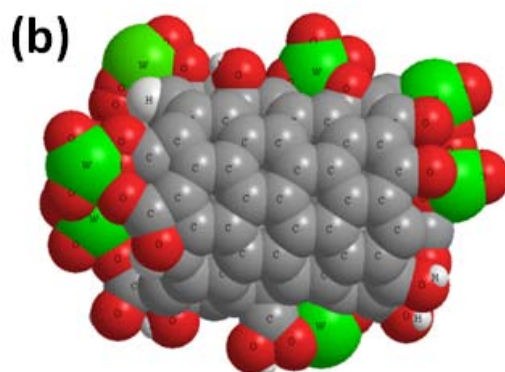
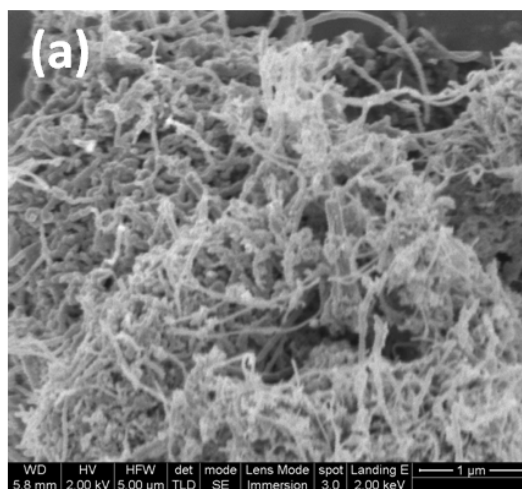


Figure 5-19 FESEM images (a) and Space Filling model (b) and EDX (c) of MWCNT/WO₃

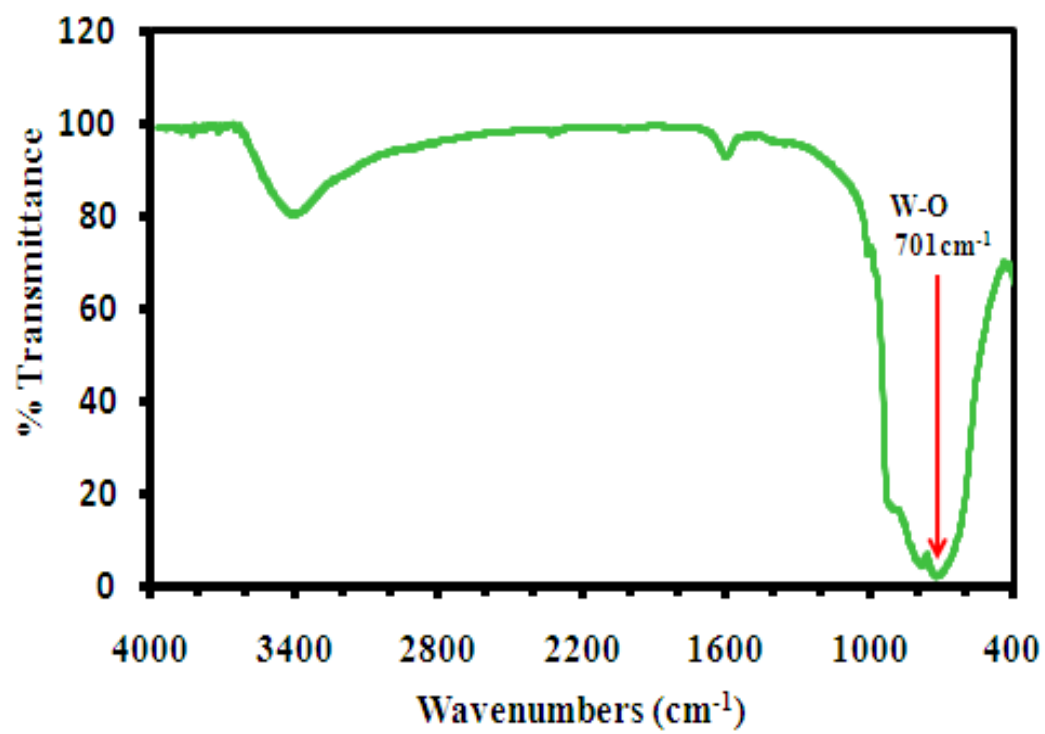


Figure 5-20 IR spectrum of WO₃ nanoparticles

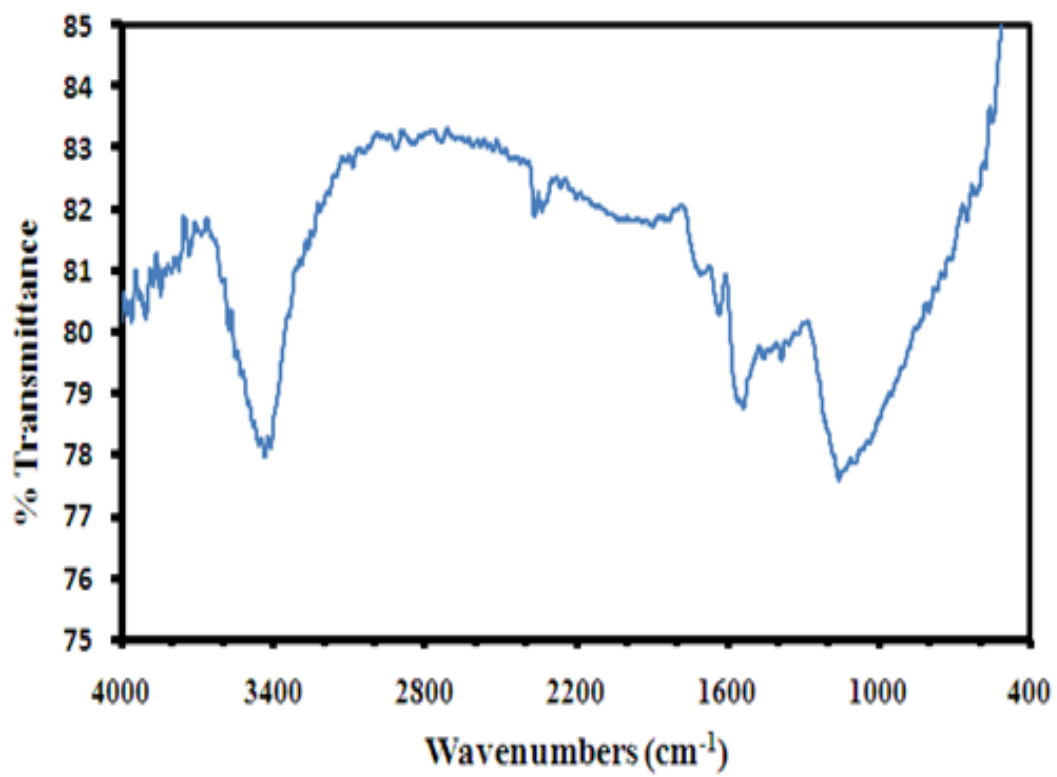


Figure 5-21 IR spectrum of MWCNT/WO₃ composite

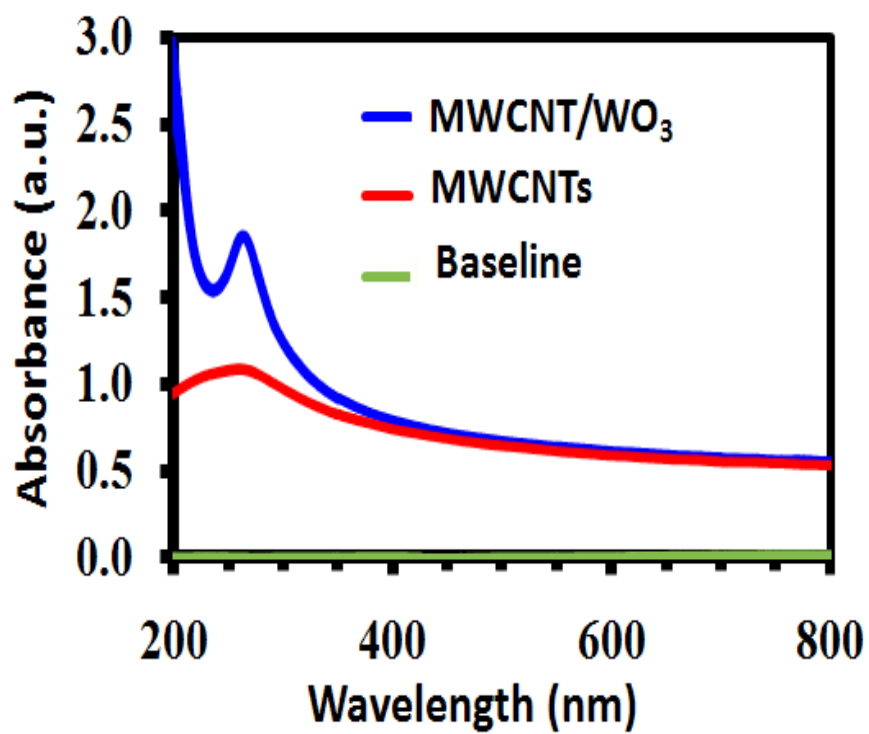


Figure 5-22 UV-vis spectrum of MWCNT/WO₃

CHAPTER 6

APPLICATION OF MWCNT/ALUMINA COMPOSITE

In the previous chapters, we have discussed how the composites were synthesized and characterized using different techniques. In this chapter, the results of the application of the multiwall carbon nanotube/alumina composite (MWCNT/alumina), for the removal of lead is presented. The chapter begins with introduction followed by experimental section. Finally, the results are presented and discussed.

6.1. INTRODUCTION

It is noteworthy that composite materials play a very important role in membrane and ceramic field and in many water treatment processes, such as formation of catalysts as for photo-degradation. Carbon nanotube-based composite is one of the more recent area of research related to the formation of membrane. Their attractiveness to researchers lies in their intrinsic outstanding electrical, optical, and mechanical properties. Composites of carbon nanotube (CNT) with different metal oxides have been reported to tackle various environmental pollution problems. Carbon nanotube/aluminum oxide composites are extremely important materials with applications in ceramic and membrane; and in general in water treatment units. The materials have become an intriguing field of intense research. Attempts to assemble CNTs with aluminum oxide

have yielded hybrid materials holding attractive multifunctional properties or considerably improved properties relative to those exhibited by the alumina.

6.2. HIGHLIGHTS

Alumina is one of the most widely used ceramic materials because of its high hardness, good oxidation resistance and chemical stability. However, its applications are limited because of its low fracture toughness. CNTs have been widely used to reinforce and increase the fracture toughness of alumina owing to their unique one-dimensional structure with robust mechanical and thermal properties (Keshri, et al., 2010). However, the reported deal mostly with the mechanical mixing methods of preparation and do not discuss the chemistry of the prepared composite. In here, we will discuss the applicability of the alumina/CNT composite to be used in the removal of lead ions from aqueous media in two modes batch and fixed bed mode.

Adsorbents such as alumina, silica and zirconia are well known by their high surface area, high mechanical properties and good resistivity to thermal degradation, and they exist in several structures and amphoteric properties. Alumina has been used for removal of different heavy metals such as nickel, lead and cadmium [Tarun et al., 2009]. Besides, activated alumina is considered as one of the common adsorbent used for heavy metal removal, pre-concentration and separation of trace amounts of elements in flow injection- inductively coupled plasma.

CNT has been used for removal of lead from water [Li et al., 2005; Anna et al., 2007]. However, the uses of CNT as support of metallic oxides introduce new chemistry. The advantages of this chemistry is that materials with higher sorption capacity, larger surface area and supported metallic oxides with better orientation degree with regard to net metallic oxides can be obtained.

In most wastewater flowing systems, because the contact time is not sufficiently long for the attainment of equilibrium, it is required to perform equilibrium studies by using columns. Fixed bed column tests have been widely used to predict the performance of full-scale fixed bed absorbers and to evaluate the mass transport parameters of many contaminants. Short bed adsorber column, is a fixed bed column with a bed of sufficiently short length that immediate concentration breakthrough occurs. Activated carbon, zeolite, cellulose were used as packing materials in a fixed-bed column for the removal of lead.

This work aims to investigate the adsorption behavior of alumina supported on carbon nanotube for the treatment of lead aqueous solutions. For this purpose, MWCNT/ Al_2O_3 composites were synthesized and characterized. The effect of contact time, dosage of adsorbent and agitation speed was studied and the relationship between pH and removal efficiency was analyzed. For comparison purposes, the same study was carried using functionalized uncoated MWCNTs. We were further interested in preparing a column filled with Al_2O_3 -coated MWCNTs composite. Different parameters, such as composites layer thickness and flow rate were investigated.

6.3. EXPERIMENTAL DESIGN

The contact time of lead is an important factor for lead ion removal. Adsorption experiments were conducted by preparing a 50-mL glass pyramid bottle containing 10mg of the adsorbent and 25 ml of 20ppm Pb^{+2} at a fixed pH. The glass bottle was placed on a slow-moving platform shaker and aliquots were taken from the suspension at different time intervals of the reaction. The concentration of Pb^{+2} in effluent solutions were analyzed by inductively coupled plasma spectrometer and removal or adsorption (%) versus reaction time was determined according to the following procedure. Adsorption experiments were performed in 50-mL glass pyramic bottles containing 25mL of different concentrations of lead.

To investigate the effect of adsorbent dosage, different doses adsorbents were added to each bottle. The influence of solution pH values on lead removal was also studied by adding defined amount of the MWCNT adsorbents into the glass pyramic bottles containing 25mL of different lead solution with pH values ranging from 3 to 7. All batch experiments were carried out at ambient temperature (25 ± 2 °C) and all the suspensions were shaken on a rotary shaker at 200rpm for 24 h.

The fixed-bed system, the column was packed with the synthesized composites. Then the prepared lead (II) solutions were passed through them in the bed to study their adsorption capacity. The different layer thickness of the adsorbent and the flow rate of the solutions were used as specified for each experiment. The metal uptake capacity

(amount of removal of lead ion) and the adsorption capacity (percentage of lead ion removal) were calculated using the following equations:

Metal Uptake Capacity = Initial lead ion concentration – Final lead ion concentration.

Adsorption Capacity or Lead Removal (%) = (Metal Uptake Capacity X 100) / Initial lead ion concentration.

6.4. PARAMETERS OPTIMIZATION

6.4.1. Batch mode

Effect of contact time: The effect of contact time on the removal of lead ions by the uncoated-MWCNT and alumina-coated MWCNTs is depicted in Figure 1. In both adsorbents, a rather fast adsorption of the lead ions occurs during the first hour of the adsorption process followed by a slower stage as the adsorbed amount of lead reaches its equilibrium value. Thus, 60 min were sufficient for the sorption equilibrium to be achieved. Coated-MWCNT has higher capacity for adsorption toward lead comparing with uncoated-MWCNT, as can be seen in Figure 1.

Effect of pH: pH is one of the most important parameters controlling the metal ion adsorption process. Thus, the influence of pH on adsorption capacity was studied over a range of pH values from 3 to 7 and not more than 7 for avoiding lead precipitation. As depicted in Figure 2, it was observed that lead adsorption increased when pH increased from 3 to 7. One explanation suggested that one of the contributions of MWCNTs

adsorption toward lead ions resulted from electrostatic attraction between the negatively charged MWCNTs adsorbent surface and the positively charged cationic lead.

The pH is a significant factor for determining the form of the metallic species in aqueous media. It influences the adsorption process of metal ions, as it determines the magnitude and sign of the charge on ions. The distribution of lead species as a function of pH is important. In case of low pH (<6), positively charged lead (II) species are dominant. In case of high pH values (pH = 7-11), however, there are several lead species with different charges. This includes Pb(OH)^+ and Pb(OH)_2 and thus the removal of Pb is possibly accomplished by simultaneous precipitation of Pb(OH)_2 and sorption of Pb(OH)^+ .

Effect of composite dosage: As depicted in Figure 3, it was observed that the percentages of lead adsorbed increased as the composite dosage was increased over the range 1mg to 50mg. The removal of approximately 100% was achieved when 50mg of the coated MWCNTs was soaked in 25 ml of 20 ppm lead solution comparing with 85% removal when 50mg of uncoated MWCNTs was used. Thus, the mechanism of composite adsorption toward cationic lead may be derived from three reasons. One reason might be based on van der Waals interactions occurring between the hexagonally arrayed carbon atoms in the graphite sheet of MWCNTs and the positively charged lead ions. The second one might be due to the electrostatic attraction between the positive cationic lead and the negative charged MWCNTs adsorbent surface. The third one might be due to the electrostatic attraction between the pairs of electrons on the oxygen atoms

of alumina and the positive cationic lead. The first two reasons are supported by the removal ability of unmodified carbon nanotube, as depicted in Figure 8. The third reason is supported by improvement in removal when alumina modified carbon nanotube was used for removal of lead, comparing the adsorption ability of carbon nanotube only.

Effect of agitation speed: The agitation speed plays an important role in the adsorption process. It was observed that the percentages of lead adsorbed increased as the agitation speed was increased up to 150 rpm. The removal ratio of lead increased from 20 to around 99% when the synthesized MWCNT/Al₂O₃ composites were used and from 10 to 50% in case of MWCNTs adsorbent. The adsorption capacity was greatest when 150 rpm speed was used, as shown in Figure 4.

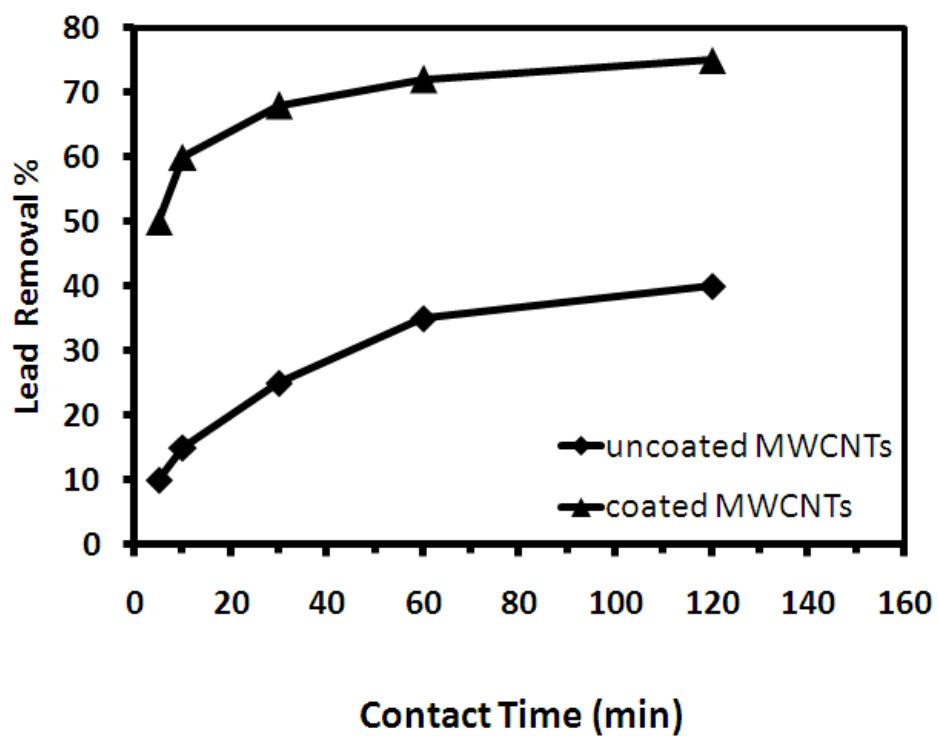


Figure 6-1 Effect of contact time on the percent removal of Pb(II) by uncoated MWCNTs and the alumina-coated MWCNTs. pH=5.5, agitation speed= 150 rpm, adsorbent dosage= 10mg

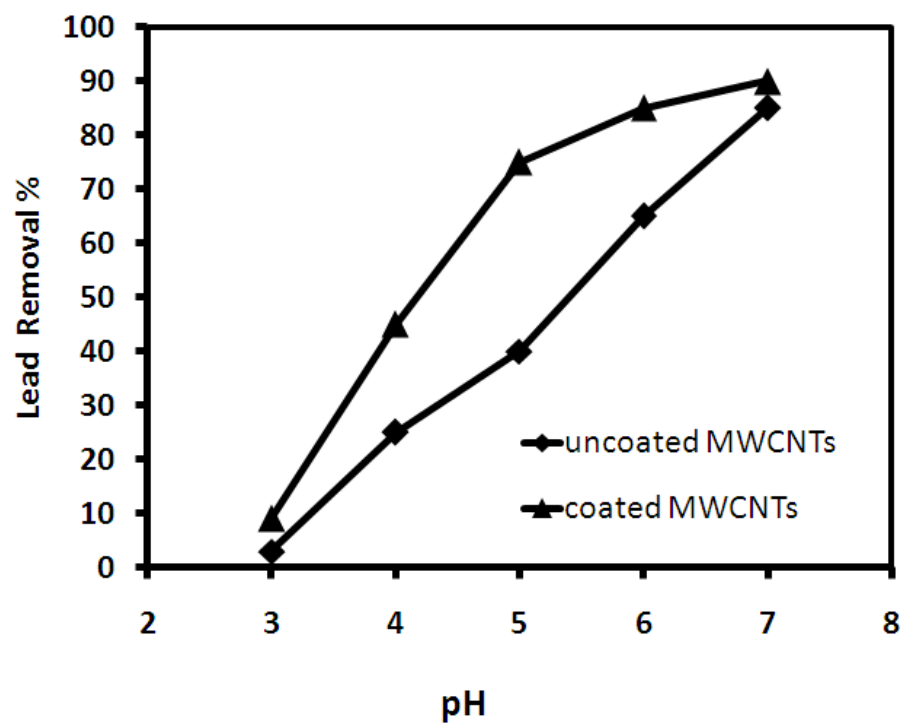


Figure 6-2 Effect of pH on the adsorption of Pb(II) ions. Initial Pb(II) conc.

Agitation speed= 150 rpm, adsorbent dosage= 10mg, Contact time 120 min.

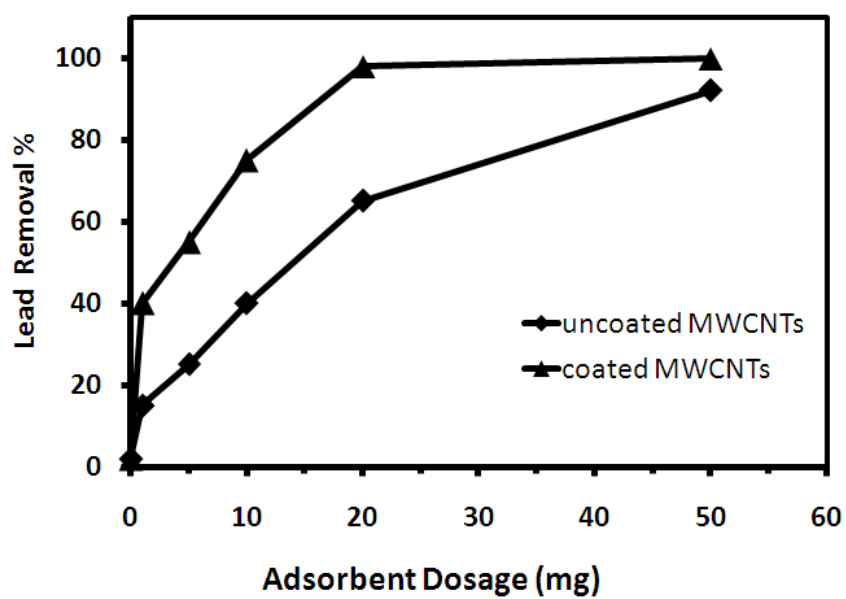


Figure 6-3 Effect of adsorbent dosage on adsorption of Pb(II) ions. Initial Agitation speed= 150 rpm, pH= 5.5, Contact time 120 min.

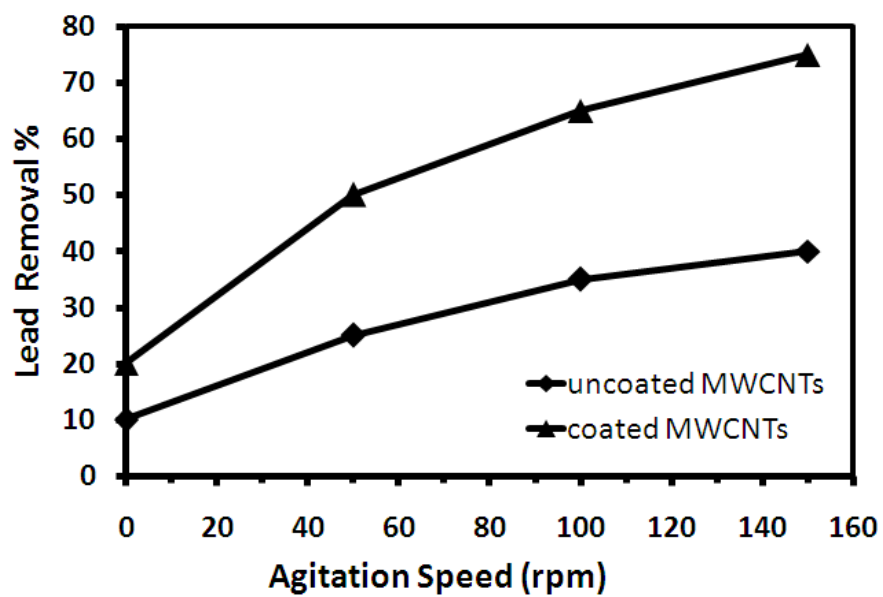


Figure 6-4 Effect of agitation speed on adsorption of Pb(II) ions. pH= 5.5, contact time 120 min, adsorbent dosage= 10mg

6.4.2. Fixed bed column experiments

To overcome the problems associated with the batch system, fixed mode is used. In fixed bed column, several parameters require to be optimized like bed thickness, flow rate and pH of the solution. The solution pH is an important factor in adsorption equilibrium and kinetics of metal ion. The curve for the percentage removal, adsorption of lead ions, at different initial pH values is shown in Figure 5.

Effect of layer thickness

Figure 6 shows the percentage removal of lead by coated-MWCNT of different thickness and at a flow rate of 7 mL/min. Increasing the thickness of the layer produces an increase in the adsorption of lead ions. This may be due to an increase of the surface area of adsorbent that provided more binding sites for adsorption of lead with a thicker layer and the efficiency is increased by allowing sufficient time for the lead adsorbate to diffuse into the whole mass of the adsorbent.

Effect of flow velocity

To investigate the effect of flow rate on the adsorption of lead ions into the synthesized composites, both the metal concentration in the feed solution and the layer thickness were kept constant, whereas the flow rate was changed from 1.0 to 7.0 mL/min. The results are given in Figure 7, where the uptake of lead ions decreased with an increase in

flow rate. This is because the time required to reach an equilibrium state is much longer than the time allowed by the flow rate. Therefore, increasing the flow velocity causes shorter retention time. The maximum adsorption efficiency was obtained at a flow rate of 7 mL/min.

It is worth mentioning that the fixed bed mode has some advantages over batch mode. The fixed bed adsorber is capable of reducing the solute concentration in the feed stream to very low levels. The conclusion from the study is that fixed bed adsorption was faster over batch adsorption. The use of fixed-bed column contractor can offer an advantage over batch-contact because it can achieve better separation and higher concentration ratio over several consecutive sorption-desorption cycles. In addition, in batch mode there is a need from filtration to separate the adsorber from the aqueous.

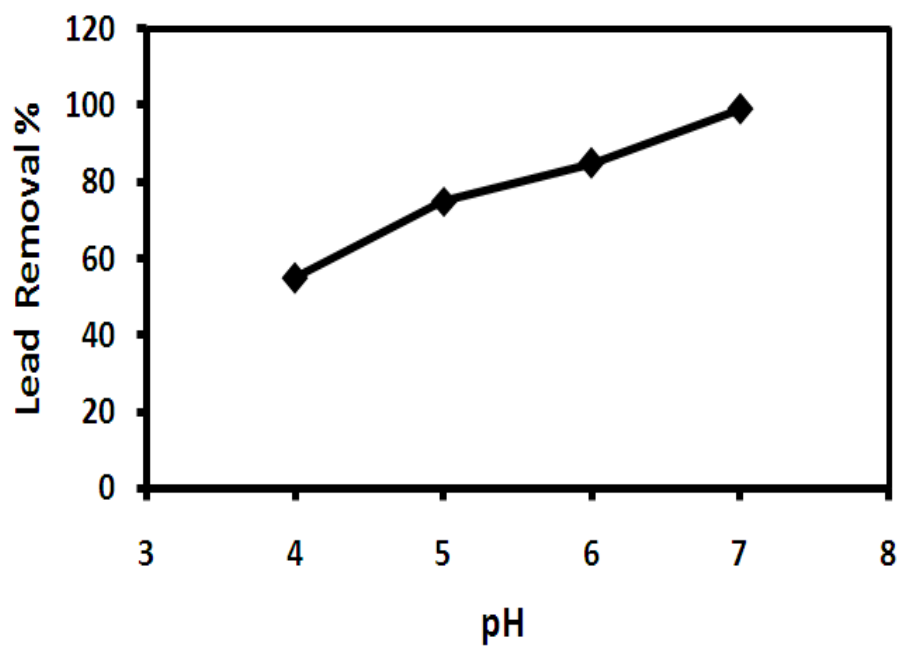


Figure 6-5 Effect of pH on adsorption of Pb(II) ions, in fixed bed system

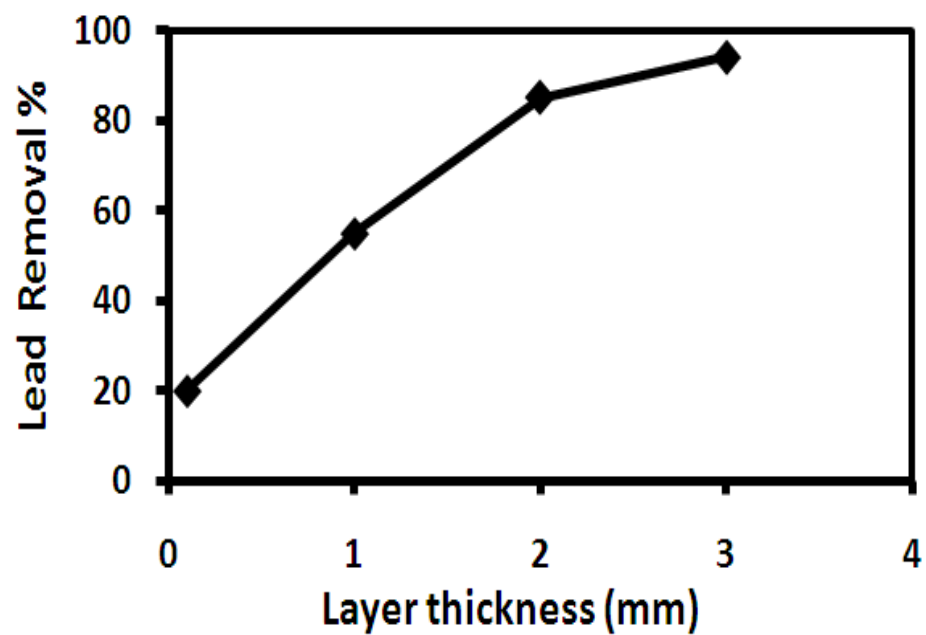


Figure 6-6 Effect of layer thickness on adsorption of Pb(II), in fixed bed system

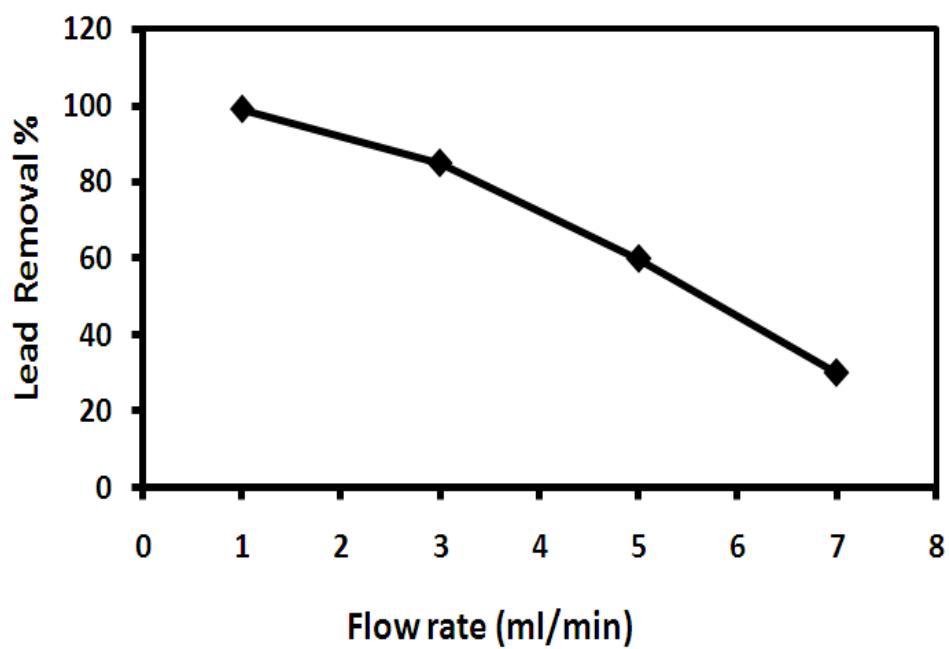


Figure 6-7 Effect of flow rate on adsorption of Pb(II) ions, in fixed bed system

CHAPTER 7

APPLICATION OF MAGNETIC-MWCNT

The application of magnetic particle technology to solve environmental problems has received considerable attention in recent years. One of the most important magnetic nanotechnologies is magnetic-carbon nanotubes. In chapter 4, we have introduced the synthesis methodology of magnetic-CNT. The characterization of such material was presented in chapter 5.

Providing a broad insight into the potential applications of magnetic-CNT composite, this chapter focuses on the possibility of utilizing such material for the removal of pollutants from aqueous media. Chromium has been used as model. Two systems have been utilized to test the applicability.

This chapter is arranged as follows; in the first section, a brief introduction is introduced to highlight the importance and rationalize the idea. In the second section, the experimental design is explained. Then, the results, of using the magnetic composite for the removal of chromium (III) in simple batch mode and fixed bed treatment mode, is presented and discussed.

7.1. OVERVIEW

Chromium remains the sole leather-tanning chemical since its first successful trial by an American dye chemist, Augustus Schultz. Tanneries use basic chromium sulphate (CrOHSO_4), which contains chrome in the trivalent oxidation state. Other main sources of chromium pollution are mining; cement ceramics and glass industries, uses in dyes, electroplating, and production of steel and other metal alloys, photographic material and corrosive paints (Rana, et al., 2004). According to EPA drinking water standards, the maximum limit of chromium in drinking water is 0.1 mg/L based on total chromium. Various naturally available adsorbents like wool, olive cake, sawdust, pine needles, almond shells, cactus leaves, charcoal used tyres, soot, hazelnut shell, coconut shell charcoal, banana peel, seaweed, dead fungal biomass, cyanobacterium, and green alga were used for the removal of chromium. However, many of these naturally available adsorbents have low chromium adsorption capacity and slow process kinetics. Thus, there is a need to develop innovative adsorbents useful both for industry and for the environment.

Unlike many adsorbents, CNTs possess different features that contribute to the superior removal capacities; such as fibrous shape with high aspect ratio, large accessible external surface area, and well developed mesopores. The pores have been reported to be mostly mesopores due to a high van der Waals interaction forces along the length axis (Wang, et al., 2006; Girifalco et al., 2000).

The application of magnetic-CNT to solve environmental problems is presented in this work. The adsorption features of multiwall carbon nanotubes (MWCNTs) with the magnetic properties of iron oxides have been combined in a composite to produce a magnetic adsorbent. The materials have the advantages of high sorption capacity, large surface area and supported metallic oxides.

7.2. EXPERIMENTAL DESIGN

Batch adsorption experiments were conducted by adding the composite mass to 50ml of different Cr(III) test solutions at different pH (3-7) in an Erlenmeyer flask (100ml capacity). The initial solution pH was adjusted using 0.1 M HCl or 0.1 M NaOH. The flasks were agitated at different speed (0-to-150rpm) in a rotary shaker for different contact time (10-60min). The composite mass was separated from the test solution by magnet followed by filtration using a vacuum filter. For the fixed-bed system, the column surrounded with a magnet was packed with the synthesized composites. Then the prepared Cr(III) solutions were passed through to study the adsorption capacity. The column diameter and length used in every experiment were kept constant with a bed depth of 1 cm and diameter of 0.3mm. The different layer thickness of the adsorbent and the flow rate of the solutions were used as specified for each experiment.

All experiments were carried out at ambient temperature (25 ± 2 °C). The amount of chromium adsorbed was calculated from the difference between its concentration in test solution and in the supernatant liquid. The initial and final concentrations of chromium

were analyzed by using inductively coupled plasma mass spectrometry (ICP-MS). The samples were filtered prior to spray chamber applications to remove the possible agglomerates.

7.3. PARAMETERS OPTIMIZATION

The adsorption capability of the magnetic-composites was tested in batch and fixed bed modes. Different parameters, such as contact time, agitation speed and pH, in the batch mode; and on flow rate and the bed thickness in the fixed bed mode, were optimized. In this section, the results will be presented with discussion.

7.3.1. 2 Results of Batch experiments

Effect of contact time

The influence of contact time on the adsorption capacity of activated carbon, MWCNTs and the produced composite is depicted in Fig. 1. Less than 5% adsorption by activated carbon was observed. According to the literature reports, activated carbon is expected to have a poor adsorption capacity for removal of contaminants comparing with MWCNTs. It is clearly stated that one of the disadvantages of using activated carbon is that it presents problems with the adsorption of hydrophilic substances (Kandah and Meunier, 2007; Pillay et al., 2009). Both MWCNTs and the MWCNTs/nano-iron oxide by contrast, show a good ability to remove Cr(III) from aqueous solution. The MWCNTs/nano-iron oxide, however, show a greater ability, approximately 90%

adsorption after 60min contact time. This can be explained by the additional adsorbing sites provided by the oxygen atoms of iron oxide nanoparticles, average size is 18 nm, on the surface of MWCNTs, which are also available for electrostatic interaction with the chromium. It should be noticed that in the composite there are two sorts of adsorbing sites; MWCNTs and iron oxide nanoparticles.

Effect of pH

The pH effect on the adsorption of Cr(III) onto the prepared composite was studied by evaluating the adsorption at pH values of 3, 4, 5, 6, and 7 as shown in Fig. 2. It was found that the composite effective for the adsorption of Cr(III) above pH 3 and below pH 7, since Cr(III) at strongly acidic media did not adsorb to the composite. Fig. 2 illustrates that maximum adsorption capacity at pH 5-6.

The result could be explained based on the reported speciation diagrams (Zhang, et al., 2008; Chuan, And Liu, 1996). It has been reported that at pH less than 3.6 , Cr(III) is present as Cr^{3+} while at pH higher than 4 and lower than 6.5, it is present as $\text{Cr}(\text{OH})^{2+}$ $\text{Cr}(\text{OH})_2^+$. However, it is present as neutral $\text{Cr}(\text{OH})_3$ species at pH between 7 and 12.

On the other hand, the point of zero charge (PZC) of oxidized MWCNTs was reported to be approximately 4 (Lu, and Chiu, 2006; Gao, et al., 2009). Thus, when it is placed in aqueous solutions of pH below its PZC=4 it becomes protonated and exhibits a positive net charge on its surface, thus it could not well adsorb the Cr^{3+} . In contrast, when placed

in solutions above its PZC=4, the net surface charge turns negative by deprotonation and it could adsorb the positively charged chromium species. At pH 7, the chromium presents as neutral $\text{Cr}(\text{OH})_3$ species, which has low affinity for electrostatic interaction with the positively charged composite of MWCNTs.

Therefore, at pH 7, coulombic or electrostatic interactions do not favor the adsorption of chromium. The maximum Cr(III) removal was 82 and 88% at pH 5 and 6, respectively. The association between Cr(III) and the composite is therefore governed by $\text{Cr}(\text{OH})^{2+}$ species, since $\text{Cr}(\text{OH})^{2+}$ dominates the system within this pH range (Chuan, and Liu, 1996).

Effect of agitation speed

The effect of agitation speeds was investigated by a range from 0 to 150 rpm, Fig. 3. The adsorption of Cr(III) was low without or at low agitation speed and rose as the agitation speed was increased to 150 rpm. This effect can be attributed to the decrease in boundary layer thickness around the adsorbent particles being a result of increasing the degree of mixing.

Effect of adsorbent dosage

Various amounts of adsorbent ranging from 5-100mg were used. The percentage removal of Chromium ions varied linearly with the amount of the adsorbent as shown in Fig. 4.

7.3.2. Results of fixed bed experiments

In this section, the results of the parameters' optimization is be presented and discussed in details. The optimized-parameters are flow rate and bed thickness. Then, the advantages of the system will be highlighted.

Effect of flow rate

Experiments were performed with flow rates of 1 to 5 ml/min whereas the thickness of the adsorbent was 3mm. As depicted in Fig. 5, it was observed that the lower the flow rate the higher the chromium removal. This is due to the more contact time when the flow rate is low.

Effect of bed thickness

The removal of Cr(III) by MWCNTs /nano-iron oxide fixed bed composite of different thickness at a constant flow rate of 1 mL/min. As shown in Fig. 6, by increasing the thickness of the fixed bed layer, the uptake of chromium ions increases. Increasing the fixed bed layer leads to increase of the available interaction sites of the composite that provided more sites for adsorption of chromium ions with a thicker layer and the efficiency is increased by allowing sufficient time for the adsorbate to diffuse into the adsorbent.

When the thickness of the layer of the composite was increased from 0.5mm to 3mm, the percentage removal was increased from 40 to 90%. Comparing with its efficiency in

batch mode, the prepared adsorbent displayed the main advantage of separation convenience when a fixed bed column was used. This is because the chromium anions are forced to interact with the active adsorbing sites on the large surface-area composite during the penetration.

Advantages

Along with the high surface area of the MWCNTs, the advantage of the magnetic composite is that it can be used as adsorbent for contaminants in water and can be subsequently controlled and removed from the medium by a simple magnetic process

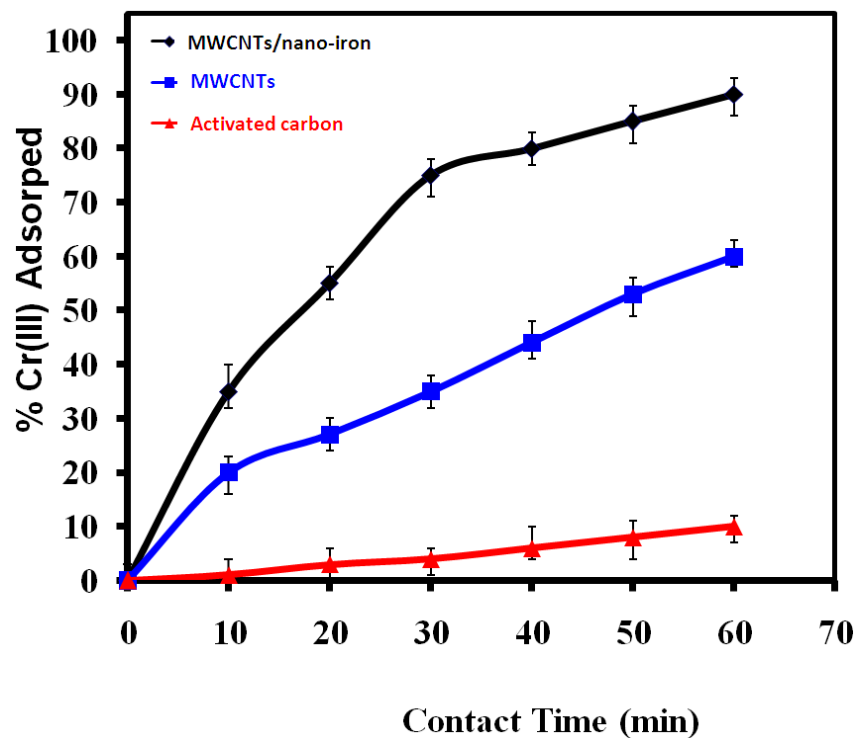


Figure 7-1 Effect of contact time on the amount of Cr(III) adsorbed on different adsorbents

Conditions: initial Chromium concentration 20ppm; Dosage of adsorbent = 50mg; pH 6;

Agitation speed = 150 rpm

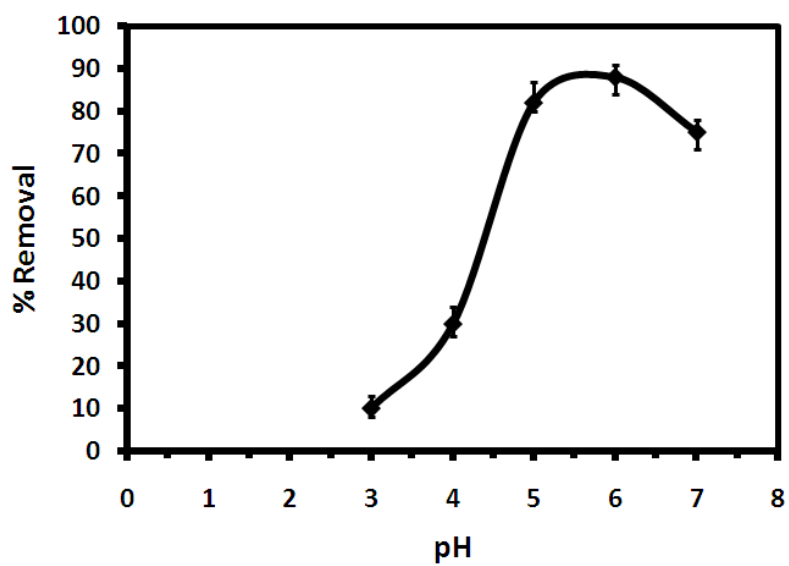


Figure 7-2 Effect of pH on the amount of Cr(III) adsorbed on the MWCNT/nano-iron oxide

(Other conditions: as in Fig.7-1)

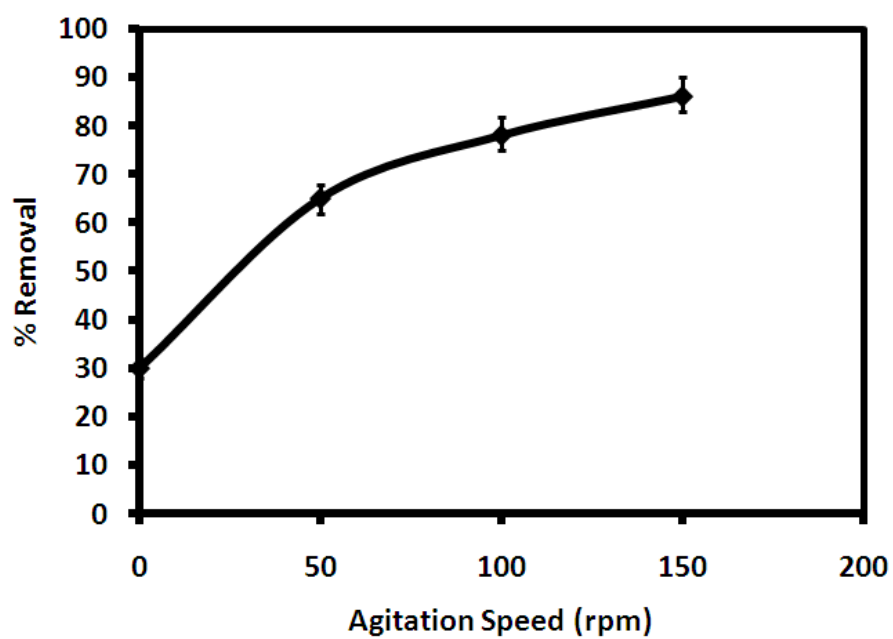


Figure 7-3 Effect of agitation speed on the amount of Cr(III) adsorbed on the MWCNT/nano-iron oxide

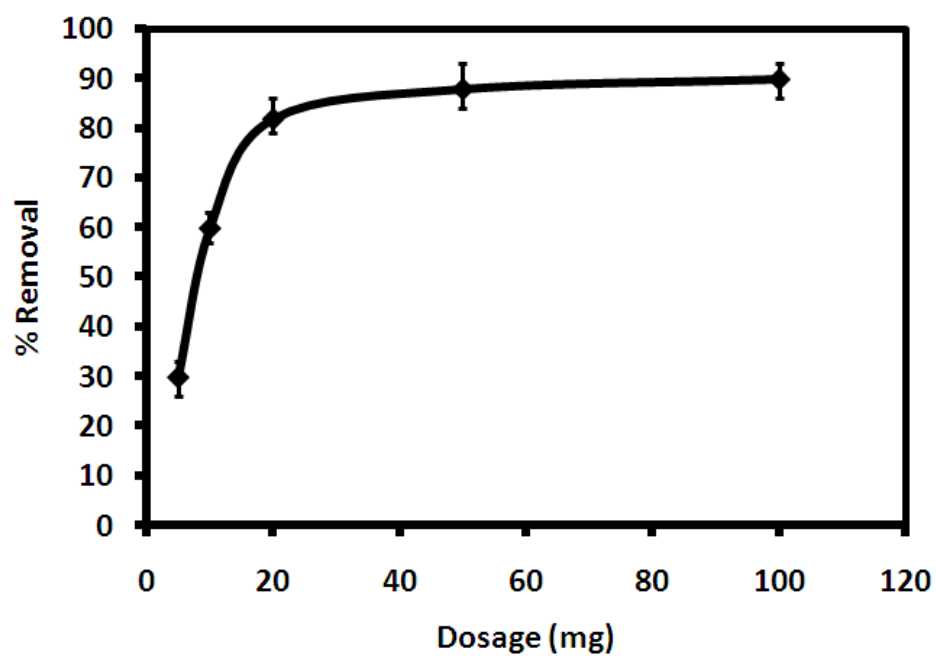


Figure 7-4 Effect of dosage on the amount of Cr(III) adsorbed on the MWCNT/nano-iron oxide

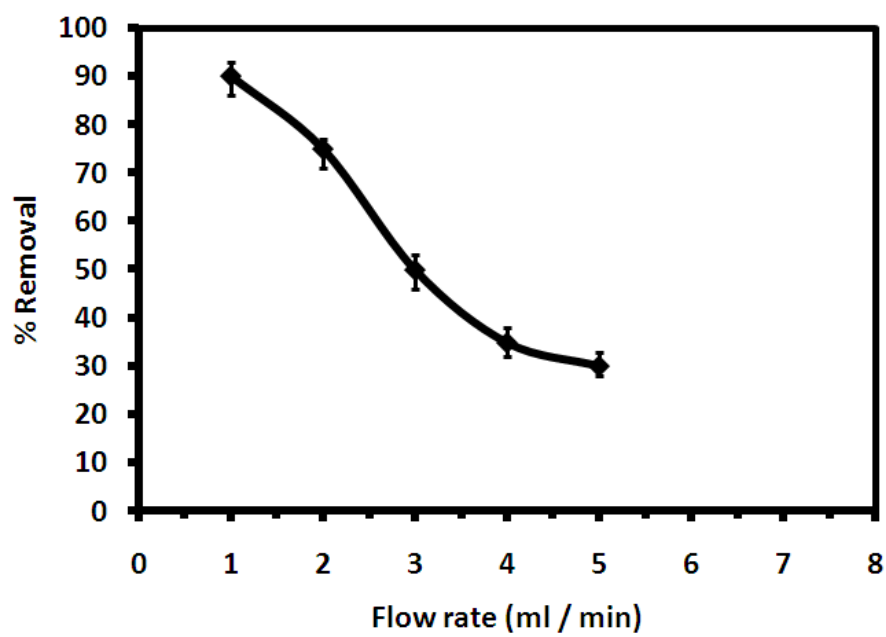


Figure 7-5 effect of flow rate (ml/min) on the amount of Cr(III) adsorbed on the MWCNT/nano-iron oxide

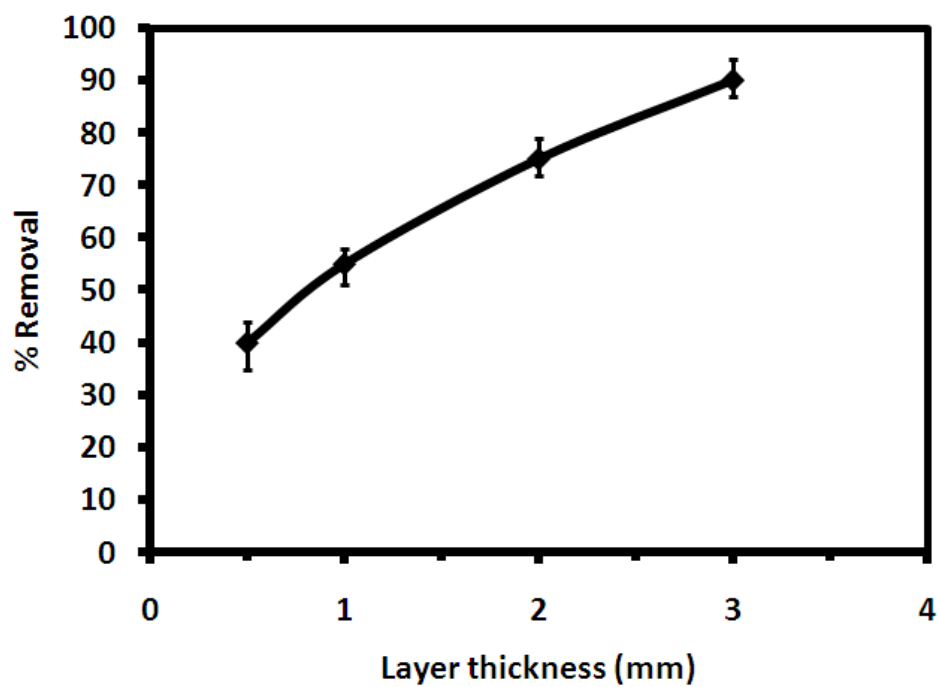


Figure 7-6 Effect of layer thickness on the amount of Cr(III) adsorbed on the MWCNT/nano-iron oxide

CHAPTER 8

APPLICATION OF MWCNT/MANGANESE COMPOSITE

8.1. INTRODUCTION

The chapter provides the application of the synthesized multiwall carbon nanotube/manganese oxide (MWCNT/MnO₂) composite for removal of arsenic selected as a model to show the applicability of the composite in water treatment. In the first part, a short rationalize of the work is introduced. The second part provides with the materials used and the experimental design. In the third part, the results are presented with interpretation and discussion.

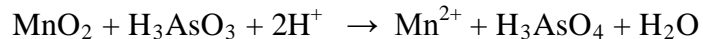
8.2. HIGHLIGHTS

It is well known that arsenic is one of the most toxic and carcinogenic substances that can pollute the water. Generally, arsenic exists mainly in two forms arsenite with oxidation state of (III) and arsenate with oxidation state of (+V). At natural waters, As(V) exists as anionic species; a monovalent (H₂AsO₄⁻) or divalent (HAsO₄²⁻) anion, while As (III) exists as neutral species (H₃AsO₃) [Smedley and Kinniburgh, 2002]. Thus, As (III) is more mobile in natural waters than As(V), and in turn it is less

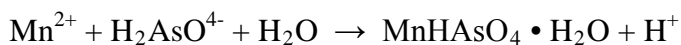
efficiently removed in adsorption processes than arsenate because of its low affinity for adsorbents. Therefore, oxidation of As(III) species to As(V) is desirable to enhance the immobilization [Lee and Choi, 2002]. Several technologies are used to remove arsenic from waters based on oxidizing As(III) to As(V) and then adsorb the As(V). Out of different materials, it has been found that manganese oxide (birnessite) [Driehaus et al., 1995], is considered the best for oxidation of arsenite to arsenate and adsorption of the resulted form. However, the problem associated with manganese oxide is its precipitation with the arsenate to form manganese (II) Arsenate [Tournassat et al., 2002].

The As(III) species is substantially more toxic than As(V) and tends to be more weakly bound to soils than As(V). This is most probably due to the tendency for As(III) to adsorb more weakly to most aluminum oxide and aluminosilicate soil minerals than As(V). An important reaction in the environmental fate of As(III) is heterogeneous oxidation on soil mineral surfaces. Manganese oxides are extremely important minerals because they readily oxidize many reduced species such as As(III), Co(II), Cr(III), and organic molecules. The crystalline structures of Mn oxides are of environmental interest because of the adsorptive and oxidative capabilities of these minerals.

Details about the chemical mechanism of As(III) heterogeneous oxidation by birnessite indicates that the oxidation of As(III) by synthetic birnessite is coupled with the reductive dissolution of the MnO₂ surface and results in the release of both As(V) and Mn(II) to solution at low pH. The net stoichiometry of the reaction is (Manning et al., 2002)



The ion activity product of Mn(II) and As(V) reached after 74 h reaction time was the solubility product of a protonated manganese arsenate. The manganese arsenate precipitate formed long fibers that aggregated at the surface of H-birnessite. The oxidation reaction transforms a toxic species, As(III), to a less toxic aqueous species, which further precipitates with Mn^{2+} as a mixed As-Mn solid (Tournassat et al., 2002)



Therefore, an alteration of the MnO_2 surfaces during oxidation by creating new adsorption sites for As(V) is needed. To help overcome the formation of manganese arsenate precipitate, a composite of multiwall carbon nanotube and manganese oxide (MWCNT/ MnO_2) has been synthesized. The composite combines the high adsorption capacity of MWCNT with oxidation ability of MnO_2 . In this work, this composite has been tested for oxidation of As(III) and adsorption of As(V) and the results are presented.

8.3. EXPERIMENTAL DESIGN

This section provides a description of the materials used and the experimental designed for this application. It contains the materials and chemicals used in this work. Then, explanation of how the oxidation and adsorption experiments were performed. The

results then are presented and discussed, in details, to reflect the efficiency of the multiwall carbon nanotube/manganese oxide (MWCNT/MnO₂) composite.

8.3.1. Materials

The arsenate stock solution was prepared from sodium heptahydrate arsenic salt Na₂HAsO₄·7H₂O (Sigma, purity 98%). The arsenite stock solution was prepared from arsenic trioxide As₂O₃ (Sigma, purity 99%). A stock solution (1000 mg/l) As(III) was prepared in distilled water by dissolving 1.320 g of arsenic trioxide in 10 ml of concentrated hydrochloric acid. The resulting solution was diluted and then neutralized with 3.6 M potassium hydroxide and diluted to 1L. A stock solution (1000 mg/l) As(V) was prepared by dissolving 4.16 g of sodium heptahydrate arsenic salt in distilled water.

8.3.2. Oxidation and adsorption experiments

Dry o-MWCNTs or MWCNT/MnO₂ composite suspensions were used to carry the experiments in presence of arsenite or arsenate solutions in closed flasks. The flasks were on a rotary shaker at 100 rounds per minute at room temperature (25 °C ±1). Samples were collected at various time points and arsenic concentration was measured by ICP-AES.

8.3.3. Desorption experiments

Arsenic desorption was performed by immersing the dry As-loaded MWCNT/MnO₂ composite in 100 ml of 1.5 M NaOH solution. The solution was then filtered and the solid was put in contact with the same arsenic solution as in the first retention stage. The concentration of arsenic was determined by ICP-AES

8.4. RESULTS AND PARAMETERS OPTIMIZATION

This section presents the results obtained by the application of the composite for the oxidation of arsenite to arsenate and the adsorption of arsenate. The optimization of the experimental parameters is described and rationalized. A mechanism is provided at the end with a rationalization description.

8.4.1. Contact time effect

First, the equilibrium time was determined with an As(III) or As(V) concentration of 20ppm. At regular time intervals, arsenic concentration was determined. Equilibrium time was obtained within 1h. It should be noted that no significant soluble Mn was observed in the solution after the composite adsorbent reacted with As(III).

The effect of contact time (0–60 min) on the adsorption of As(III) and As(V) is depicted in Fig. 1. The o-MWCNTs show low adsorption efficiency toward As(III). This is in consistent with previous studies findings that As(III) is less strongly sorbed than As(V)

to a variety of sorbents [Mohan and Pittman, 2007]. So, pre-oxidation step is required to convert As(III) to As(V) in order to achieve the removal of As(III) [Maji et al., 2008]. As it is depicted in Fig. 1, with the composite consisting of MnO₂ as oxidant and MWCNTs as adsorbent, As(III) removal efficiency increases rapidly with an increase in contact time up to 60 min; and a maximum removal efficiency of more than 95% was achieved. In addition, it is clear from the figure that most of the removal (55%) occurs in a contact time of 10 min. One reason for the higher adsorption efficiency of the composite comparing with o-MWCNTs is that the MnO₂ nanoparticles, decorated on the surface of MWCNTs, oxidize As(III) to As(V), which in turn is absorbed by MWCNTs. Fig 2 shows that As(V) adsorption by o-MWCNTs and the composite increases with an increase in contact time. It is noticed also that no significant difference in the adsorption of As(V) between the composite and o-MWCNTs. However, the slightly higher As(V) adsorption ability of o-MWCNTs comparing with MWCNT/MnO₂ is attributed to the difference in surface area, which was measured using the BET method, and found to be 130 and 110 m²/g for the o-MWCNTs and MWCNT/MnO₂ respectively.

8.4.2. pH effect

The effect of variation of the initial solution pH on the adsorption of As(III) and As(V) was investigated by changing the initial pH as 4, 5.5, 7 and 9. As presented in Fig 3, the efficiency of arsenic removal increases with increasing pH from 4 to 5.5 and then there

is no significant change by increasing the pH to 7. However, the efficiency decreases by increasing the pH to 9. The maximum As(III) and As(V) removal efficiency at pH 5.5 was 90 and 95%, respectively.

This can be explained based on the arsenic speciation. At pH range between 1 and 9 As(III) is present as neutral H_3AsO_3 and as AsO_2^- species at pH higher than 9 while As(V) is present as anionic species $\text{H}_2\text{AsO}_4^{-1}$ in the pH range of 3-7 and as HAsO_4^{-2} in pH range between 7 and 12. Thus, within our experimental pH range 4 to 9, As(III) is present as neutral HAsO_2 species and As(V) is present as anionic species. The point of zero charge (pH_{PZC}) of the experimented MWCNT/ MnO_2 nanomaterial composite was found to be 4. Therefore, at the pH value > 4 , the net surface charge of the composite was expected to be negative. Therefore, columbic or electrostatic interactions do not favor the sorption of arsenic. Thus, this retention could be attributed to other mechanisms of chemical interactions through, e.g. surface complexation and ion exchange [Ouvrard et al., 2002].

These results are consistent with findings of previous studies regarding arsenic removal by sorption onto manganese oxides. Previous studies have suggested that pH should not affect the redox reaction between arsenate(III) and MnO_2 . A definite influence of pH is only obvious at pH-values below 5 with a reaction order of zero with respect to H^+ activity [Driehaus et al., 1995].

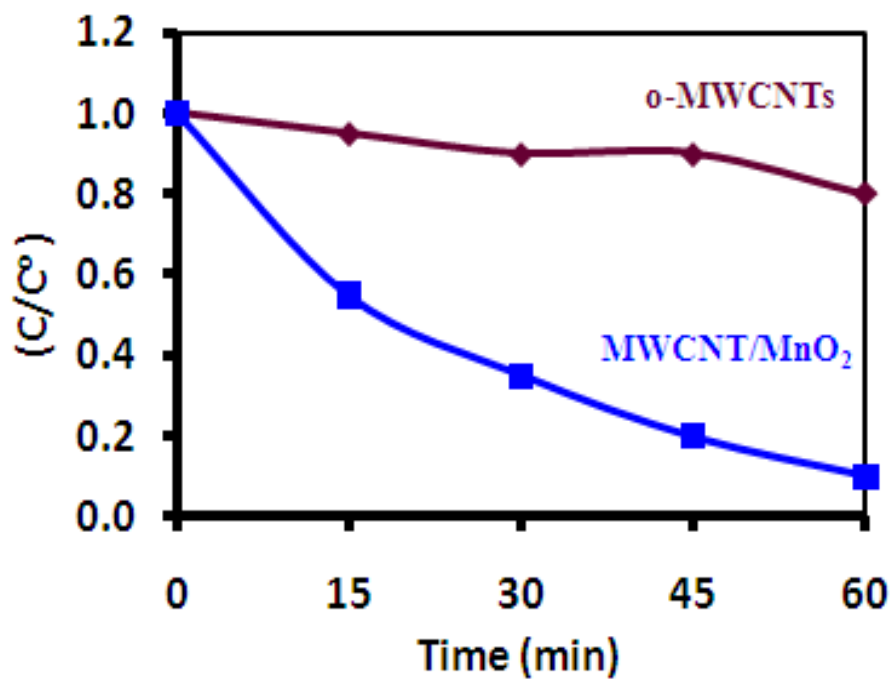


Figure 8-1 Change in As(III) content in solution vs. time (min) reaction for *o*-MWCNTs and MWCNT/MnO₂

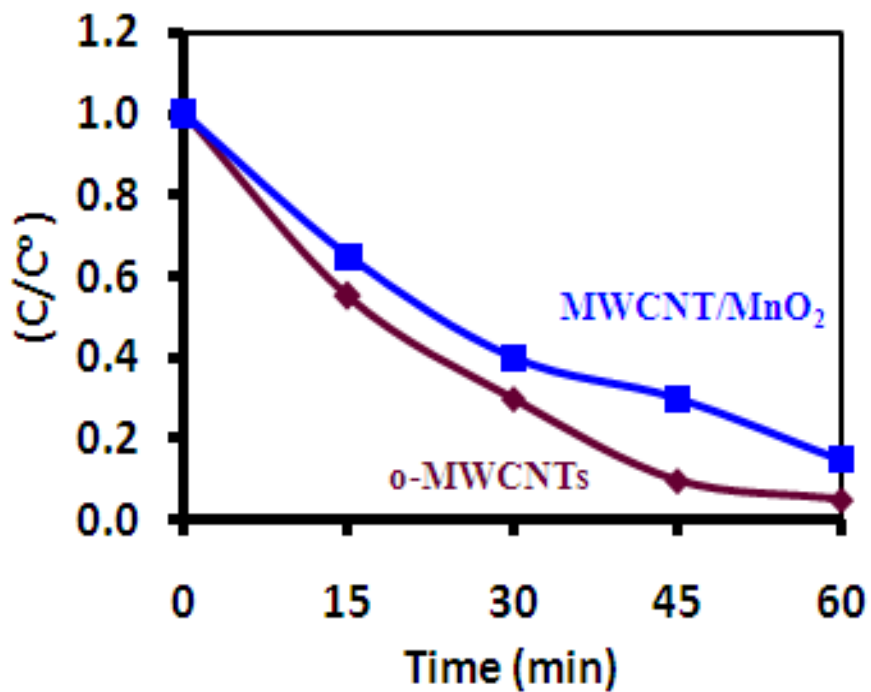


Figure 8-2 Change in and As(V) content in solution vs. time (min) reaction for o-MWCNTs and MWCNT/MnO₂

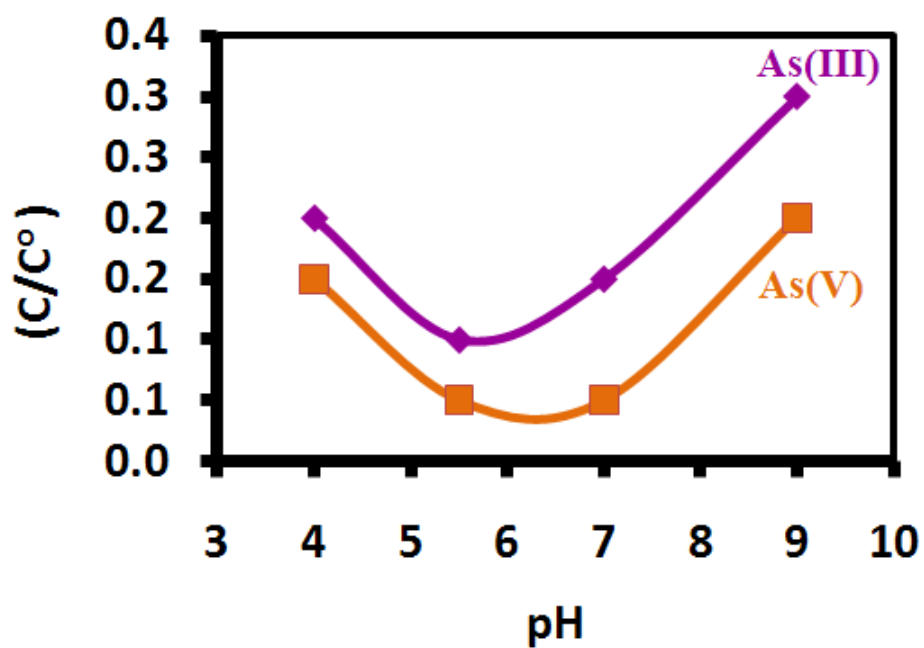


Figure 8-3 Influence of pH of the solution on As(III) and As(V) adsorption;
Experimental conditions: Amount of dosage 0.2g/L; Contact time 60 min.

8.4.3. Desorption

After the arsenic adsorption process by the MWCNT/MnO₂ composite, the SEM image and EDX analysis was conducted and presented in Fig. 4a,b. The composition consists of carbon, oxygen, manganese and the arsenic as adsorbate. As illustrated in Fig. 4, the desorption process was conducted by immersing the matrix of adsorbent-adsorbate in NaOH solution for 1h. It was then filtered and rinsed with deionized water. This followed by drying at 100 °C prior to the SEM image and EDX analysis. The regeneration of the composite was noticed to be successful since the adsorbate was removed without effect on the composite structure. This was confirmed also by FTIR spectrum, which shows the same peaks as of the composite. This composite was used for removal of As(III) under the same conditions. The arsenic percentage removal in the second stage was almost similar with that of the first and the difference was within the experimental errors.

It should be noted that to have a good representative EDX analysis, SEM image should be taken of large surface sample, i.e. the SEM would be of low resolution. Figure 5 depicts SEM image of MWCNT/MnO₂ composite after regeneration. It shows the presence of manganese oxides nanoparticles on the surface of MWCNTs. Schematic representation of the regeneration process is depicted in Fig. 6.

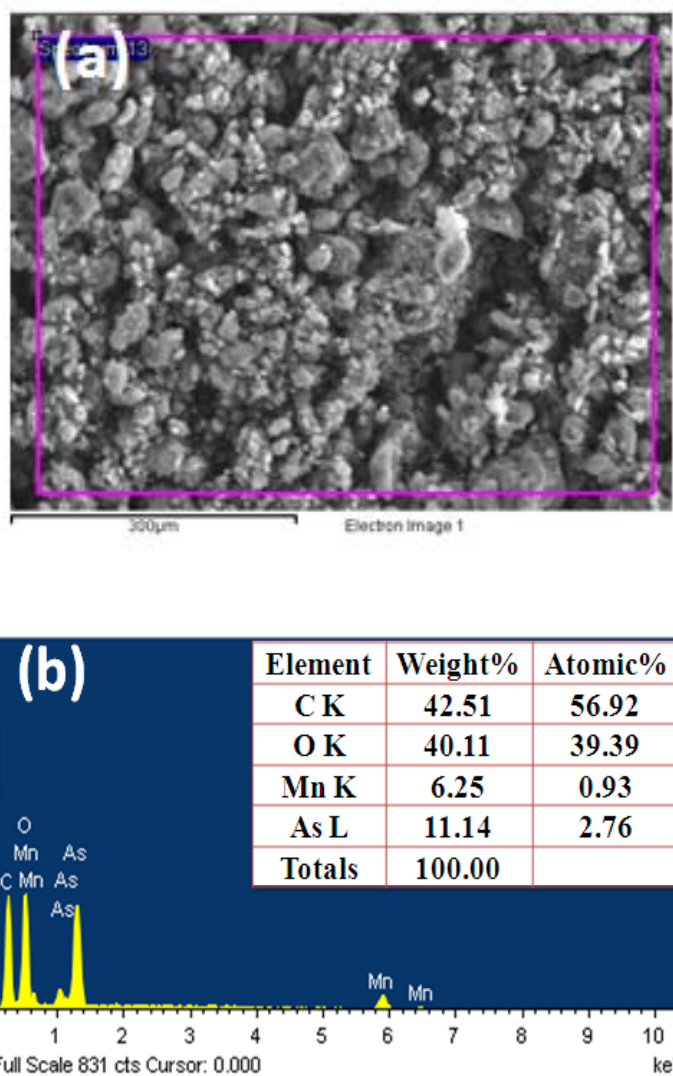


Figure 8-4 SEM image of MWCNT/MnO₂ composite after adsorption of arsenic

(a); with Energy dispersive X-ray (EDX) spectrum (b)

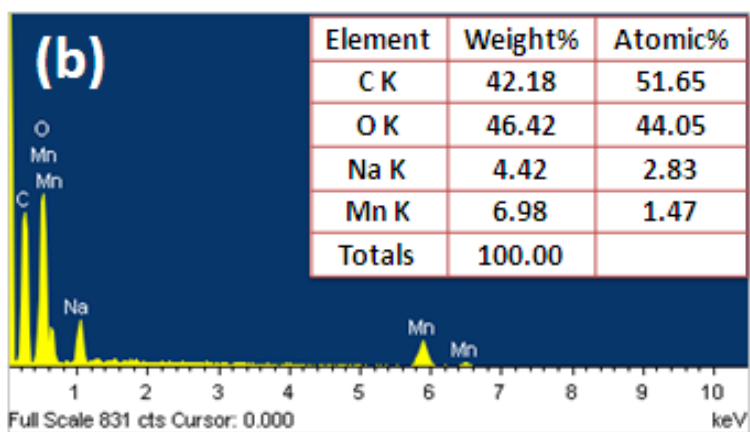
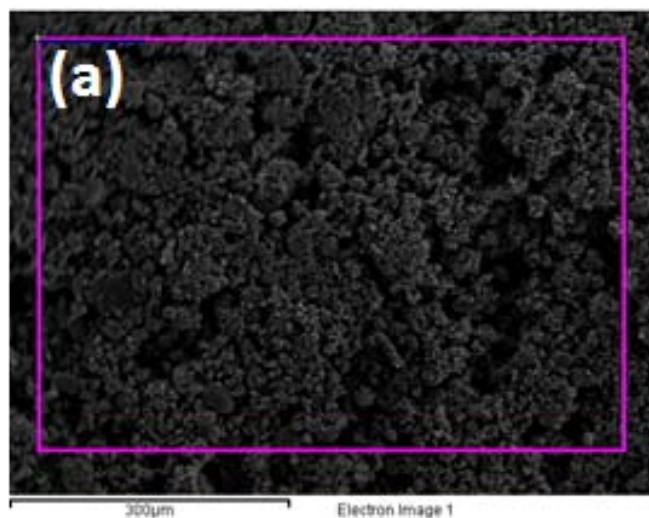


Figure 8-5 SEM image of MWCNT/MnO₂ composite after regeneration (a); with energy dispersive X-ray (EDX) spectrum (b)

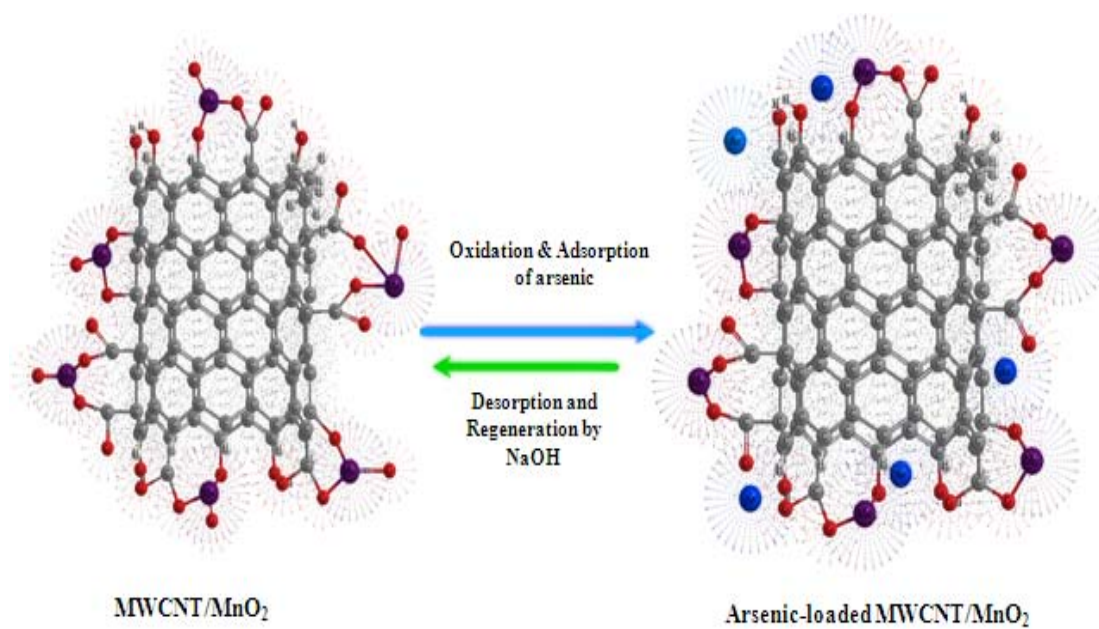


Figure 8-6 Schematic representation of the regeneration process

8.5. MECHANISM

The proposed mechanism consists of two steps; (1) oxidation of As(III) to As(V); (2) adsorption of resulted As(V), Fig. 7. A possible explanation of the first step is that manganese (IV) oxide of the composite oxidizes As(III) to As(V) [Lenoble et al., 2004], reduction of Mn(IV) to Mn(II) accompanied by oxidation of As(III) to As(V). The resulted reduced manganese (II) oxide is fixed by bond with the oxygen atoms of o-MWCNTs. At the same time electrons transfer from As(III) to the manganese and release of As(V).

The adsorption process is explained as follow. It is well known that the oxygen electronegativity, 3.44, is higher than that of arsenic, 2.18. Thus the electrons of O-As bond are attracted to the more electronegative atom of the bond, resulting in a shift of electron-density toward the oxygen atom. As a result the dipolar nature of these bonds leads to positive ends towards arsenic. Therefore, interaction between these positive ends and the pair of electrons on the oxygen atoms bonded with MWCNTs. Another possible interaction is between these arsenic positive ends and the out-of-plane bond (the π -bond) of MWCNTs. It should be noticed that the out-of-plane bond results from the curvature structure of nanotube, which plays a key role in determining the binding affinity [Mu et al., 2008]. Although this interaction is relatively weak contribution, it is more available on the non-decorated zones of MWCNTs' surface. This is because the electron density of the π -bonds is more in the outer surface of MWCNTs than inner surfaces as a result of the curvature. Other reports demonstrated that as a result of

curvature, the open carbon tubes are slightly positive on the inner surfaces and negative [Wang and Bu, 2007] on the outer lateral surfaces. The other possibility is the interaction between oxygen of arsenic oxyanions and hydrogen on the surface of MWCNTs through formation of hydrogen bond.

Stirred reactor experiments indicate that As(III) is oxidized by MnO_2 followed by the adsorption of the As(V) reaction product on the composite.

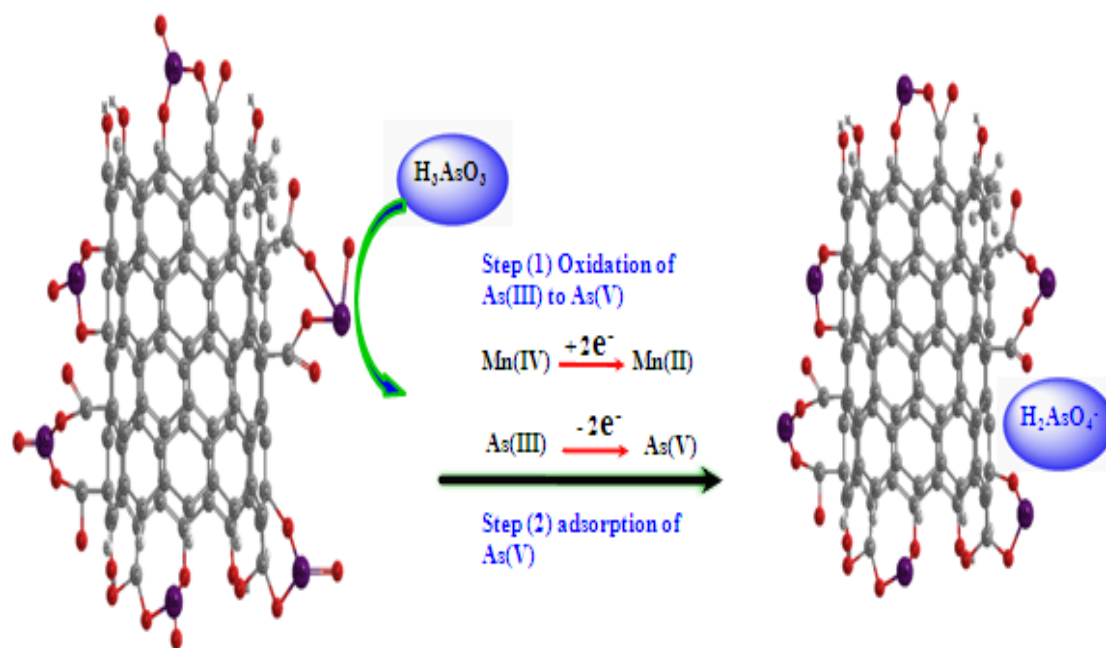


Figure 8-7 Proposed mechanism of oxidation and adsorption process of arsenic

CHAPTER 9

APPLICATION OF MWCNT/ZINC OXIDE COMPOSITE

This chapter discusses the applicability of multi-walled carbon nanotube to be used as support for catalysts. In this work, multi-walled carbon nanotube/zinc oxide (MWCNT/ZnO) composites was prepared as discussed in chapter 4, and characterized as presented in chapter 5. In this chapter, the results of the application of MWCNT/ZnO for the degradation of cyanide are presented and discussed in details.

9.1. INTRODUCTION

Being a very toxic compound, cyanide compounds originate, in the environment, from different sources, mainly industrial sources. These sources include metal mining, metal refining, metal plating, metal cleaning and electroplating industries. For instance, potassium cyanide and sodium cyanide are frequently employed and used in mining for releasing precious metals such as gold and silver from the ore. From these sources, cyanide compounds enter the environment by different pathways. As a result, these compounds can release free cyanide and HCN, which are extremely toxic to animal and human. For example, cyanide at concentration as low as 50 ppb can kill brown trout. Thus, in Asia, started in the early 1960s mainly in Philippines, cyanide is used for

fishing. Therefore, its use spreads throughout Southeast Asia and many other areas of the world. In addition, cyanide leaching, which is one of many gold extraction technologies, has replaced the mercury amalgamation. It involves spraying NaCN solution, approximately 200 to 600 ppm, on piles of ground ore or waste rock. Gold forms a distilled water-soluble compound with the cyanide. Gold then can be extracted by passing the solution over an activated carbon. The leftover cyanide solution is stored in covered ponds. Monitoring of cyanide is demanded for environmental control.

9.2. HIGHLIGHTS

Cyanide-contaminated water is often treated by physical (ion exchange, adsorption or separation), biological and/or chemical methods involving oxidation of cyanide by reagents such as SO₂-air, chlorine, permanganate, hydrogen peroxide, air and/or ozone [Bozzi et al., 2004]. However, these physical methods are only used to separate cyanide into another phase without degrading them and therefore require secondary process for complete removal of cyanide.

The advanced oxidation processes can be used, and photo-catalytic oxidation of cyanide at semiconductor surface offers distinct advantages for disposing of cyanide form waste water. It ensures complete mineralization of cyanide without the use of large amount of chemicals and waste generation that could create additional environmental problems. Thus, photo-degradation method for cyanide removal is considered to be relatively an environmentally friendly method. A large number of semiconductor catalysts have been

applied as photo-catalysts. The photo oxidation of cyanide using various photo catalysts such as TiO_2 , ZnS , ZnO , CdS , V_2O_5 , SiO_2 and Fe_2O_3 has been investigated.

The unique properties of ZnO such as high sensitivity for UV–vis light, wide bandgap (3.3 eV), high stability & catalytic activity, large excitonic binding energy of 60 meV and low resistivity, have motivated the researchers to utilize it as catalyst for different applications. Due to these unique properties, ZnO has been used extensively in the field of photocatalysis either alone or with other elements [Wang et al., 2009; Anandan et al., 2007]. However, its efficiency is not high as a result of the recombination process. ZnO nanocrystals-coated MWCNTs composite was prepared through noncovalent modification of MWCNTs with sodium dodecyl sulfate has been reported [Jiang and Gao, 2005]. However, it is difficult to remove the surfactant used in this method, which may affect the photocatalytic activity for removal of pollutants. In our simple preparation method of ZnO nanocrystals-coated MWCNTs, there is no need to use surfactants, as discussed in chapter 4.

The as-prepared material has been used as catalyst for the photo-degradation of cyanide. In the next part, the experimental setup will be discussed. This is followed by a discussion of the obtained results.

9.3. EXPERIMENTAL SETUP

In this experiment, a 2 mm diameter aperture was located inside the path of UV beam in order to get a uniform beam shape. Cyanide -water solution in known concentration was

prepared and added inside the reaction chamber. To this solution, an appropriate amount of the MWCNT-ZnO composite was added. The source of the UV is a Q-switched Nd-YAG laser (Spectra Physics Model, GCR 100) operating at 355 nm wavelength using third harmonic generator was employed as an excitation source. It can deliver maximum pulse energy of 300 mJ with a pulse width of 8 ns and operates at a 10 Hz pulse repetition rate. Different parameters such as irradiation power, exposure time, composite dosage and cyanide concentration were optimized.

9.4. PHOTO CATALYTIC DEGRADATION OF CYANIDE

For the cyanide removal by photo-degradation, the system was installed, and it is also of important to optimize several experimental parameters. In this section the results of the parameters optimization are presented and discussed.

9.4.1. Parameters' Optimization

The parameters that have been optimized are irradiation time and energy, the pH of the solution, and the dosage of the catalyst composite.

Influence of Laser Irradiation Time

Irradiation time plays important role on the efficiency of the cyanide removal was investigated and is depicted in Fig. 1. It can be observed that almost 90% cyanide has been decomposed after the 30 min laser irradiation.

However, increasing the laser irradiation time, up to 40 min, results in total removal of cyanide. It confirms that cyanide is surely decomposed by the photo-catalytic reaction in presence of MWCNT/ZnO nanocomposite. In order to understand the effect of various parameters on removal process like cyanide adsorption on MWCNTs, or laser photolysis in degradation of cyanide without catalyst or the effect of photocatalytic process using MWCNT/ZnO, in depth study for cyanide removal was conducted.

For this purpose, four series of experiments were performed for the purpose of finding out the efficiency of the composite. In the first set, the cyanide solution was irradiated with 200 mJ UV laser without MWCNT/ZnO presence. In the second set of experiment, the cyanide solution was irradiated in presence of synthesized pure ZnO nanoparticles. In the third and fourth set of experiments, the cyanide solution was irradiated in presence of MWCNTs alone and MWCNT/ZnO composite respectively. As depicted in Fig. 1a, very little degradation was observed with the laser photolysis without presence of any catalyst for 60 min laser irradiation. Similarly less than 10 % degradation was achieved due adsorption of cyanide on the surface of MWCNTs as shown in Fig. 1b when 10mg of pure MWCNTs was added into the cell and solution was irradiated.

Approximately 50% of cyanide was degraded, in the presence of both ZnO and laser light, Fig. 1c. The photocatalytic degradation of cyanide in presence of semiconductor

catalyst like ZnO can be explained as follows. The process is initiated by photo-excitation of ZnO, followed by the formation of an electron-hole pair on the surface of catalyst (Equation 1). The electron and hole pair then interact with the water molecule and generates hydroxyl radicals (HO \cdot) (Equation 2 & 3) and superoxide radical (O $_2^{\bullet-}$) by reducing molecular oxygen to superoxide anion (Equation 4). The generated hydroxyl radicals (HO \cdot) oxidize CN into cyanate (Equation 5).



Cyanate is further oxidized to carbonate and nitrogen is carried out by the photo-generated radicals due presence of the zinc oxide [Rose and Nanjundiah, 1985].

The photocatalytic effect of the pure ZnO nanoparticles alone and MWCNT/ZnO composite is presented in Fig. 1c-d. Compared with pure ZnO, the decomposition efficiency of MWCNT/ZnO composites is almost double in the cyanide removal processes. This clearly indicates that the ZnO has better catalytic activity when it is loaded onto carbon nanotube. This can be explained that the presence of zinc oxide on MWCNTs helped in the electron transfer process from valence to conduction band and

thus generation of electron and hole pair. The result shown in Fig. 1 indicates that the cyanide degradation likely proceeds on 1st order in cyanide concentration. These results also suggest that the rates are limited not only by the wavelength (frequency) of excitations (the intrinsic photocatalytic activity of the materials), but also most likely by the adsorption process of cyanide as shown in Fig 1b. In this case, the surface areas of the materials, especially ZnO, plays major role that is much higher for nano structured ZnO.

A schematic diagram for the mechanism was also presented as shown in Fig. 2. It was proposed based on two roles of MWCNTs, the electron transfer and the adsorption capability. MWCNTs are conducting materials and the excited electron generated in conduction band of ZnO can be transferred to MWCNTs as depicted in Fig.2a. The electron transfer to MWCNT can help separating charges, and thus reducing the recombination, which could enhance the photocatalytic activity. This is due to the fact that MWCNTs are known to function as an electron acceptor. The electron in the conduction band of ZnO can reduce molecular oxygen to generate the superoxide anion, which is considered highly active radical. On the other hand, the positive charge generated on MWCNT/ZnO⁺ surface due to the laser absorption can create hydroxyl radicals, which are then responsible for the degradation of cyanide into cyanate. In addition to electron transfer, the large surface area of MWCNTs could enhance the adsorption capability of the composite, which is considered another major reason for augmentation in photocatalytic activity of the synthesized ZnO -coated MWCNTs as shown in Fig. 2b.

Influence of Laser Irradiation Energy

Incident laser energy effect on the removal of cyanide was investigated for this purpose, the laser energy was varied in the range of 60 and 200 mJ and the amount of cyanide degraded at different laser energies was determined. Large increase in the cyanide photo-oxidation was observed between 60 and 130 mJ while slight increase was observed when the energy was increased beyond 130mJ as depicted in Fig. 3. The increase in degradation due to the increase in laser energy may be explained as a fact that when laser energy is increased, incident photon flux increases in the solution, which excites more electrons in the catalyst.

Influence of pH on cyanide degradation

pH of the solution can also affect the degradation process. To study its effect, the variation of the cyanide removal with pH in the range of 4 to 12 has been investigated. A strong dependence of cyanide degradation on pH was observed. As depicted in Fig. 4, the cyanide removal decreases with the increase of pH, especially at pH higher than 7. This can be explained by the difference between the potential of cyanide oxidation and the potential of photogenerated holes as well as the increased electrostatic repulsion between the negatively-charged MWCNTs and ZnO surface and anionic cyanide at high pH values. The Point of zero charge (PZC) values of functionalized SWCNTs, MWCNTs and ZnO were reported to be 1.2 [McPhail et al., 2009], 4.9 [Lu and Chiu, 2006] and 9, respectively. This explains the highest cyanide removal at pH=4 since the adsorption of cyanide on MWCNTs reached its maximum amount because of the

weakest electrostatic repulsion between MWCNTs and cyanide molecules. With the increase of pH, especially at pH close to 9, both the MWCNTs and ZnO surfaces became more negative charged, leading to a reduced cyanide adsorption. This supports the idea that the adsorption is a prerequisite for efficient photodegradation [Xu and Langford, 2001].

Composite Dosage

Effect of composite dosage on elimination of cyanide is also important. Thus, the dependence of the percentage cyanide removal on the mass (substrate concentration) of the composite in suspension was investigated. Fig. 5 depicts the percentage elimination of cyanide after 10 min of laser irradiation at 200 mJ energy in 50ml solution of 20 ppm C cyanide N with pH of 5.5. The cyanide removal percentage increases linearly with the increase of composite concentration in 5 to 20 mg range and beyond 20 mg, the % removal was saturated.

9.4.2. Advantages

Carbon nanotube as catalyst support can provide different advantages:

- It helps the catalyst avoid self-poisoning

- It provides with high mechanical and thermal stability

- Its resistance to acid/basic media

- It is possible to control porosity and surface chemistry

- Its large specific surface area.

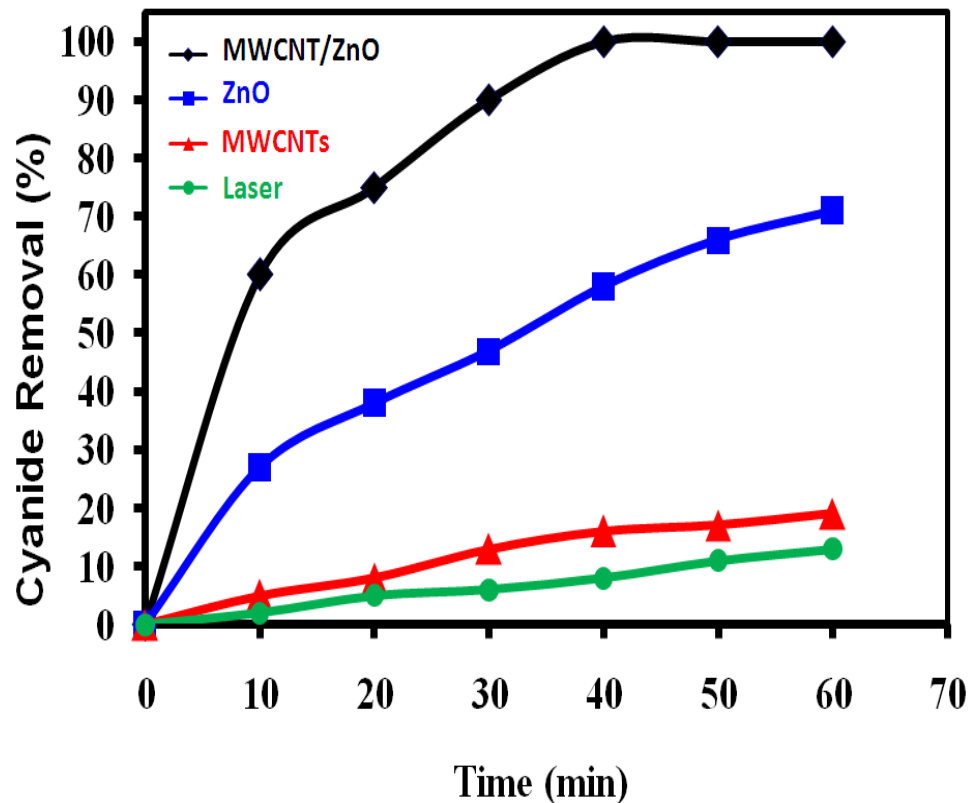


Figure 9-1 Variation of cyanide elimination with irradiation time in present of dosage of different material

(a) no dosage; b) MWCNTs; c) ZnO nanoparticles; d) MWCNT/ZnO composite.

Dosage mass: 10mg; Volume of cyanide solution: 50 ml; initial cyanide concentration:

20ppm; irradiation energy: 200mJ; pH: 5.5.

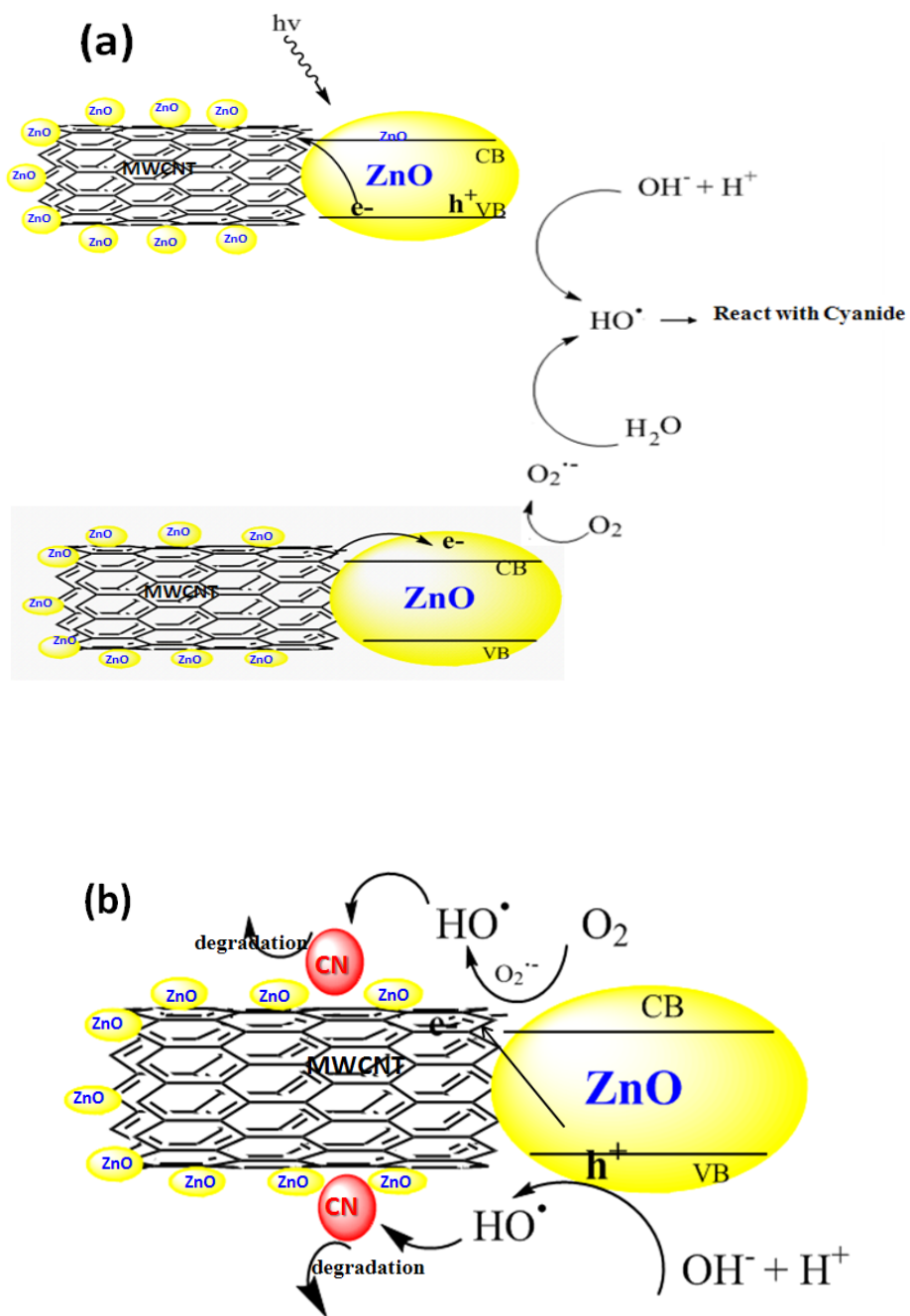


Figure 9-2 Proposed mechanism of cyanide photodegradation over CNT/ZnO

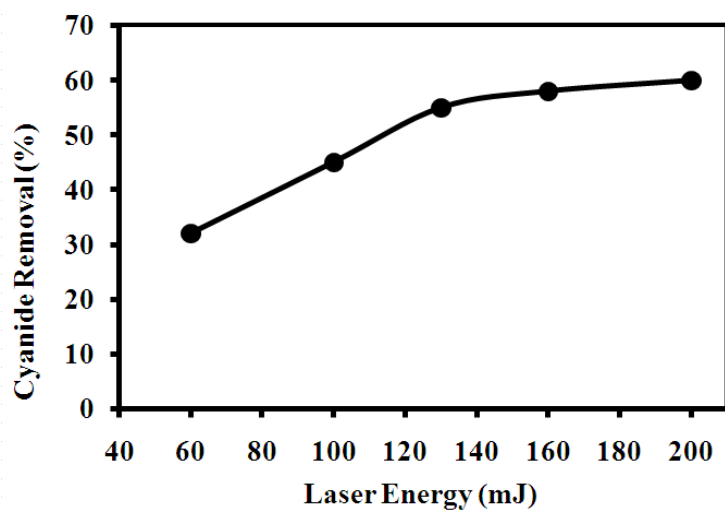


Figure 9-3 Variation of cyanide elimination with the irradiation energy

Dosage mass: 10mg; Volume of cyanide solution: 50 ml; initial cyanide concentration: 20ppm; irradiation time: 10min; pH: 5.5.

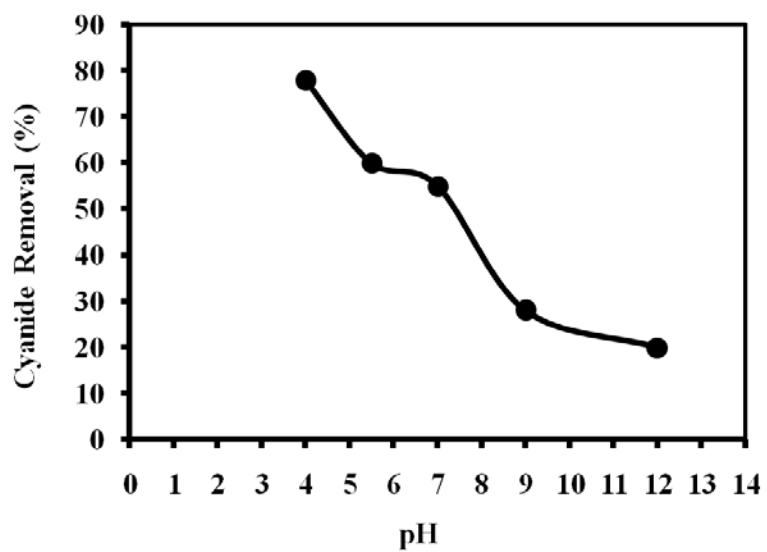


Figure 9-4 Variation of cyanide elimination with pH

Dosage mass: 10mg; Volume of cyanide solution: 50 ml; initial cyanide concentration: 20ppm; irradiation time: 10min; irradiation energy: 200mJ.

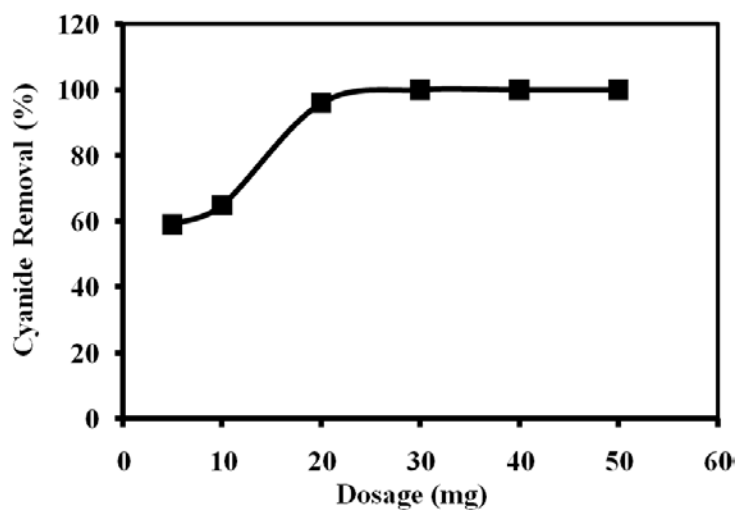


Figure 9-5 Variation of cyanide elimination with the catalytic composite dosage

Volume of cyanide solution: 50 ml; initial cyanide concentration: 20ppm; irradiation time: 10min; irradiation energy: 200mJ; pH: 5.5.

CHAPTER 10

APPLICATION OF MWCNT/TUNGSTEN OXIDE COMPOSITE

This chapter presents and discusses the application of MWCNT/WO₃ as a catalyst for degradation of pollutants under the sun light. The rhodamine B has been selected as a model due to its toxicity and spread use in the industry.

10.1. HIGHLIGHTS

The catalytic activities are strongly dependent on composition, size, and shape of the catalyst. In photocatalytic technique, irradiation of semiconductor with a photon of sufficient energy, greater or equal to band gap energy could promote an electron from valence band (VB) to conduction band (CB). As a result, the electron leaves a vacancy behind in the valence band called positive holes which could oxidize the organic material by removal of an electron or react with water or hydroxyl forming a powerful oxidant; a hydroxyl radical. The conduction band electrons reduce dissolved oxygen producing superoxide anion radical that is highly reactive and can oxidize any organic compound.

Due to its unique properties in particular the strong oxidizing power, physical and chemical stability and its large (3.2 eV of anatase titania) bandgap energy, titanium oxide (TiO_2) is the most widely studied catalytic material for environmental applications including water and air purification. TiO_2 under ultraviolet wavelength is an excellent photocatalyst for degradation of a wide variety of inorganic and organic substances. However, TiO_2 absorbs only solar light in the UV region because of its large band gap. Since only about 4-5% of the solar spectrum falls in this UV range, it is necessary to shift the absorption towards visible light or to have catalyst that can absorb in the visible region in order to utilize more energy of solar light. Many doping methods, such as nitrogen doped TiO_2 and sulfur doped TiO_2 , have been intensively investigated; however, their ability to completely oxidize organic compounds under visible light has not been satisfactory.

Because of its small band gap (2.4-2.8 eV), high oxidation power of VB holes (+3.1-3.2 V vs. NHE; almost the same as that of TiO_2), no toxicity, and stability, the ideal candidate is tungsten oxide (WO_3). It has the potential ability to promote photocatalytic reactions under visible light ($\lambda > 440$ nm) irradiation. Generally, in order to allow efficient consumption of photoexcited electrons and subsequent oxidative decomposition of organic compounds by holes, CB bottom potentials of a semiconductor should be more negative than the potential for the single-electron reduction of oxygen ($\text{O}_2 + e^- = \text{O}_2^-$ (aq), $E^0(\text{O}_2/\text{O}_2^-) = -0.3$ V vs NHE; $\text{O}_2 + \text{H}^+ + e^- = \text{HO}_2$ (aq), $E^0(\text{O}_2/\text{HO}_2) = -0.05$ V vs. NHE) (14-15). However, the problem is that the CB level of WO_3 is more positive (+0.3 to +0.5 V vs NHE) comparing with that of TiO_2 (around -0.2 to -0.4 V vs NHE).

Therefore, reduction of oxygen by the electron on CB of WO_3 could be more difficult than that of TiO_2 . Thus, pure WO_3 is not an efficient photocatalyst because of the lower CB edge that does not provide a sufficient potential to reduce O_2 . As a result of oxygen inability to track CB electrons, fast recombination could take place and hence lower photocatalytic activity.

To reduce the recombination and increase the efficiency of WO_3 , different investigations have been reported. Some of these methods were based on loading WO_3 with suitable cocatalysts such as CuO and Pt to trap photogenerated electrons and enhance the photoresponse of WO_3 . Some others based on controlling the synthesis process of WO_3 , related to the particle dimension and morphology of the material to improve photoresponse and efficiency.

Due to its unique electronic properties, multi-walled carbon nanotubes (MWCNTs) have attracted considerable attention. Recently composites of semiconductors with MWCNTs have been reported. It has been reported that MWCNTs could enhance photocatalytic activity. Nevertheless, a few papers have been reported on their enhancement under visible light. MWCNT)/Pt catalyst enhanced hydrogen generation rate under visible light. MWCNT/ TiO_2 composites were used as photocatalyst for phenol degradation under irradiation of visible light, which showed higher efficiency compared to pure TiO_2 . Thus far, little information on the solar photocatalytic degradation using this kind of composite has been presented. To the best of our knowledge the catalytic activity MWCNT/ WO_3 under sun-light has not been investigated yet. Therefore we offer a new

contribution by having tested the catalytic activity of the synthesized nanoscale MWCNT/ WO₃ under solar irradiation.

10.2. EXPERIMENTAL DESIGN

Experiments were carried out with a system of Pyrex glasswares placed outside the laboratory building. Different sets of experiments have been carried out to optimize the experimental parameters that affect on the process. To compare the catalytic activity of the synthesized composite, different materials have been used. In this consideration, the composite was compared with tungsten oxide nano-particles and carbon nanotube. In addition, a mixture of tungsten oxide nano-particles and carbon nanotube has been used to test the catalytic activity and compare it with that of the composite.

10.2.1. Photocatalytic Reaction

The photocatalytic activity of MWCNT/WO₃ composites was tested using Rh B degradation in aqueous solution under solar irradiation. The experiments were carried out in an open wide glass photochemical reactor charged with 50 mL of suspension. In a typical experiment, 50 mL of Rh B aqueous solution with 1×10^{-5} M was mixed with MWCNT/WO₃ composites. Prior to moving the system under the sun, the suspension was constantly stirred in dark for 2 h to reach equilibrium absorption. The concentration of the solution was determined, which was considered as initial concentration (C^0) of the Rh B solution. Then the system was moved outside under solar irradiation. Then, aliquot

of degraded solution was taken out with the help of a syringe and then examined regularly by UV–vis spectrophotometer in scheduled irradiation time

10.2.2. Absorbance Measurement

The absorbance's of the dye solutions before and after degradation was measured at different degradation times and different investigated parameters such as pH, dosage and initial concentration of the dye. Measurements were carried out using a spectrophotometer in the photon energy range of wavelength from 400 to 700 nm. The percentage of degradation (efficiency) was calculated from the following equation:

$$\text{The percentage of degradation} = [(C^{\circ} - C)/C^{\circ}] * 100$$

Where C° is the initial concentration of dye and C is the concentration at time t . All C/C° values were obtained by the maximum absorption at 559 nm in the absorption spectrum in order to evaluate the degradation efficiency.

10.3. RESULTS OF PHOTOCATALYTIC ACTIVITY

In this section, the results of the experimental work related to the parameters optimization will be introduced and discussed. The results of a comparison between the composite and WO_3 nanoparticles, CNT and mechanical mixtures of CNT and WO_3 nanoparticles will be presented and discussed.

10.3.1. Parameters' optimization

Different parameters have been optimized, such as time of contact, type of material, pH of the solution, dosage, and initial concentration.

Time Effect

The change in photocatalytic degradation of RhB under solar irradiation was monitored by UV-visible spectral changes, Figure 1. The characteristic absorption band of RhB at 559 nm diminished with increasing the time of exposure to the sunlight. The shift observed in the maximum absorption band resulted from the formation of a series of intermediates of RhB [Fu et al., 2008; Yu et al., 2009; Horikoshi et al., 2003].

The results of photocatalytic reaction over the composites and the mixture were fitted according to the apparent first-order equation $\ln(C^0 / C) = kt$, (Figure 2). The slope of the curve belongs to the composite is almost two times as that of the mixture which signify the rate of the composite is two times higher.

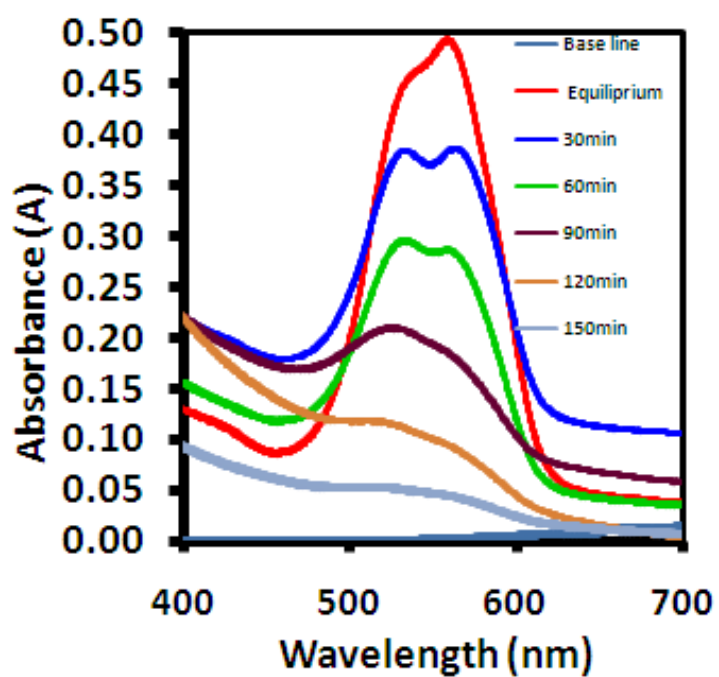


Figure 10-1 UV/vis spectral changes of RhB under solar irradiation for the composite, spectra from top to bottom refer to irradiation for 0 (after equilibrium), 30, 60, 90, 120 and 150 min, respectively

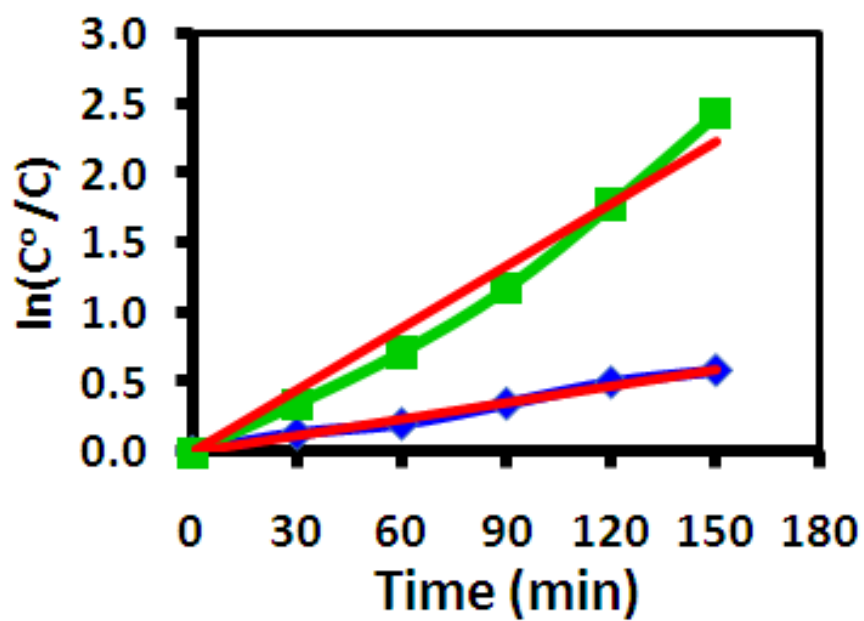


Figure 10-2 Apparent first-order linear transform $\ln(C^0 / C) = kt$ of Rh B degradation kinetic plots for the composite and the mixture of MWCNTs

Figure 3 shows decrease in absorption of Rh B as a result of adsorption, the experiment was run in dark to get equilibrium. Figure 4 depicts the results of photodegradation of Rh B over various systems. The first is a blank experiment, which was performed in dark without any catalyst as a control. The second was performed in sunlight without catalyst. The others were performed under the sun over different materials. When MWCNTs was used, a small removal was observed which is most probably as a result of adsorption. More than 92% of Rh B was decomposed after irradiation for 150 min while degradation of only 49 and 44% was observed when WO_3 and MWCNTs+ WO_3 mixture were applied.

This might be attributed to the synergistic effect of adsorption, due to large surface area, and electron transfer from WO_3 to MWCNTs, due to the formation of ester bond and strong interaction. The adsorption can be explained by the presence of hydroxyl sites on the surface of MWCNTs as a result of strong oxidation conditions should improve/enhance adsorption of RhB because of the electrostatic attractive interaction between the hydroxyl sites on the composite and RhB dye. As a result, the degree of adsorption and in turn the rate of degradation of the RhB dye has dramatically increased in case of using the composite comparing with both the mechanical mixture and WO_3 . Another physical role of MWCNTs is acting as dispersing agent preventing WO_3 from agglomerating, thus providing a high active surface area of the catalyst. This support the notion that preadsorption of the dye on the surface of catalyst particles is a prerequisite for efficient photodegradation. Moreover, the findings support the idea that degradation occurs at the particle surface and not in the solution bulk [Zhao et al., 1998].

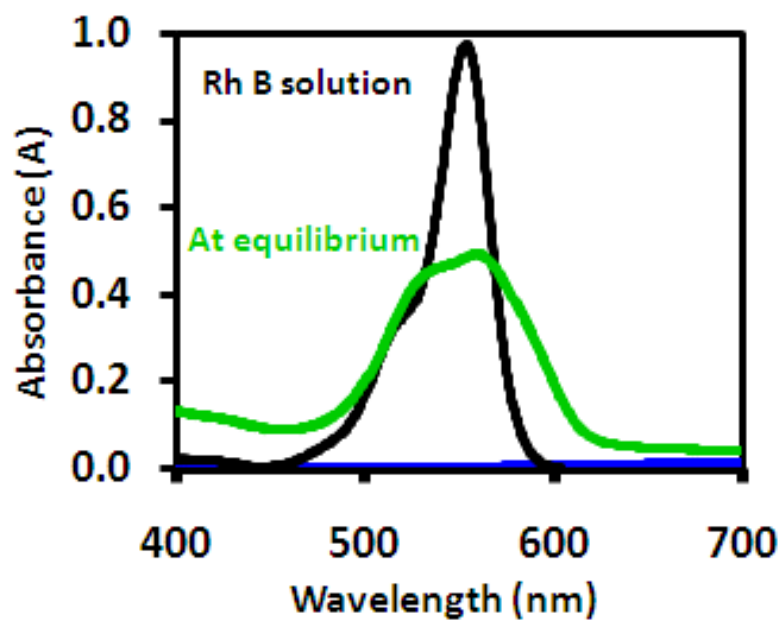


Figure 10-3 Equilibrium of Rh B in CNT/tungsten oxide nanocomposite

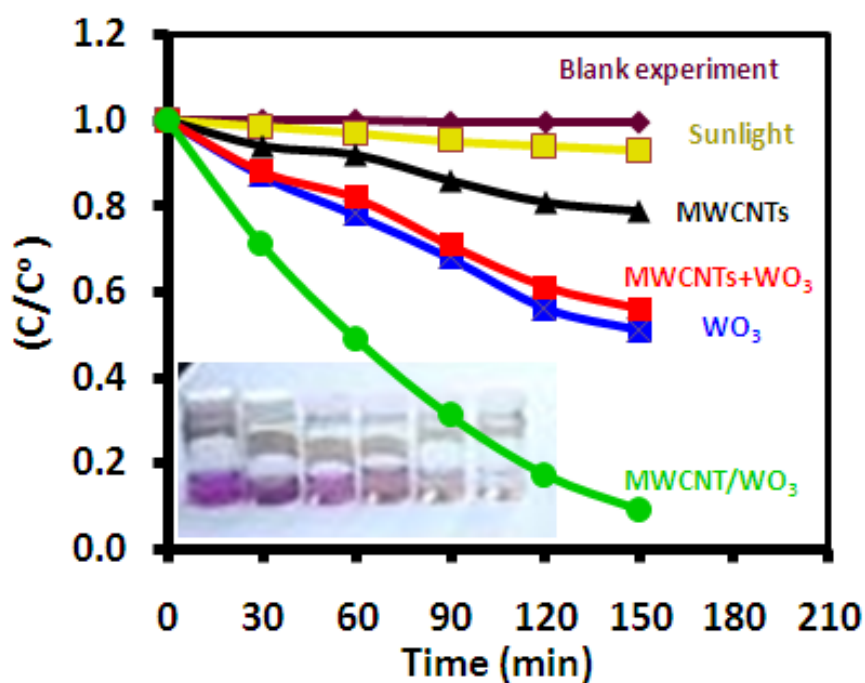


Figure 10-4 Photodegradation of RhB vs irradiation time for several systems

Blank experiment, Sunlight with no catalyst, sunlight with: MWCNTs, WO₃, MWCNTs + WO₃ and MWCNT/WO₃ composite (initial concentration of Rh B 1×10^{-5} M, dosage: 10mg g/50mL, pH5.5. Picture: color change of the corresponding dye solutions in the MWCNT/WO₃ composite.

Dosage

Experiments of photodegradation of Rh B solution of 2×10^{-5} M over different dosage of MWCNT/WO₃ composite were carried out to study the effects of catalyst dosage. The dosage ranges from 0.1 to 50 mg/50ml in aqueous solutions at pH 5.5, and the exposure time of irradiation is 150 min. It was observed that the decay was enhanced significantly by increasing the doses of the composite. However, increasing the dosage to from 10 to 50 mg/50ml results in an insignificant increment to the decay. The optimum was found to be 5 mg/ 50ml.

Initial Concentration Effect

The influence of initial Rh B concentration on the photodegradation process over the composite was studied by varying the concentration from 0.1-100 $\times 10^{-5}$ M. It was found that the photodegradation ratio decreased as the initial concentration increased. This can be explained that at higher dye concentrations, greater molecules adsorbing on the MWCNTs surface which could lead into reduction in the light intensity, which is screened, by the solution and fewer photons could reach the catalytic surface. Thus, the generation of $e^- - h^+$ pair is reduced leading to absence of oxidizing species since the rate of degradation is affected by amount of HO• radicals formed on or near the catalyst surface. A similar trend was observed for the photocatalytic degradation of Methyl Orange over TiO₂ Nanotubes [Smith et al., 2009].

pH Effect

With respect to the adsorption of particular ions on MWCNTs, pH value plays an important role. In order to investigate the photodegradation process of Rh B, the experiments were carried out at pH values of 3.0, 5.5, 7.0 and 9.0, respectively (Figure 4). The results showed that the efficiency of the composite on the photodegradation of RB was improved with the increase pH. The discussion of this effect is valuable but complicated since several reaction mechanisms contribute to dye degradation, such as hydroxyl radical attack, direct oxidation by positive holes, and direct reduction by electrons. pH value had significant effect on the absorption behavior of the dye on the composite surface. Therefore, considering PZC when the MWCNT/WO₃ composite placed in aqueous solutions of pH below its PZC=4 (for details see the Supporting Information) it becomes protonated and exhibits a positive net charge on its surface, thus it could not well adsorb the Rh B dye. In contrast, when placed in solutions above its PZC=4, the net surface charge turns negative (from deprotonation) and adsorbs well the Rh B dye. Increasing the adsorption leads to diffuse the dye to the photocatalytic tungsten oxides and thus the degradation. Also, the presence of a large quantity of OH⁻ under alkaline conditions, pH>7, facilitates formation of OH radicals which enhance Rh B degradation.

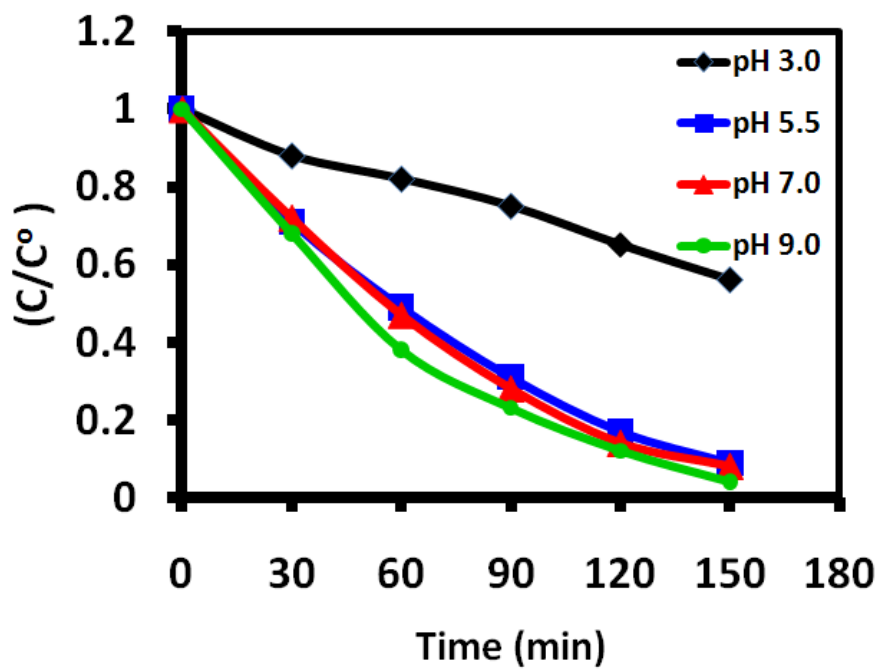


Figure 10-5 Photo catalytic degradation of Rh B at various pH values

10.3.2. Mechanism

Based on our experimental results, the enhancement in photocatalytic performance of MWCNT/WO₃ composite can be rationally explained based on electron transportation and adsorption.

Under solar irradiation, electrons (e⁻) are excited from the valence band (VB) to the conduction band (CB) of WO₃ creating a charge vacancy, hole (h⁺), in the VB. In the absence of MWCNTs, most of these charges quickly recombine without doing efficient degradation. Using the composite, the strong interaction and formation of ester bonds (-COO-W-), resulting in a close contact between WO₃ and MWCNTs leads to form a barrier junction which offers an effective route of reducing electron-hole recombination by improving the injection of electrons into MWCNTs, Figure 5. This supported by being MWCNTs relatively good electron acceptors [Riggs et al., 2000; Subramanian et al., 2004] while WO₃ is an electron donor under illumination [Geng et al., 2008]. Hence, MWCNTs acts as a photogenerated electron acceptor to promote interfacial electron transfer processes. The electrons react with O₂, which can trigger the formation of very reactive superoxide radical ion (O₂^{•-}) that can oxidize the dye and generate hydroxyl radical (•OH) to oxidize the dye. Compared with the pure WO₃, the enhanced photoactivity shown by the composite signifies the presence of strong interfacial combination in MWCNT/WO₃. The electrons in CB may also directly react with O₂, which can trigger the formation of very reactive superoxide radical ion (O₂^{•-}).

Since the adsorption is a key process in the photocatalysis, we propose the mechanism in Figure 5b. Oxygen and dye can be adsorbed on the composite surface. The e^- in MWCNTs could catch the adsorbed O_2 and finally yields $O_2^{\bullet-}$ and $\bullet OH$, to oxidize the dye. Simultaneously, a positive charged hole (h^+), formed with electron transfer from VB in WO_3 to CB, catches OH^- derived from H_2O to form $\bullet OH$ which oxidizes the adsorbed Rh B dye. Dye adsorbed on MWCNTs transfer to WO_3 surface, where it undergoes the photocatalytic degradation. The driving force for this transfer could be the difference in the dye concentration on MWCNTs and WO_3 , resulting in dye diffusion from MWCNTs to WO_3 .

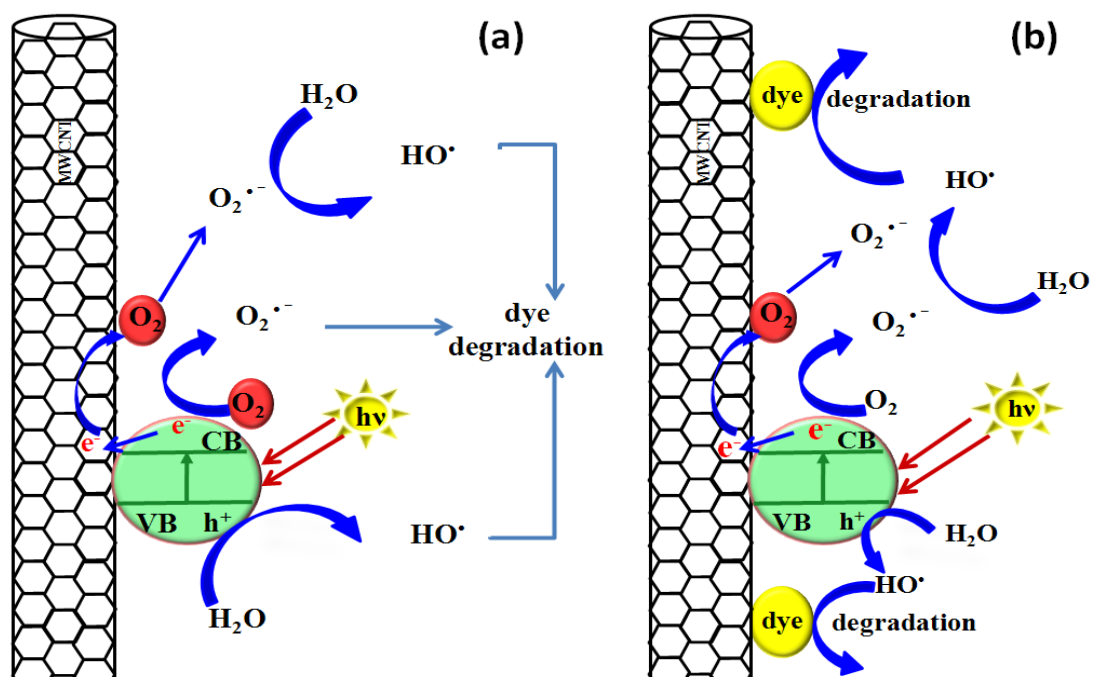


Figure 10-6 Schematic representation of the reasonable reaction mechanism of Rh B photodegradation over MWCNT/WO₃ presented in this work

CHAPTER 11

CONCLUSIONS

In this dissertation, composites of carbon nanotubes with different metal oxides have been successfully synthesized. The composites like CNT/alumina, magnetic-CNT, CNT/manganese oxide, CNT/zinc oxide, and CNT/tungsten oxide, were then characterized. Characterization of the as-prepared carbon nanotube/metal oxides nanocomposites is performed by means of different characterization tools like high resolution transmission electron microscope (HRTEM), field emission scanning electron microscope (FESEM), energy dispersive X-ray (EDX), thermogravimetric analysis (TGA), Raman spectroscope, UV-vis spectrometer and fourier transformed infrared spectroscope (FT-IR) and X-ray photoelectron spectroscope (XPS). The techniques are complementary.

The dissertation has analyzed the methodology of functionalization and activation of the nanotubes as a first step for preparation of CNT/MO nanocomposites. The details of functional groups characterization have also been discussed. The synthesis of CNT/MO nanocomposites is detailed with the characterization interpretation.

The new class of prepared CNT/MO nanomaterials offers great potential applications in different fields. Some application-studies have been carried out referring to a realistic

use of CNT/MO nanocomposites as adsorbents that have excellent adsorption ability for many kinds of pollutants like inorganic and organic compounds.

The advantage is that CNTs provide large number of nucleation centers available on its surface for receiving the nanoparticles and preventing their agglomeration. This makes such material not only good in adsorption but also in enhancement of the catalytic activity. The reason given for the high catalytic performance is the optimum dispersion of MO on the CNTs. The mechanism of enhancing the photo-catalytic activity is discussed based on adsorption ability of the nanotube and the transfer of promoted electrons from metal oxide to CNT. The most important processing issue is the interfacial strength between the CNTs and the MO nanoparticles.

RECOMMENDATION

Over the last years, much progress has been made in adsorption applications of CNT/MO nanocomposites. In spite of high costs, using CNTs as adsorbents may be advantageous in future owing to their high adsorption capacities. However, there are still much to do to enhance CNT/MO nanocomposites' adsorption properties in future. Efforts in synthesis methods to develop a cost effective way of CNTs production are required. Investigations on CNT/MO nanocomposites on applications in adsorption and catalysis are recommended.

REFERENCES

- [1] Shih, Y. H.; Li, M. S. Adsorption of selected volatile organic vapors on multiwall carbon nanotubes. *J. Hazard. Mater.* 2008, 154, 21–28.
- [2] Gotovac, S.; Hattori, Y.; Noguchi, D.; Miyamoto, J.; Kanamaru, M.; Utsumi, S.; Kanoh, H.; Kaneko, K. Phenanthrene adsorption from solution on single wall carbon nanotubes. *J. Phys. Chem. B* 2006, 110, 16219–16224.
- [3] Gotovac, S.; Song, L.; Kanoh, H.; Kaneko, K. Assembly structure control of single wall carbon nanotubes with liquid phase naphthalene adsorption. *Colloid Surf., A* 2007, 300, 117–121.
- [4] Wang, X.; Chen, X.; Yoon, K.; Fang, D.; Hsiao, B. S.; Chu, B. High flux filtration medium based on nanofibrous substrate with hydrophilic nanocomposite coating. *Environ. Sci. Technol.* 2005, 39, 7684–7691.
- [5] Pan B., Xing B., “Adsorption mechanisms of organic chemicals on carbon nanotubes”, *Environmental Science & Technology*, 42, 2008, 24, pp. 9005-9013.
- [6] Li Q., “Antimicrobial nanomaterials for water disinfection and microbial control: potential applications and implications”, *Water Res* 42, 2008, 18, 4591-4602.
- [7] Upadhyayula V., “Adsorption kinetics of Escherichia coli and Staphylococcus aureus on single-walled carbon nanotube aggregates”, *Water Science & Technology*, 58, 2008, 1, pp. 179-184.
- [8] Sharma Y., et.al., “Nano-adsorbents for the removal of metallic pollutants from water and wastewater”, *Environmental Technology*, 30, 2009, 6, 583-609.

- [9] Jorg J. Schneider, Nadezda I. Maksimova, Jorg Engstler, Ravi Joshi, Roland Schierholz, Rudolf Feile, Catalyst free growth of a carbon nanotube–alumina composite structure, *Inorganica Chimica Acta* 361,2008, 1770–1778.
- [10] Iijima S., Helical microtubules of graphitic carbon, *Nature* 354(1991)56–58.
- [11] Johann Cho, Silke Schaab, Judith A. Roether, Aldo R. Boccaccini, Nanostructured carbon nanotube/TiO₂ composite coatings using electrophoretic deposition (EPD), *J Nanopart Res* (2008) 10:99–105.
- [12] Chen Ming-Liang, Zhang Feng-Jun, Won-Chun Oh, Synthesis, characterization, and photocatalytic analysis of CNT/TiO₂ composites derived from MWCNTs and titanium sources, *New Carbon Materials*, 2009, 24(2): 159–166
- [13] Yan-Hui Li, Yanqiu Zhu, Yimin Zhao, Dehai Wu, Zhaokun Luan, Different morphologies of carbon nanotubes effect on the lead removal from aqueous solution, *Diamond & Related Materials* 15 (2006) 90– 94.
- [14] C. Quintelas, Z. Rocha, B. Silva, B. Fonseca, H. Figueiredo, T. Tavares, Removal of Cd(II), Cr(VI), Fe(III) and Ni(II) from aqueous solutions by an *E. coli* biofilm supported on kaolin, *Chem. Eng. J.* 149 (2009) 319–324.
- [15] V.K. Gupta, D. Mohan, S. Sharma, Removal of lead from wastewater using bagasse fly ash, sugar industry waste material, *Sep. Sci. Tech.* 33 (1998) 1331–1343.
- [16] V.K. Gupta, I. Ali, Removal of lead and chromium from wastewater using bagasse fly ash—a sugar industry waste, *J. Colloid Interface Sci.* 271 (2004) 321–328.

- [17] V.K. Gupta, P. Singh, N. Rahman, Adsorption behavior of Hg(II), Pb(II) and Cd(II) from aqueous solution on duolite C-433: a synthetic resin, *J. Colloid Interface Sci.* 275 (2004) 398–402.
- [18] V.K. Gupta, A. Rastogi, Biosorption of lead from aqueous solutions by green algae *Spirogyra*: kinetics and equilibrium studies, *J. Haz. Mater.* 152 (2008) 407–414.
- [19] V. K. Gupta, S. K. Srivastava, D. Mohan, S. Sharma, Design parameters for fixed bed reactors of activated carbon developed from fertilizer waste for the removal of some heavy metal ions, *Waste Management* 17 (1997) 517-522
- [20] V.K. Gupta, M. Gupta, S. Sharma, Process development for the removal of lead and chromium from aqueous solutions using red mud—an aluminium industry waste, *Water Res.* 35 (2001) 1125–1134.
- [21] Tarun Kumar Naiya, Ashim Kumar Bhattacharya, Sudip Kumar Das, Adsorption of Cd(II) and Pb(II) from aqueous solutions on activated alumina, *Journal of Colloid and Interface Science* 333 (2009) 14–26
- [22] Jun Yin, Zucheng Jiang, Gang Chang, Bin Hu, Simultaneous on-line preconcentration and determination of trace metals in environmental samples by flow injection combined with inductively coupled plasma mass spectrometry using a nanometer-sized alumina packed micro-column, *Analytica Chimica Acta* 540 (2005) 333–339
- [23] C. L. Chen, X. K. WANG , and M . Nagatsu, Europium Adsorption on Multiwall Carbon Nanotube/Iron Oxide Magnetic Composite in the Presence of Polyacrylic Acid, *Environ. Sci. Technol* 43 (2009) 2362–2367

- [24] Li YH, Di Z, Ding J, Wu D, Luan Z, Zhu Y. Adsorption thermodynamic, kinetic and desorption studies of Pb²⁺ on carbon nanotubes. *Water Res* 39 (2005)605–9.
- [25] Anna Stafiej, Krystyna Pyrzynska, Adsorption of heavy metal ions with carbon nanotubes, *Separation and Purification Technology* 58 (2007) 49–52
- [26] Renata S. Amais Juliana S. Ribeiro, Mariana G. Segatelli, Inez V.P. Yoshida, Pedro O. Luccas and César R.T. Tarley, Assessment of nanocomposite alumina supported on multi-wall carbon nanotubes as sorbent for on-line nickel preconcentration in water samples, *Sep.Pur. Tech.* 58 (2007) 122-128
- [27] P. Westerhoff, D. Highfield, M. Badruzzaman, Y. Yoon, Rapid small-scale column tests for arsenate removal in iron oxide packed bed columns, *J. Environ. Eng. - ASCE* 131 (2005) 262–271.
- [28] Sperlich, A. Werner, A. Genz, G. Amy, E. Worch, M. Jekel, Breakthrough behavior of granular ferric hydroxide (GFH) fixed-bed adsorption filters: modeling and experimental approaches, *Water Res.* 39 (2005) 1190–1198.
- [29] C.N. He, F. Tian, S.J. Liu, A carbon nanotube/alumina network structure for fabricating alumina matrix composites, *Journal of Alloys and Compounds* 478 (2009) 816–819
- [30] V.K. Gupta, Suhas, Application of low-cost adsorbents for dye removal – A review, *Journal of Environmental Management* 90 (2009) 2313–2342
- [31] Gupta, V.K., Mittal, A., Gajbe, V., Mittal, J., 2008. Adsorption of basic fuchsin using waste materials–bottom ash and deoiled soya–as adsorbents. *J. Colloid Interface Sci.* 319, 30–39.

- [32] Hyung, H. & Kim, J.H., (2008). Natural organic matter (NOM) adsorption to multi-walled carbon nanotubes: effect of NOM characteristics and water quality parameters, *Environ. Sci. Technol.* 42: 4416–4421.
- [33] Goering, J.; Kadossov, E. & Burghaus, U. (2008). Adsorption kinetics of alcohols on single wall carbon nanotubes: an ultra high vacuum surface chemistry study, *J. Phys. Chem. C* 112: 10114–10124.
- [34] Cho, H. H.; Wepasnick, K.; Smith, B.A.; Bangash, F.K.; Fairbrother, D.H. & Ball W.P. (2010). Sorption of aqueous Zn[II] and Cd[II] by multiwall carbon nanotubes: the relative roles of oxygen-containing functional groups and graphenic carbon, *Langmuir* 26: 967–981.
- [35] Peng, K.; Liu, L.Q.; Li, H.; Meyer, H. & Zhang, Z. (2011). Room temperature functionalization of carbon nanotubes using an ozone/water vapor mixture, *Carbon* 49: 70–76
- [36] Hojati-Talemi, P.; Simon, G. (2009) Microwave-based treatments for multi-walled carbon nanotubes, *Phys. Status Solidi C* 6, 10: 2170–2173
- [37] Smith, B.; Wepasnick, K.; Schrote, K. E.; Cho, H. H.; Ball, W. P.; Howard Fairbrother, D. (2009). Influence of Surface Oxides on the Colloidal Stability of Multi-Walled Carbon Nanotubes: A Structure-Property Relationship, *Langmuir* 25: 9767–9776
- [38] Wang, H.; Wang, H. & Jiang, W. (2009). Solar photocatalytic degradation of 2,6-dinitro-p-cresol (DNPC) using multi-walled carbon nanotubes (MWCNTs)–TiO₂ composite photocatalysts, *Chemosphere* 75: 1105–1111

- [39] Chiang, Y.; Lin, W. H. & Chang, Y. C. (2011). The influence of treatment duration on multi-walled carbon nanotubes functionalized by H₂SO₄/HNO₃ oxidation, *Applied Surface Science* 257 2401–2410
- [40] Wepasnick, K. A., B. A. Smith, K. E. Schrote, H. K. Wilson, S. R. Diegelmann , D. H. Fairbrother, Surface and structural characterization of multi-walled carbon nanotubes following different oxidative treatments, *Carbon* 49(2011) 24 –36
- [41] Wang, Z., M. D. Shirley, S. T. Meikle, R. L.D. Whitby, S. V. Mikhalovsky, The surface acidity of acid oxidised multi-walled carbon nanotubes and the influence of in-situ generated fulvic acids on their stability in aqueous dispersions, *Carbon* 47 (2009) 73-79
- [42] Boehm, H. P., Some aspects of the surface chemistry of carbon blacks and other carbons. *Carbon* 32(1994) 759–69.
- [43] Eder, D. (2010). Carbon Nanotube-Inorganic Hybrids. *Chem Rev.* 110: 1348-1352.
- [44] Zhang, Hong-Bin, Guo-Dong Lin, Zhen-Hua Zhou, Xin Dong, Tong Chen, Raman spectra of MWCNTs and MWCNT-based H₂ adsorbing system, *Carbon* 40 (2002) 2429–2436
- [45] Wang J., L. P. See, J. Ma, One-Pot Synthesis of Hierarchically Assembled Tungsten Oxide (Hydrates) Nano/Microstructures by a Crystal-Seed-Assisted Hydrothermal Process, *Crystal Growth & Design* 2009, 9, 2243-22499
- [46] Stobinski L., B. Lesiak, L. Kover, J. Toth, S. Biniak, G. Trykowski, J. Judek, Multiwall carbon nanotubes purification and oxidation by nitric acid studied by the

- FTIR and electron spectroscopy methods, *Journal of Alloys and Compounds* 2010, 501, 77–84
- [47] Xiang Q., G. F. Meng, H. B. Zhao, Y. Zhang, H. Li, W. J. Ma, J. Q. Xu, Au Nanoparticle Modified WO₃ Nanorods with Their Enhanced Properties for Photocatalysis and Gas Sensing, *J. Phys. Chem. C* 2010, 114, 2049–2055
- [48] Y. J. Xu, Y. Zhuang, X. Fu, New Insight for Enhanced Photocatalytic Activity of TiO₂ by Doping Carbon Nanotubes: A Case Study on Degradation of Benzene and Methyl Orange, *J. Phys. Chem. C* 2010, 114, 2669–2676
- [49] Keshri A. K., Jun Huang, Virendra Singh, Wonbong Choi, Sudipta Seal, Arvind Agarwal, Synthesis of aluminum oxide coating with carbon nanotube reinforcement produced by chemical vapor deposition for improved fracture and wear resistance, *Carbon*, 48, 2010: 431-442
- [50] Tarun, K.N., K.B. Ashim, K.D. Sudip, Adsorption of Cd(II) and Pb(II) from aqueous solutions on activated alumina, *J Colloid Interf Sci.* 333 (2009) 14-26.
- [51] Li Y.H., Z. Di, J. Ding, D. Wu, Z. Luan, Y. Zhu, Adsorption thermodynamic, kinetic and desorption studies of Pb²⁺ on carbon nanotubes, *Water Res.* 39 (2005) 605-609.
- [52] Anna S., P. Krystyna, Adsorption of heavy metal ions with carbon nanotubes, *Sep Purif Technol.* 58 (2007) 49-52.
- [53] Chuan, M. C. And Liu, J. C. 1996. Release behavior of chromium from tannery sludge, *Wat. Res.* 30, 932-938,

- [54] Gao, Z., Bandosz, T. J., Zhao, Z., Han, M., Qiu, J., 2009, Investigation of factors affecting adsorption of transition metals on oxidized carbon nanotubes, *Journal of Hazardous Materials* 167 (2009) 357–365
- [55] Girifalco, L.A., Hodak, M. and Lee, R.S. 2000. Carbon nanotubes, buckyballs, ropes, and a universal graphitic potential, *Physical Review B* 62 (19) 13104-13109.
- [56] Kandah, M.I., Meunier, J.L., 2007. Removal of nickel ions from water by multiwalled carbon nanotubes. *Journal of Hazardous Materials* 146, 283–288.
- [57] Lu, C., Chiu, H., 2006. Adsorption of zinc(II) from water with purified carbon nanotubes, *Chemical Engineering Science*, 61, 1138 – 1145
- [58] Pillay, K., Cukrowska, E.M., Coville, N.J., 2009. Multi-walled carbon nanotubes as adsorbents for the removal of parts per billion levels of hexavalent chromium from aqueous solution. *Journal of Hazardous Materials* 166, 1067–1075.
- [59] Rana, P., Mohan, N., Rajagopal, C., 2004. Electrochemical removal of chromium from wastewater by using carbon aerogel electrodes. *Water Research* 38, 2811–2820
- [60] Wang, X. Z., Li, M. G., YChen, . W., Cheng, R. M., Huang, S. M., Pan, L. K., Sun, Z., 2006, Electrosorption of ions from aqueous solutions with carbon nanotubes and nanofibers composite film electrodes, *Applied Physics Letters* 89, 053127-053134
- [61] Zhang, N., Suleiman, J. S., He, M., Hu, B., 2008. Chromium(III)-imprinted silica gel for speciation analysis of chromium in environmental water samples with ICP-MS detection, *Talanta* 75, 536–543

- [62] Tournassat C., L. Charlet, D. Bosbach, A. Manceau, Arsenic(III) oxidation by birnessite and precipitation of manganese(II) arsenate, *Environ. Sci. Technol.* 36 (2002) 493–500
- [63] Manning B. A., S. E. Fendorf, B. Bostick, D.L. Suarez, Arsenic(III) oxidation and arsenic(V) reactions on synthetic birnessite, *Environ. Sci. Technol.* 36 (2002) 976–981.
- [64] Smedley P.L., D.G. Kinniburgh, A review of the source, behaviour and distribution of arsenic in natural waters, *Applied Geochemistry* 17 (2002) 517–568
- [65] Lee H., W. Choi, Photocatalytic oxidation of arsenite in TiO₂ suspension: kinetics and mechanisms, *Environ. Sci. Technol.* 36 (2002) 3872–3878.
- [66] Driehaus W., R. Seith, M. Jekel, Oxidation Of Arsenate(III) With Manganese Oxides In Water Treatment, *Water Res.* 29 (1995) 297-305
- [67] Mohan D., C. U. Pittman, Arsenic removal from water/wastewater using adsorbents—A critical review, *J. Hazard. Mater.* 142 (2007) 1-53
- [68] Maji S. K., A. Pal, T. Pal, Arsenic removal from real-life groundwater by adsorption on laterite soil, *Journal of Hazardous Materials* 151 (2008) 811–820
- [69] Ouvreard S., M. O. Simonnot, M. Sardin, Reactive behavior of natural manganese oxides towards the adsorption of phosphate and arsenate. *Ind Eng Chem Res* 41 (2002) 2785 –2791.
- [70] Lenoble V., C. Laclautre, B. Serpaud, V. Deluchat, J. C. Bollinger, As(V) retention and As(III) simultaneous oxidation and removal on a MnO₂-loaded polystyrene resin, *Science of the Total Environment* 326 (2004) 197–207

- [71] Mu Q., W. Liu, Y. Xing, H. Zhou, Z. Li, Y. Zhang, L. Ji, F. Wang, Z. Si, B. Zhang, B. Yan, Protein Binding by Functionalized Multiwalled Carbon Nanotubes Is Governed by the Surface Chemistry of Both Parties and the Nanotube Diameter, *J. Phys. Chem. C* 112 (2008) 3300-3307
- [72] Wang Y., Y. Bu, Noncovalent Interactions between Cytosine and SWCNT: Curvature Dependence of Complexes via $\pi \dots \pi$ Stacking and Cooperative CH $\pi \dots \pi$ /NH $\pi \dots \pi$, *J. Phys. Chem. B* 111 (2007) 6520-6526
- [73] Bozzi A, Guasaquillo I, Kiwi J, Accelerated removal of cyanides from industrial effluents by supported TiO₂ photo-catalysts, *Applied Catalysis B: Environmental* 51, 2004, 203-9.
- [74] Fu H., S. Zhang, T. A. Xu, Y. Zhu, J. Chen, Photocatalytic Degradation of RhB by Fluorinated Bi₂WO₆ and Distributions of the Intermediate Products, *Environ. Sci. Technol.* 2008, 42, 2085–2091
- [75] Yu K., S. Yang, H. He, C. Sun, C. Gu, Y. Ju, Visible Light-Driven Photocatalytic Degradation of Rhodamine B over NaBiO₃: Pathways and Mechanism, *J. Phys. Chem. A* 2009, 113, 10024–10032
- [76] Horikoshi S., A. Saitou, H. Hidaka, N. Serpone, Environmental Remediation by an Integrated Microwave/UV Illumination Method. V. Thermal and Nonthermal Effects of Microwave Radiation on the Photocatalyst and on the Photodegradation of Rhodamine-B under UV/Vis Radiation, *Env. Sci. Technol.* 2003, 37, 5813-5822
- [77] Zhao J., T. Wu, K. Wu, K. Oikawa, H. Hidaka, N. Serpone, Photoassisted Degradation of DyePollutants. 3. Degradation of the Cationic Dye Rhodamine B in

- Aqueous Anionic Surfactant/TiO₂ Dispersions under Visible Light Irradiation: Evidence for the Need of Substrate Adsorption on TiO₂ Particles, *Environ. Sci. Technol.*, 1998, 32, 2394–2400
- [78] Smith Y. R., A. Kar, R. Vaidyanathan, Subramanian Investigation of Physicochemical Parameters That Influence Photocatalytic Degradation of Methyl Orange over TiO₂ Nanotubes, *Ind. Eng. Chem. Res.* 2009, 48, 10268–10276
- [79] Riggs J. E., Z. Guo, D. L. Carroll, Y. P. Sun, Strong Luminescence of Solubilized Carbon Nanotubes, *J. Am. Chem. Soc.* 2000, 122, 5879-5880
- [80] Subramanian V., E. Wolf, P. V. Kamat, Catalysis with TiO₂/Gold Nanocomposites. Effect of Metal Particle Size on the Fermi Level Equilibration, *J. AM. CHEM. SOC.* 2004, 126, 4943-4950
- [81] Geng Q., Q. Guo, C. Cao, L. Wang, Investigation into NanoTiO₂/ACSPCR for Decomposition of Aqueous Hydroquinone, *Ind. Eng. Ch. R.* 2008, 47, 2561-2568
- [82] Wang J, Xie Y, Zhang Z, XiaChen J, Zhang L, Xu R, Zhang X, Photocatalytic degradation of organic dyes with Er³⁺:YAlO₃/ZnO composite under solar light, *Solar Energy Materials & Solar Cells* 93, 2009, 355-9.
- [83] Anandan S, Vinu A, Mori T, Gokulakrishnan N, Srinivasu P, Murugesan V, Ariga K, Photocatalytic degradation of 2,4,6-trichlorophenol using lanthanum doped ZnO in aqueous suspension, 2007 *Catal. Commun.* 8 1377-82.
- [84] Jiang L and Gao L 2005, Fabrication and characterization of coated multi-walled carbon nanotubes with enhanced photocatalytic activity, *Mater. Ch. Phys.* 91 313.

- [85] Rose TL and Nanjundiah C 1985 , Rate enhancement of photooxidation of CN with TiO₂ particles. *J. Phys. Chem.* 89 3766-71.
- [86] McPhail MR, Sells JA, He Z, and Chusuei CC 2009, Charging Nanowalls: Adjusting the Carbon Nanotube Isoelectric Point via Surface Functionalization, *J. Phys. Chem. C* 113 14102–14109
- [87] Lu C, Chiu H 2006, Adsorption of zinc(II) from water with purified carbon nanotubes, *Chemical Engineering Science* 61 1138 – 1145
- [88] Xu Y and Langford CH 2001, UV- or Visible-Light-Induced Degradation of X3B on TiO₂ Nanoparticles: The Influence of Adsorption, *Langmuir* 17 897-902
- [89] Osorio, A. G.; Silveira, I. C. L.; Bueno, V. L. & Bergmann, C.P. (2008). H₂SO₄/HNO₃/HCl Functionalization and its effect on dispersion of carbon nanotubes in aqueous media, *Applied Surface Science* 255 2485–2489
- [90] Droste, R.L., *Theory and Practice of Water and Wastewater Treatment*. John Wiley & Sons, Inc., 1997 New York.
- [91] Franklin, L.B. *Wastewater Engineering: Treatment, Disposal and Reuse*. McGraw Hill, Inc., 1991 New York.
- [92] Nemerow N., Dasgupta A., *Industrial and Hazardous Waste Treatment*. Van Nostrand Reinhold, 1991 New York.

APPENDIX A - LIST OF PUBLICATION

During my Ph.D. program, I have published many peer-reviewed papers, and book chapter; and given presentations in conferences. Here are some *representative papers*:

- Synthesis of MWCNT/MnO₂ and their application for simultaneous oxidation of arsenite and sorption of arsenate, *Applied Catalysis B: Environmental*, 106, 1-2 (2011) 46-53
- Functionalization of MWCNT with Tungsten Oxide and its Application for Sun-Light-Induced Degradation of Rh B, *J. Colloid and Interface Sci.* 362,2(2011)337-344
- Preparation of a MWCNT/ZnO nanocomposite and its photocatalytic activity for the removal of cyanide from water using a laser, *Nanotechnology* 21, 49 (2010) 8
- Synthesis and characterization of alumina-coated carbon nanotubes and their application for lead removal, *Journal of Hazardous Materials* 185, 1 (2011)17-23
- Chromium removal combining the magnetic properties of iron oxide with adsorption properties of carbon nanotubes, *Water Research*, 45, 6 (2011) 2207-2212
- The influence of treatment temperature on the acidity of MWCNT oxidized by HNO₃ or a mixture of HNO₃/H₂SO₄, *Applied Surface Science*, 257 (2011) 7746-7751
- Testing the effectiveness of visual aids in chemical safety training, *Journal of Chemical Health and Safety, American Chemical Society*, March/April 2011, doi:10.1016/j.jchas.2010.03.012,

- Statistical Analysis of Cooperative Strategy Compared with Individualistic Strategy: An Application Study, *Journal of Effective Teaching, University of North Carolina Wilmington* 11, 1(2011) 19-27,

APPENDIX B - CURRICULUM VITAE

Tawfik Abdo Saleh Awadh

Current Address: Chemistry Department, King Fahd University of Petroleum and Minerals, Dhahran, Saudi Arabia.

Tel. +966 3860 4870

Mobile +966 506065323

Email: tawfik@kfupm.edu.sa

Permanent Address: Yemen, Wosab, Tel. 009673206847.

Email: tawfikas@hotmail.com

Email: tawfikas@gmail.com

Doctor of Philosophy in Chemistry from King Fahd University of Petroleum and Minerals, [Dhahran, Saudi Arabia].